Phil. Trans. R. Soc. Lond. B **321**, 263–324 (1988)
Printed in Great Britain

AMACRINE CELLS IN THE RETINA OF A TELEOST FISH, THE ROACH (*RUTILUS RUTILUS*): A GOLGI STUDY ON DIFFERENTIATION AND LAYERING

BY H.-J. WAGNER AND E. WAGNER

Institut für Anatomie und Zellbiologie, Philipps Universität Marburg, Robert-Koch-Strasse 6, *D*-3550 *Marburg, F.R.G.*

(*Communicated by B. B. Boycott, F.R.S. – Received* 11 *June* 1987)

[Plates 1–6; pullout 1]

CONTENTS

We studied 250 amacrine cells in the retina of the tetrachromatic cyprinid *Rutilus rutilus* (roach) after rapid Golgi impregnation. All cells were recorded in camera lucida drawings from 50–80 μm sections. For classifications we used independent criteria of presumed functional relevance, most of which could be quantified. These included 'gross morphological' features such as size, symmetry and orientation of the dendritic field, pattern of branching and number of ramification points as well as fine

structural details like process diameter and the occurrence of spines and varicosities. We also took into account the pattern of radial distribution of dendrites.

To obtain information about the subdivision of the inner plexiform layer, we used the relative stratification levels of stratified amacrine cells to plot a frequency distribution diagram showing that the dendrites of these cells are clustered in seven discrete sublayers of unequal width; four sublayers occupy the distal half of the inner plexiform layer (sublamina a) and three sublayers are present in the proximal half (sublamina b). The subdivision was compared with densitometric data of the inner plexiform layer after various staining methods and with previous observations about the location of bipolar terminals and neurochemical bandings. Our findings suggest that this layer is composed of complementary structural components, each of which is subject to a specific layering pattern.

On this basis we could distinguish 43 different types of amacrine cell. If individual types occurred in more than one sublayer, they were considered as subtypes; of these, we found 70 different ones. Among the 43 types, 6 were observed only once. In comparison with amacrine cells described in other species, six 'new' types were identified. For each individual type, an identity chart was prepared summarizing camera lucida drawings of tangential views at low and high magnification, a semischematical drawing of the radial location of the dendrites, and the most relevant quantitative data.

Our observations are discussed in the context of available evidence about light-evoked responses of identified amacrine types in other species, and possible transmitter content. They substantiate a functional concept according to which amacrine cells provide (i) a multicellular aggregate for coupled membrane potential; (ii) unit activity by the action of entire individual cells; and (iii) local microcircuits caused by isolated activation of single dendrites or parts thereof. The great variety of morphological differentiation, and the numerous transmitters found, suggest that within this basic framework individual amacrine types serve highly complex and sophisticated roles in retinal information processing. Our attempt towards a detailed classification and description of amacrine cell types is intended to provide a reference for future intracellular and neurochemical work, to facilitate precise identification.

Introduction

Amacrine cells are the main local circuit neurons of the second synaptic layer of vertebrate retinae. They differ from classical projection neurons by the apparent lack of an axon, which led Cajal (1894) to alter the original name of 'spongioblasts' and to call them 'axonless' cells. Their dendrites extend in the inner plexiform layer and engage in synaptic contacts with bipolar terminals, ganglion-cell dendrites, and other amacrine cell processes (see Dowling (1979) for review). Furthermore, they establish two-way connections with interplexiform cells (Dowling & Ehinger 1975) and may receive input from horizontal-cell axon terminals (Naka 1976; Marshak & Dowling 1984) and centrifugal fibres (Marchiafava 1976). This means that amacrine cells contact every retinal neuron class except photoreceptors. The nature of signal transmission in amacrine cells is diverse. They are coupled to other amacrine cells and certain bipolar cells by gap junctions (Naka & Christensen 1981; Kolb & Nelson 1984), and by chemical synapses to bipolar, interplexiform, ganglion and amacrine cells. The transmitters used in these synapses are of an extraordinary variety and comprise small molecules such as acetylcholine, biogenic amines and amino acids (for review, see Marc (1986)) as well as neuroactive peptides like enkephalins, tachykinins and somatostatins (for review, see Brecha

et al. (1984)). In some cases, co-localization of two transmitters has been observed (Weiler & Ball 1984; Lam *et al.* 1986).

Light-evoked responses of amacrine cells can be broadly divided into sustained and transient, the former being either depolarizing 'on' or hyperpolarizing 'off' (Werblin 1970; Kaneko 1973; Murakami & Shimoda 1977; Marchiafava & Weiler 1982; Kolb & Nelson 1984; Djamgoz *et al.* 1985). A more detailed analysis of the response profiles has shown further response characteristics such as 'brisk' or 'sluggish' components, light-dependent membrane noise and afterpotentials; these results suggest that the physiology of amacrine cells is highly sophisticated and diversified (Djamgoz *et al.* 1985).

The physiological, neurochemical and synaptic complexity is only paralleled by the morphological diversity of amacrine cell types initially shown by Cajal (1894). Depending on whether amacrine cells were examined in whole-mounts or radial sections, and on the criteria used for classification, different numbers of cell types have been identified in various species: carp, 14 (Cajal 1894), 10 (Ammermüller & Weiler 1981); catfish, 3 (Naka & Carraway 1975); bogue, 5 (Vallerga & Deplano 1984); *Nannacara anomala*, 10 (Wagner 1973); turtle, 27 (Kolb 1982); rat, 9 (Perry & Walker 1981); ground squirrel, 5 (West 1976); cat, 22 (Kolb *et al.* 1981); macaque, 8 (Boycott & Dowling 1969); man, 19 (Linberg *et al.* 1986). Traditionally, parameters such as size of the dendritic field, degree of ramification, and pattern of stratification have been examined; more recently, shape and symmetry of the dendritic field, pattern of ramification, and number of branching points have also been taken into account (Ammermüller & Weiler 1981). Furthermore, attention has also focused on details such as the occurrence of spine-like appendages and varicosities as well as on dendritic diameter (Vallerga & Deplano 1984).

Because a substantial part of amacrine output is to ganglion cells (Dowling & Werblin 1969; Witkovsky & Dowling 1969; West & Dowling 1972) it is generally assumed that their function consists in creating the antagonistic peripheral zone of ganglion receptive fields (Miller 1979; Dowling 1979). However, in view of the great variety of morphological types and physiological responses, it would be surprising if the role of amacrine cells could be adequately described by such a general statement. In fact, where morphologically identified cells have been tested for their light-evoked responses and their synaptology (Kolb & Nelson 1984, 1985) a much more sophisticated picture begins to emerge. According to these studies in the cat, specific amacrine cell types may mediate the off inhibition of on-centre ganglion cells (A13), have local adapting effects on rod bipolar cells (A17), or serve as interneurons in the rod pathway from bipolar to off-centre ganglion cells (AII).

Such detailed information about the role of amacrine cells in cat retinal circuitry has been possible only because a correlation was made between anatomical and physiological data. An essential prerequisite for the success of any correlative approach of this type is that in both categories a set of well-defined parameters is at hand, which allows a precise identification and classification of the observations. In teleosts, first attempts towards a correlation have already been undertaken (for review, see Djamgoz & Wagner (1987)). However, at least on the morphological side, we feel that a comprehensive classification of amacrine cell types, based on a broad array of functionally relevant criteria, is not available at present, because most of the previous reports have focused preferentially on either overall features of the dendritic field (see, for example, Ammermüller & Weiler 1981) or fine structural details (see, for example, Vallerga & Deplano 1984).

In many species, the chromatic types of photoreceptors are morphologically discernable (Scholes 1975; Stell & Harosi 1976; Levine & McNichol 1979) and even chromatic types of bipolar cells have been identified (Scholes 1975). Because amacrine cells have been shown to have chromatic components in their light-evoked responses (Kaneko 1973; Mitarai *et al.* 1978; Djamgoz & Ruddock 1983; Djamgoz *et al.* 1985) the teleost retina is a suitable model for the elucidation of the involvement of amacrine cells in the different colour channels. Furthermore, the comparison of species with different chromatic capabilities may facilitate the identification of cell types with specialized functions and others with basic functions common to all species.

In the present investigation, we chose the retina of the tetrachromatic roach (*Rutilus rutilus*) (Avery *et al.* 1982). In this cyprinid species, closely related to carp and goldfish, the functional relation of photoreceptors, horizontal and bipolar cells is well characterized (Scholes 1975; Djamgoz 1984; Djamgoz & Downing 1983; Djamgoz *et al.* 1985). Furthermore, a number of observations on amacrine cells in this species are also available (for review, see Djamgoz *et al.* (1985)). For the morphological characterization of amacrine cells we chose as a staining method the classical rapid Golgi method (Cajal 1894), and used as criteria size, shape and symmetry of the dendritic field, number and distribution of ramification points, pattern of stratification within the inner plexiform layer, diameter of individual processes, and the occurrence of varicosities and spines. Wherever possible, we attempted to quantify our observations. On this basis, we could distinguish 43 different types of amacrine cell. To allow an easy means of identification and correlation with cells stained by other methods, we prepared a catalogue of identification charts for each cell type in which qualitative and quantitative data are summarized (see pp. 303–324).

As regards the radial distribution of amacrine-cell dendrites within the inner plexiform layer we found it difficult to reconcile our observations with the often-used subdivision of this layer into five sublayers of equal thickness. Alternative approaches to define these sublayers, for example on the basis of the location of bipolar terminals (Scholes 1975; Haesendonck & Missotten 1983; Deplano & Vallerga 1983) also did not appear to provide a suitable framework for the observed levels of amacrine dendrites. For this reason, we established a frequency distribution of the stratification levels of all stratified amacrine cells. This analysis showed that amacrine-cell dendrites in the roach's inner plexiform layer form seven discrete sublayers of varying thickness, the borders of which are not in agreement with those found for bipolar terminals. However at present, it is not possible to correlate these sublayers with the functional on–off subdivision of sublamina a and b, as introduced by Famiglietti & Kolb (1976) and Famiglietti *et al.* (1977). Further combined morphological and physiological work should reconcile the various concepts of functional subdivisions of the second synaptic layer, as well as yielding new insights into the diverse role of amacrine cells in retinal circuitry.

Materials and methods

We used retinae of adult roach (*Rutilus rutilus*, Cyprinidae, body length more than 20 cm) obtained from their natural environment (River Lahn, Edersee) during July–October 1984. The animals were dark-adapted for two hours before decapitation, enucleation and hemisection of the eye. In order to minimize morphofunctional variations due to endogenous factors, all animals were killed between 10h00 and 12h00. The posterior pole was held upside down; the

retina was gently detached from the pigment epithelium and the optic nerve was cut. Retinae were fixed in a mixture of 2.5% (by volume) glutaraldehyde and 1% (by mass) paraformaldehyde in 0.06 M phosphate buffer with 3% (by mass) sucrose at pH 7.3 for 2 h. During subsequent rinses in buffer, several radial incisions were made before the tissue was placed between two pieces of curtain net, which were sewn together at the edges to keep the wholemounts flat. These preparations were then impregnated according to the rapid Golgi method (Cajal 1894; Stell 1975) and embedded in Epon after removal of the stabilizing net. Sections 50–80 μm thick, in the tangential and radial planes, were cut on a sliding microtome by using West's technique (1972) of warming the blockface.

In 35 retinae, we found the density of impregnated cells suitable for further analysis of individual cells. These were studied in a light microscope equipped with a drawing tube and recorded as camera lucida drawings at medium (×300) and high (×1500) magnification. Individual cells with parts in more than one section could be reconstituted in this way. In addition, light micrographs were taken of characteristic cells and specific details.

We based our analysis essentially on tangential views and used radial sections as controls to establish the radial distribution of the dendritic ramification. The depth of every process within the inner plexiform layer (IPL) was determined by focus readings at maximum magnification (×1200). These measurements were expressed both as relative values with respect to the inner and outer borders of the IPL and as absolute values. In cells with a homogeneous, narrowband fibre plexus, focal measurements were taken every 50–100 μm for each process, whereas in cases with irregular or wavy dendrites the position of every process was assessed at 10 μm intervals. We used two additional methods to control the layering information derived from focus readings. First, five stratified and five diffuse cells were resectioned and the distribution of processes observed directly in radial views. Comparisons with the results from focus measurements confirmed the reliability of this method at a 96% confidence level, equivalent to an error margin of ±1 μm. These values are in good agreement with the theoretical observations of Harris (1985) about the preciseness of light microscopic focus measurements. Secondly, in cases of very irregular dendritic fields, combined values derived from radial and tangential sections were entered interactively via a graphics tablet into a computer system (IPS, Kontron) and 3-D representations obtained according to a procedure outlined by Wagner & Speck (1985) and Djamgoz *et al.* (1987).

No correction factors were introduced for shrinkage due to fixation and embedding.

Results

1. *Definition and evaluation of parameters for classification*

A total of 250 amacrine cells were identified by their lack of processes connecting them to the outer plexiform or optic fibre layer and thus distinguishing them from displaced ganglion and interplexiform cells. Their essential characteristic is a field of processes within the IPL, which determines their 'view of the world' (Palay & Chan-Palay 1975) and thus is likely to play a major part in the determination of their function(s). The morphological differentiation of their dendritic field provides the key parameters for the classification in the present paper. As pointed out by Rodieck & Brening (1982) any attempt to introduce a system of classification relies on the evaluation and comparison of similarities and reproducible differences; ideally this then leads to the establishment of an inventory of exemplary types of cell as attempted in this

study. Obviously, the choice of such parameters has important bearings on the selectivity and the number of cell types that result from a classification. The parameters chosen have to fulfil several requirements: they have to be independent from one another; they must be quantifiable, they have to be morphological constants and they should be of functional relevance. We have focused our attention on fine structural as well as gross morphological features: occurrence and size of varicosities and spines, calibre and terminal characteristics as well as size, symmetry, branching frequency and pattern, and radial localization and spread of the dendritic field.

1.1. *Wholemount views of dendritic fields*

1.1.1. *Extent of the dendritic field.* To take into account the different types of symmetry of the dendritic field, we measured the distance between the centre of the projection of the soma and the most distant dendritic terminal in camera lucida drawings. This value, D, ranged from 50 μm to 1.06 mm. In figure 1, the frequency distribution of the maximum distances, D, of all individual amacrine cells is shown; because the distribution cannot be fitted to a Gaussian we found it difficult to derive a 'natural' classification based on size, as has been proposed by Vallerga & Deplano (1984). Instead, we termed cells with $D > 450$ μm widefield, those with $D = 100$–450 μm mediumfield, and cells with $D < 100$ μm smallfield. Narrowfield amacrine cells, as found in the bogue, have not been found in the roach.

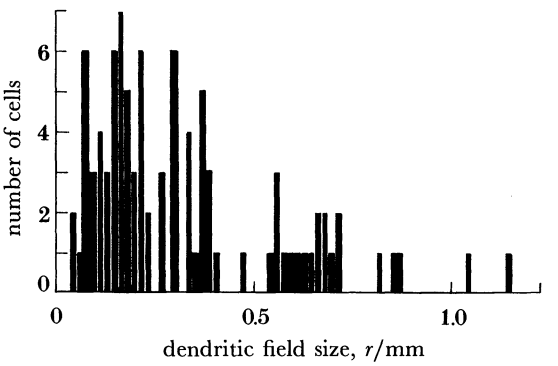

FIGURE 1. Frequency distribution diagram of greatest radii (r) in all amacrine cells recorded ($n = 250$).

Some cell types were observed in sufficient numbers to assess the question of systematic variation in the extent of dendritic field in relation to the eccentricity of a given cell. Figure 2 indicates that such a correlation cannot be established for type 4 cells. This corresponds well to the relative homogeneity of cone density; according to cell counts in whole mounts (H.-J. Wagner, unpublished data), there is a region of increased cone density only in the ventrotemporal quadrant; however, even in this part, the density does not exceed 2.1 times that of the remaining regions and is therefore considered to be of minor importance, compared with situations in teleost species with foveas (Schwassmann 1968) or species with central areas (cat (Boycott & Wässle 1974)). Because similar evaluations of two other cell types gave no indication of a regional dependence of dendritic size, we used the parameter without taking into account the specific location of a given cell within the retina. Similar observations have been made for horizontal cells in the roach (Djamgoz *et al.* 1985) and for amacrine cells in the carp (Ammermüller & Weiler 1981) and in the bogue (Vallerga & Deplano 1984).

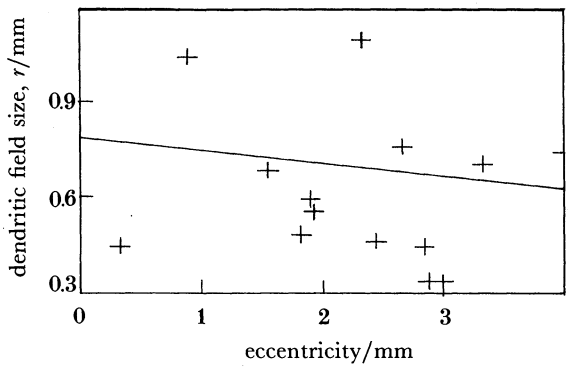

FIGURE 2. Correlation between eccentricity (distance from optic disc) and dendritic field size (r) in 15 A4 cells; the correlation coefficient is -0.144.

1.1.2. *Symmetry of the dendritic field.* We used the method of Ammermüller & Weiler (1981) to analyse the symmetry of the dendritic arborization pattern and to differentiate between uniformly radiate, polar, and asymmetrical (marked edge) cells. After placing a transparent sheet, with concentric circles at distances corresponding to 17 μm as well as radial lines subdividing the circles into twelve 30° sectors with the centre on the perikaryon, we counted the intersections of every process with a circle. Uniformly radiate cells had dendrites in roughly equal numbers in each sector. In polar cells, all sectors contained processes too, but with a clear concentration of processes in only a few sectors. Often, two peaks of process densities were found at an angle of *ca.* 180°; such cells were characterized as bipolar. Asymmetrical cells had most of their processes restricted to a small number of neighbouring sectors, some sectors even containing no dendrites at all.

Slightly less than one half of all amacrine cell types (46%) had a dendritic field with uniformly radiate symmetry; 40% of all types had a polar organization with processes often covering two 90° sectors in opposite directions. In the remaining 14%, the asymmetrical dendritic field spread over angles between 20° and 210°.

1.1.3. *Orientation of the dendritic field.* Contrary to cells with uniformly radiate dendritic fields, in asymmetrical and polar organized cells the orientation of the preferred direction of the dendritic field with respect to the optic papilla may be of functional significance, for example for the perception of directional selectivity. Therefore, we determined the long axis of a dendritic field and recorded the angle subtended by the ganglion cell axons or a radial line through the optic papilla. Especially in amacrine cell types with so-called distal dendrites (Djamgoz *et al.* 1984) (types 6 and 26, figures 25–27) a clear majority of cells extended their dendrites preferentially at right angles to the ganglion-cell axons. Considering the entire population of these cells, a ringlike, concentric distribution results from such an orientation. On the other hand, asymmetrical cells with a very narrow field of processes (like type 42) (figures 36–38) could be divided into two populations, one with a tangential or orthogonal, and the other with a parallel orientation with respect to the ganglion-cell axons (figure 8). Finally, there were cell types with preferred-direction dendritic fields in which an apparent random orientation was observed (types 5, 8, 20 and 30).

1.1.4. *Branching pattern of dendrites.* Quantitative evaluation of the dendritic branching pattern has been shown by Weiler & Ammermüller (1981) to be a reliable criterion for the

differentiation of cell types. The following parameters were assessed: total number of branching points, absolute and relative distance between the most distant ramification points, number of branching points, and number of processes at various distances from the soma. The analysis was again performed with the help of an overlay of concentric circles (with intervals of 17 μm); the number of dendrites was determined by counting the intersections with the circles and the number of branching points was recorded in each ring. Cells with up to 20 branching points were classified as sparsely branched; they constituted 56% of our cell types. Profusely branched cells, which had more than 40 branching points, made up 9% of all cell types; the remaining 35% had between 21 and 40 branching points.

The distance of the branching points from the soma or the stem process is another significant parameter with functional consequences for the cable properties. Its differentiation power is readily illustrated with the type 4 cell, which, at first glance, may look like a 'starburst cell' as known from mammalian retinas (Famiglietti 1981; Masland & Tauchi 1986). However, whereas the mammal starburst cell is characterized by 3–7 bifurcations at roughly equal intervals throughout the entire length of a process, the type 4 cells have only a single branching point close to the tip of the stem process; furthermore, several varieties of cell types with starburst-like properties can be distinguished by using this criterion (types 12 and 14).

1.1.5. *Diameter of processes; morphology of dendritic terminals.* According to the cable theory the diameter of a dendritic process is of major importance for signal propagation (Rall 1962; Sasaki-Sherrington *et al.* 1984); it has therefore been used to categorize cell types in several species by West (1976), Kolb (1982), Kolb *et al.* (1981) and Vallerga & Deplano (1984). The thickness of a given process may remain constant up to its terminal (figures 26, 27 and A26) or it may taper gradually (figures 22 and A15). Therefore, as a rule, two measurements of profile thickness were taken, the first at or near the origin and the second at or near the tip of every major dendrite (table 3). Four categories of diameters could be clearly distinguished: thick processes (4–7 μm), medium thick (2–3 μm), thin (1–1.5 μm) and delicate fibres (no more than 0.5 μm). In three distinct cell types, all with coarse dendrites, the diameter did not change markedly from the origin to the terminals. Such processes terminated in a short conical structure, which made up about the last 10 μm. In addition, these cells had in common the occurrence of one or two so-called 'distal' dendrites (Djamgoz *et al.* 1985): very long (up to 1 mm), delicate and mostly unbranched processes that began with an abrupt tapering of one of the secondary dendrites (figures 26, 27 and A26).

Another cell type (A4) was remarkable: from a primary dendrite, about 30 delicate branches emerged, most of which became thicker towards the periphery and terminated as thin processes more than 1 mm away from the point of origin (figures 15, 16 and A4).

1.1.6. *Varicosities.* Various kinds of dendritic swelling were observed along the course of the medium thick, thin, and delicate processes, whereas thick branches were devoid of them. Their size, shape and distribution have long been recognized as specific features of the various cell types. Although, strictly speaking, the size of these swellings was almost never constant in a given cell but rather followed a normal distribution, it was not difficult to determine the dominant size and to use it as a parameter. We have discerned regular, spherical varicosities (figures 28 and A29) and irregularly shaped swellings (figures 18 and A13). The former occurred in two broad sizes, large ones measuring 2.5–4 μm and small ones 0.5–1.5 μm. The irregular ones had diameters of 1–2 μm.

Sometimes amacrine cell types had very few, sparse and indistinct swellings. These were in

general disregarded; only if more than five varicosities were found in the course of a major dendrite was a cell type considered as having varicosities.

1.1.7. *Spines.* Dendritic spines are specific postsynaptic structures best known from a number of central neurons. Similar structures, i.e. elongated, knoblike protuberances with a length of 2–4 μm and a diameter of 1–2 μm, were often observed in amacrine cells (figures 14 and A3). As for varicosities, dendrites completely devoid of spines were observed only rarely; we therefore differentiated between processes bearing few (up to three) and many (up to ten) spines. In some cases, the presence of spines seemed to be at the expense of varicosities (types 2, 3, 8, 10, 11, 14 and 25); however, no strict correlation could be established between the occurrence of both these structures (see table 3).

1.2. *Radial views: stratification of amacrine cells*

The existence of parallel 'stripes' within the IPL had been recognized by Dogiel (1888), before Cajal (1894) was able to relate them to the processes of amacrine and ganglion cells. The disagreement about the number of such strata, stated by Cajal, has, however, not convincingly been resolved since then. For the five sublayers of unequal thickness in the IPL of fish and reptiles, a further subdivision for each stratum was proposed consisting of a 'triplet' of amacrine-, bipolar- and ganglion-cell processes. Irrespective of this cautious approach, the majority of subsequent researchers chose to use a 20% criterion to define five sublayers in the IPL (Kolb *et al.* 1981; Famiglietti & Vaughn 1981; Ammermüller & Weiler 1981). Alternatively, differences in optical density after various staining procedures or histochemical labelling experiments have been exploited to analyse the layering (Wagner 1973; Scholes 1975; West 1976; Marc 1986) whereas Deplano & Vallerga (1983), Haesendonck & Missotten (1983) and McGuire *et al.* (1984) based their layering paradigm on the location of bipolar terminals. From these observations it is safe to conclude that the stratification pattern of the IPL is not generally pentalaminar, but that there are at least species-specific differences which may be supplemented by cell-class-specific features. For this reason, we have attempted to use the amacrine-cell processes as constitutive elements for layering and have analysed their depth distribution within the IPL.

1.2.1. *Stratified and diffuse cells.* Before such an evaluation, we had to establish the pattern of radial ramification of amacrine cells without respect to their exact location within the IPL, because we felt the classical subdivision into 'stratified' and 'diffuse' cells insufficient. If the dendrites had a straight course, they occupied a layer not more than 4 μm (or, at an average total IPL width of *ca.* 40 μm, 10%) thick; such cells were considered as strictly stratified. With only a single horizon of stratification, they were monostratified; in other cases, two or more distinct layers of dendrites originated from a radially orientated primary, or stem process and thus formed bi-, tri- or multistratified cells. Stratification was by far the most common type of radial ramification, accounting for 71% of our amacrine cell types. By exclusion, all non-stratified cells were called diffuse. Sometimes the dendrites of these cells had a wavy course or showed two or three processes running on top of each other with very narrow intervals. If the radial extent did not exceed 20% of the total IPL thickness, we called such cells 'narrow-diffuse'. Two more varieties of diffuse were distinguished: 'broad-diffuse' cells had irregular dendrites occupying up to 20 μm or 50% of the IPL, and 'all-diffuse' cells spread their dendrites over half the IPL thickness. In both cases, the processes either formed a dense multilayered array (figures 36–38 and A42) or were distributed randomly with processes running obliquely and

branching at irregular angles. In cells of this latter type of ramification, the density of dendritic terminals was often very high; they often appeared as a cloudlike overall structure (figures 40 and A43).

It should be noted that our concept of diffuse cells is at variance with that of Cajal (1894) and of Boycott & Dowling (1969), who considered as 'diffuse' only cells whose dendritic fields spanned the entire width of the IPL. The following evaluation of the stratification pattern requires, however, a strict definition of stratified rather than of diffuse cells.

1.2.2. *Distribution of stratified amacrine cell dendrites: definition of sublayers.* The relative location of the narrow stratified dendrites of 184 individual cells was determined by focus readings of at least four different points along all major dendrites (for details see Materials and methods). For each neuron, all percentage values so obtained were averaged for a given layer and plotted on a graph. The result (figure 3) clearly shows a discontinuous distribution of amacrine-cell dendrites which is represented neither by a simple Gaussian nor by a linear relation. Seven peaks (or clusters of peaks) are clearly separated by troughs where either a single stratified cell or no stratified cells had their dendrites. Interestingly, a dendrite-free gap is found between 68 and 73% (corresponding to a width of 2 μm). In the immediate vicinity of the perikarya of the inner nuclear layer (INL) and the ganglion cell layer (GCL) another interval of 2–3% without stratified dendrites was recorded. Contrary to the situation in the 70% region, these apparently amacrine-dendrite-free stripes were mostly attributed to uncertainties about the exact definition of the IPL borderlines; on the other hand, amacrine dendrites were only very rarely observed directly adjacent to the cell bodies.

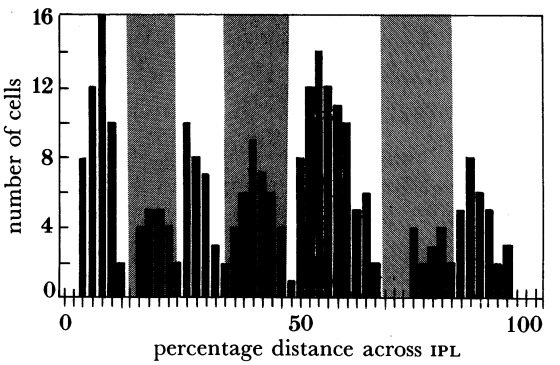

FIGURE 3. Frequency distribution of relative ramification levels of stratified amacrine cells within the inner plexiform layer. Distances across the IPL are given as percentages (border to inner nuclear layer, 0%; border to ganglion-cell layer, 100%). We used this distribution to define seven sublayers of the IPL, every other one of which is indicated as a shaded column.

Based on the distribution of maxima and minima, we introduced a subdivision of the IPL into seven sublayers (SL) of unequal thickness with borders at 15, 24, 35, 49, 68, and 83%. The first sublayer is characterized by a single, prominent peak at 10% and separated from the next sublayer by a minimum at 15%. The following sublayers contain between three and five smaller maxima, sometimes of about equal importance (SL 2, 3, and 6), sometimes with a heterogeneous distribution as in sublayer 4, 5, and 7. In two parts of the graph, the definition of sublayers is less obvious: from 49 to 68%, there is a fairly broad region which consists of three narrow, high peaks and two less conspicuous, broader 'shoulders'. Because these two latter

groups of processes were not clearly separated from the former peaks we included the entire region in sublayer 5, which thus occupies a prominent place in the intermediate part of the IPL. This may be taken as an indication of the special role of the intermediate IPL, different from either pure on- or off-functions (Toyoda *et al.* 1973; Miller 1979; for review, see Djamgoz & Wagner (1987)). Secondly, the separation of layers 6 and 7 is less marked than that of the remaining ones. We introduced a subdivision of the processes between 74 and 97% mainly because of the more coherent group of dendrites at a depth greater than 83%; furthermore, the densitometric data (see below) indicate that the inner one third of the IPL does not form a homogeneous stratum.

1.2.3. *Densitometry of IPL sublayers.* The overall organization of the IPL is determined by a maze of radially and horizontally orientated fibres in which 'beads' of various sizes, representing dendritic varicosities and bipolar and axon terminals, are interspersed with 'fibre elements' of different calibres. Attempts to analyse IPL sublayers by densitometric methods must take into account the following points: (i) different staining methods generally label different structures; (ii) owing to additive effects, increased section thickness may be of crucial importance for revealing layering; (iii) precise orientation of the section is essential because the beam path has to be absolutely parallel to the extension of the sublayers; especially in thicker sections, misalignment is bound to obscure the borders of the sublayers; and (iv) in retinae with a regular orientation of photoreceptors (mosaic retinae; in the roach, double cones are essentially arranged in a square mosaic (Scholes 1975)) a regular pattern of radially oriented processes has been observed in the IPL (Pierantoni & Ogden 1982), which may interfere with the horizontal organization of dendrites. For these reasons, we used the following procedures. Pictures of IPL preparations were entered via a TV-microscope into an image analysis system (IPS, Kontron) and processed with the following sequence of steps: (i) interactive delineation of the outer and inner borders of the IPL (figures 4–7, left-hand panel); (ii) alignment of these borders with the x-axis of the cathode ray tube (CRT) screen; (iii) setting all other layers to grey level 0 = black; (iv) implementation of a lowpass filter active only in the x-direction, to eliminate inhomogeneities due to radial substructures; (v) mapping the occupied grey levels linearly to the maximum range (0 = black, 255 = white); (vi) spreading of the IPL width over the entire width of the CRT display (500 lines) (figures 4–7, centre panel); and (vii) defining a radial trace along which a grey-level profile is measured and plotted (figures 4–7, plate 1, right-hand panel).

1.2.3.1. *Non-specific staining of thick sections.* Radial sections (50 μm) were taken after rapid Golgi impregnation or indirect immunocytochemistry with the use of horseradish peroxidase to visualize various antigens. Suitable portions of IPL containing neither impregnated cells nor specific label yielded traces, representative examples of which are displayed in figures 4 and 5. In dichromate–osmium-treated material (figure 4), there were three major and three minor peaks, equivalent to light bands, separated by three deep and two minor troughs indicating dark regions. Their locations did not exactly coincide with those of the cumulative distribution of the amacrine-cell dendrites; however, the superposition of the sublayer borders, as previously defined (figure 3) indicated a number of significant similarities. Sublayer 1 corresponds to Golgi-peak 1; sublayer 2 coincides with Golgi-trough 1; and sublayer 3 is equivalent to Golgi peak 2; sublayer 4 corresponds to a minor trough and the third minimum; the broad sublayer 5 is covered by a single maximum with an additional minor shoulder; sublayers 6 and 7 are represented by a minor peak each, and separated by a minor trough.

The pattern of light layers (peaks) and dark bands (troughs) of diaminobenzidine (DAB)-stained material (figure 5) clearly differed from that in Golgi-stained sections. Yet, here again, there are striking coincidences with the system of sublayers based on the distribution of amacrine dendrites. For the first three sublayers, the alternation of the light and dark stripes is identical with that in the Golgi material. By contrast, the maximum in sublayer 4 is almost as high as in sublayer 3, instead of only a minor peak. In the DAB-stained sections, the broad sublayer 5 consists of three light bands and one dark; the 'shoulder' observed in the Golgi-stained section possibly corresponds to the second peak. In the inner part of sublamina b, the pattern of light and dark bands is reversed: both sublayers 6 and 7 coincide with deep troughs separated by a minor peak marking the border between both these sublayers.

1.2.3.2. *Thin sections.* The densitometric trace through the lowpass-filtered micrograph of a 1 μm IPL section stained with methylene blue (figure 7) shows an even more unsteady shape, which makes a reduction to fewer sublayers difficult. On the background of the sublayers derived from amacrine dendrites, however, a pattern emerges which substantiates this subdivision. The first three layers are essentially represented by minima, i.e. dark bands separated by lighter areas; both sublayers 1 and 3 are further separated by major (1) and minor (2) peaks. The sublayers 4 and 6 correspond to two lighter bands with narrow troughs, which are widely separated by a denser region corresponding to sublayer 5, which, in turn, is made up of two dark bands and one lighter one. Finally, the innermost sublayer is characterized by a dark stripe flanked by two light areas.

1.2.3.3. *Labelling of F-actin with phalloidin.* Fluorescent rhodamine-labelled phalloidin was used to stain the microfilament system in 5 μm cryostat sections (figure 7) as described in detail by Drenckhahn & Wagner (1985). This component of the cytoskeleton has been shown to be preferentially accumulated in presynapses of neural tissue (Fifkova & Delay 1982; Drenckhahn & Kaiser 1983). Unlike the above stains, which have no specific affinity to a particular cellular component, this staining can therefore facilitate the visualization of the general distribution of synapses throughout the IPL. Previous observations have already shown a distinct sublayering of fluorescence in this part of the retina (Drenckhahn & Wagner 1985).

A densitometric trace through a fluorescence micrograph of the IPL shows the labelled areas as peaks (figure 7). Roughly, there is a symmetrical distribution of phalloidin in sublamina a and b: at both borders there are F-actin-rich areas, separated by two troughs including minor peaks from two broad zones of fluorescence on both sides of a dark band in the 50% region. The pattern of phalloidin fluorescence bears little resemblence to the layers derived from the amacrine dendrite maxima: the peripheral sublayers 1 and 7 each contain both a peak and a trough; furthermore, the most intense peak coincides with the border between sublayers 3 and 4, and between sublayers 4 and 5 is the trough separating the more complex, broad bands.

1.2.4. *Discussion of layering*

1.2.4.1. *Structural basis of IPL sublayering.* A comparison of the different patterns of sublayering observed after densitometry of various staining and sectioning techniques on the one hand, and of the radial distribution of amacrine-cell dendrites on the other, shows a high degree of diversity and even divergence. Assuming that the application of the lowpass filter only suppressed the noise caused by radially orientated structures and essentially enhanced the horizontal subdivisions without introducing further artefacts, the alternating areas of light and dark indicate that different structural components contribute in different ways to the organization of the IPL.

TABLE 1. COMPARISON OF PRINCIPLES OF SUBDIVISION OF THE INNER PLEXIFORM LAYER

(Criteria used by various authors are: amacrine-cell density (ACD); optical density (OD) and position of bipolar terminals (BCD).)

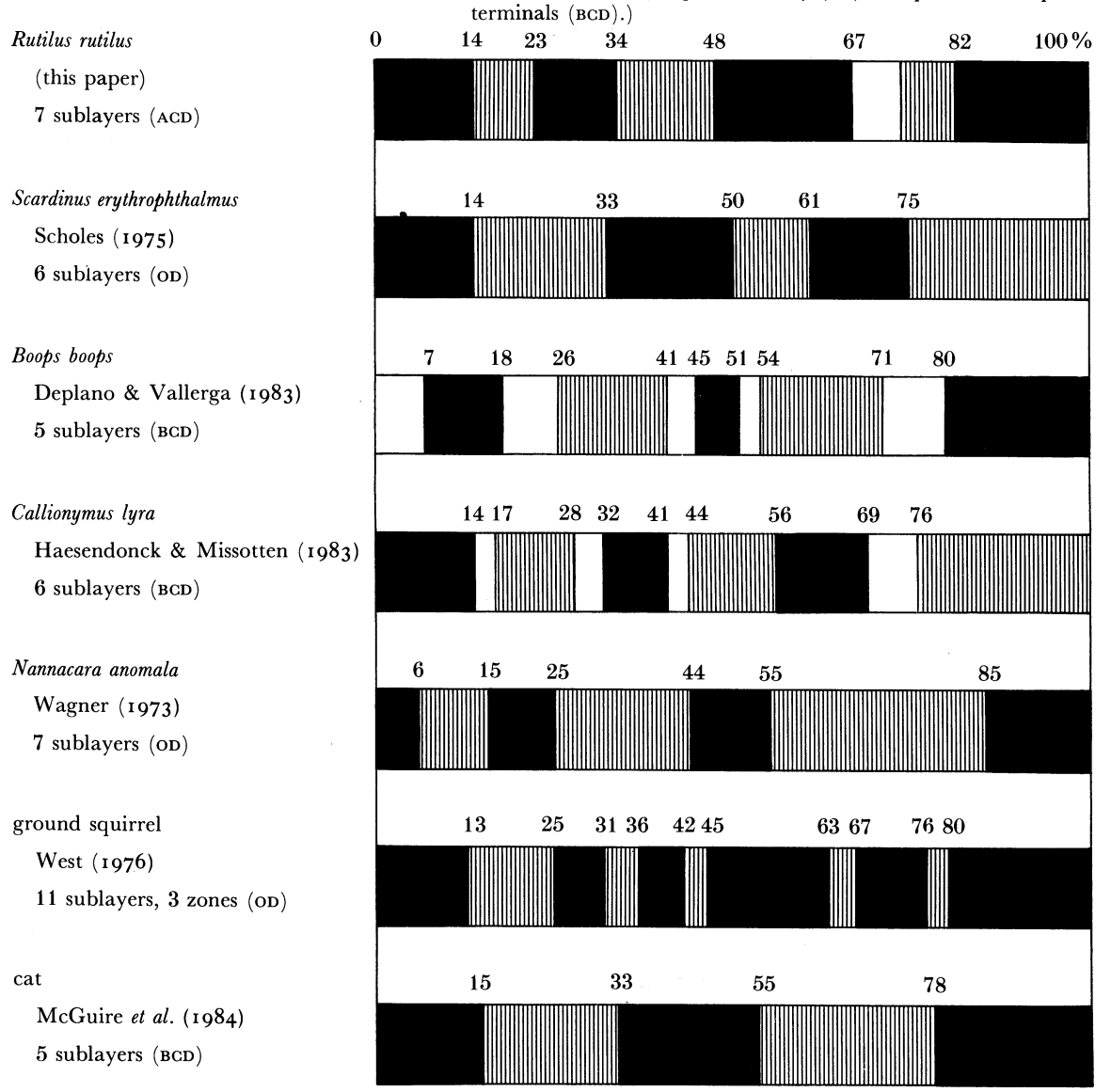

Densitometric analysis of unspecific staining of thick and thin sections shows a roughly identical banding with a tendency for a higher degree of differentiation in thinner sections. However, there is no correlation with the accumulations of amacrine dendrites, as these are represented by both light (SL 1, 3, 5) and dark bands (SL 2, 4, 7). This indicates that either the dendrites of different amacrine cell types have different staining or light-absorbing properties, or that the processes of other neurons of the IPL take part in the determination of the pattern of optical densities.

The structural elements that have been most thoroughly studied in fish are the terminals of bipolar cells (see table 1 for comparison). Unfortunately, no specific data are available for the roach, but in the closely related rudd, Scholes (1975) observed six sublayers: three of about

equal thickness in sublamina a and three others in sublamina b, the innermost of which was particularly wide (25%). An innermost sublayer of similar thickness was also reported in goldfish (Ishida *et al.* 1980) and *Callionymus lyra* (Haesendonck & Missotten 1983). Combined ultrastructural and electrophysiological studies (Saito *et al.* 1985) have shown that on-centre bipolar cells ('on-BI' cells) contacting both rods and cones terminate with conspicuous swellings close to the ganglion cell bodies; in addition, delicate telodendria of on-BII cells also occupy this sublayer. As for the distribution of bipolar axon terminals throughout the rest of the IPL, a fair degree of correspondence between the light stripes after DAB-staining and the layering of bipolar terminals may be established in *Callionymus*. Furthermore, the phalloidin fluorescence in sublayers 1 and 7 may also be attributed to the presence of bipolar terminals. However, an analysis of bipolar types and their terminations in the roach would be required before correlating densitometric data and the distribution of a second structural element besides amacrine cell dendrites.

Ganglion-cell dendrites also participate in determining the horizontal subdivision of the IPL. However, the published evidence in teleosts provides no basis for Cajal's (1894) assumption that the laminar distribution of amacrine-cell and ganglion-cell dendrites is strictly complementary. Ganglion-cell dendrites occur at different levels; the correlation of off-centre cells with dendrites in the distal IPL and on-centre cells with dendrites in the proximal IPL in the carp has been shown by Famiglietti *et al.* (1977) to be in accordance with what is known in other vertebrates (for review, see Djamgoz & Wagner (1987)). A third population of ganglion cells with dendrites in the intermediate part of the IPL gave on–off responses. Consequently, subsequent studies of the laminar distribution of ganglion-cell dendrites were restricted to a broad three-tier classification (see, for example, Dunn-Meynell & Sharma 1986). In the absence of an analysis of ganglion-cell dendrite distribution, the exact role of these dendrites in IPL sublamination cannot be assessed.

1.2.4.2. *Layering patterns after neurochemical labelling.* Immunocytochemical visualization of neuropeptides, or of enzymes involved in transmitter synthesis, as well as autoradiographic localization of tritiated transmitters taken up into neurons by specific high-affinity transport mechanisms, provide another powerful tool for characterizing the laminar organization of the IPL. With respect to our amacrine-cell-derived differentiation this is especially interesting, because all these neuroactive substances have been shown to occur in amacrine-cell perikarya and dendrites (see table 2 for comparison). Rapid uptake of [^{3}H]GABA has been observed as narrow stripes in six out of seven of our amacrine-dendrite-derived sublaminae, with the exception of sublayer 2 (Marc 1986). As for the remaining transmitters, each sublamina is characterized by a specific combination of substances. Serotonin is present in four sublayers: [^{3}H]glycine uptake and somatostatin has been localized in three strata (Marc 1986; Wagner & Zeutzius 1987); [^{3}H]choline uptake, indicating the presence of acetylcholine-containing amacrine cells, was shown in two strata, whereas substance P and neurotensin occurred in a single sublayer of the cyprinid retina (Wagner & Zeutzius 1987).

1.2.4.3. *Definition of sublayers as biological entities.* The distinction of off-centre and on-centre spaces within the IPL has clearly shown the existence of a functional basis for a laminar subdivision of this part of the vertebrate retina. The occurrence of paramorphic ganglion and amacrine cell types suggests that complementary functional roles are localized in a mirror-symmetrical way. What the exact stimulus dimensions are which are encoded in the various subdivisions of the on-centre and off-centre spaces is, however, a matter of speculation. From

TABLE 2. COMPARISON OF NEUROCHEMICAL LABELLING PATTERNS AND CUMULATIVE DISTRIBUTION OF AMACRINE DENDRITES

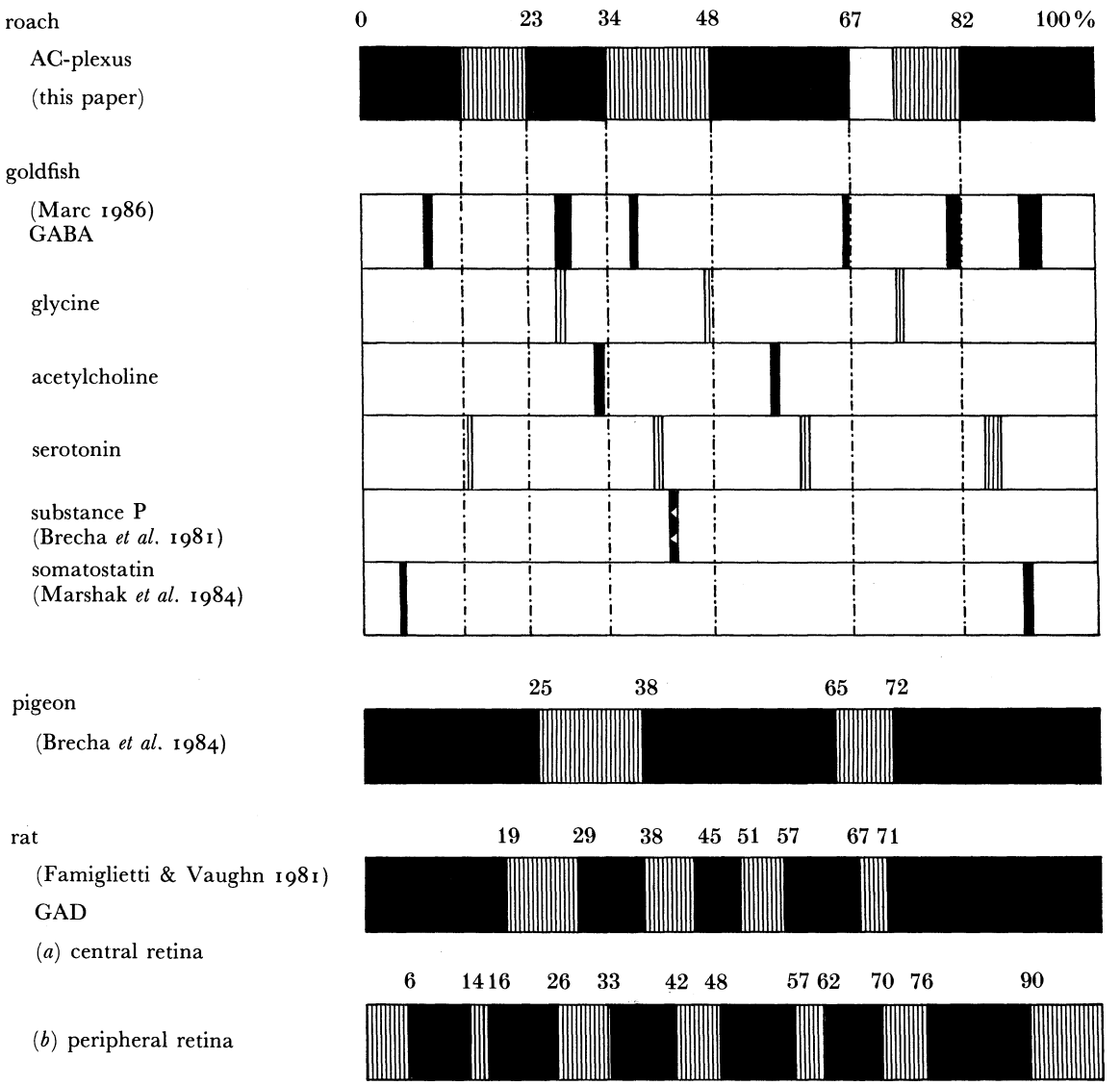

Scholes' (1975) and Haesendonck & Missotten's (1983) observations, one may get the impression that chromatic information might be processed in separate sublayers; but a more detailed analysis of bipolar connectivity is needed to substantiate this concept. A closer look at the neurochemical, densitometric, amacrine-dendrite and bipolar-derived stratification indicates that the mirror symmetry of complementary function must not be taken too literally. In many cases, there is an intermediate and an innermost layer of substantially larger width than the remaining strata; furthermore, the distal off-centre space appears more thinly laminated than the on-centre space.

Finally, the distribution of GABA activity, as well as the occurrence of narrow, broad, and

all-diffuse amacrine cells, indicates that the concept of functional entities must be supplemented by a second organizational principle, i.e. radially oriented functional subunits.

2. *Presentation of amacrine-cell types and subtypes*

Amacrine cells with perikarya in the inner nuclear layer (INL) were recorded and classified according to the criteria outlined above. Cells with individual processes that could be traced to the level of the somata of ganglion cells or even to the optic-fibre layer were identified as displaced ganglion cells and not included in this study.

Some amacrine cells have their cells bodies located in the ganglion-cell layer (GCL); such cells have been observed in many vertebrate retinae and are referred to as 'displaced' amacrine cells (Cattaneo 1922). Morphologically, they comprise a number of different types (Perry & Walker 1980; Wagner & Zeutzius 1987); numerically, they may account for some 34% of all cell bodies within the GCL of the rabbit (Vaney 1980), 40–45% in the rat retina (Hughes 1977), and possibly as much as 80% (Hughes & Wieniewa-Narkiewicz 1980; Hughes 1981). Characteristically, displaced amacrine cells are similar, with respect to ramification pattern and transmitter content, to regular amacrine cells (Masland & Mills 1979; Marshak *et al.* 1984; Brecha *et al.* 1984) so that terms like 'matching populations' (Vaney *et al.* 1981) or 'paramorphic pairs' (Kolb & Nelson 1981) have been introduced. The existence of amacrine cells with identical dendritic features and cell bodies on either side of the IPL has recently been shown in the roach (Wagner & Zeutzius 1987). In our Golgi preparations, silver chromate crystals were sometimes present in the vicinity of perikarya in the GCL, making it difficult to decide whether or not an axon was leaving the soma. Therefore, as a rule, we disregarded all dendrites originating from the GCL.

We propose to call a *type* of amacrine cell a cell with a distinct dendritic pattern, including fine-structural details as outlined above, irrespective of the location of the processes in the IPL. This latter characteristic is referred to as *subtype*. If only a single branching level was found for a given cell, such a type then had only one subtype. If, on the other hand, the same kind of branching pattern was found in more than one sublayer (paramorphism, see above), as has also been reported previously by Cajal (1894), Boycott & Dowling (1969), and Wagner (1973) such a cell type is described as having several subtypes. These are identified by the sublayer of stratification behind the number of the cell type.

In the 35 retinae examined, 250 cells were recorded which were clearly identified as amacrine cells. Among these, we could distinguish 43 cell types and 70 subtypes according to our criteria. The types of amacrine cell were numbered consecutively; for the sake of greater clarity, we divided the types into a number of groups. In figure 41, the cells are assembled for a survey in the following order:

monostratified types with several subtypes: types 1–10
monostratified types in which we found only a single subtype: types 11–24
bi- to multistratified types: 25–31
diffuse types: narrow diffuse: 32–34
broad diffuse: 35–39
all diffuse: 40–43

Within these groups we arranged the cell types according to the size of their dendritic fields.

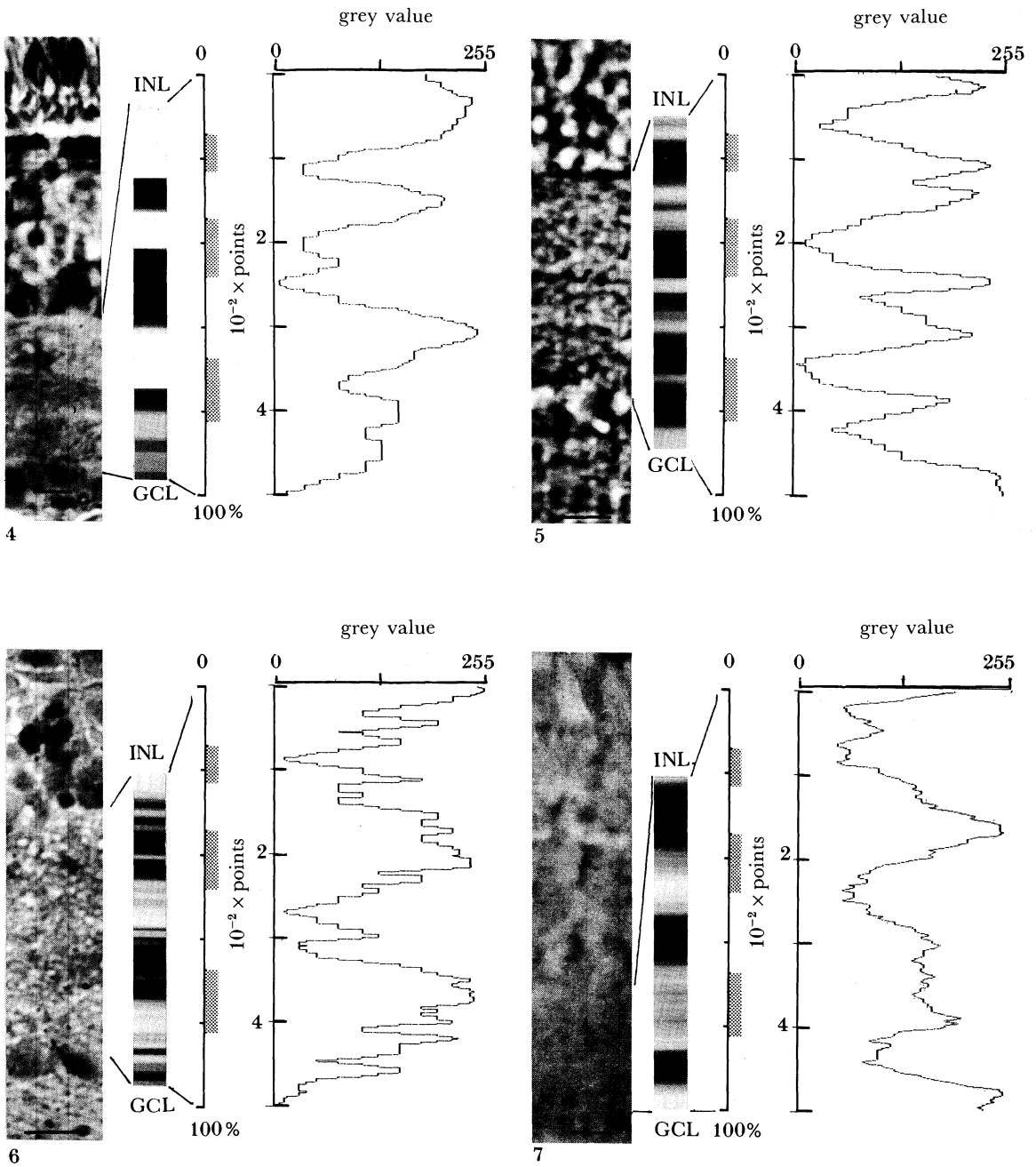

FIGURES 4–7. Densitometry of the inner plexiform layer in radial sections after various staining protocols. Each panel consists of a light micrograph of the inner plexiform layer (calibration bar 10 μm) which served as a basis for image analysis on the left; in the centre, the inner plexiform layer is shown after lowpass filtering and scaling of grey values; the densitometric scans through the processed images are shown on the right. Grey values are mapped from 0 (black) to 255 (white); the total width of the IPL is given as a percentage (0 indicates the outer border and 100 the border to the ganglion-cell bodies) and in a resolution of 500 points. (See text for details of the image analysis procedure.)

FIGURE 4. A 50 μm plastic section of Golgi-impregnated material in a region with no impregnated cells.

FIGURE 5. A 50 μm plastic section of control material after immunocytochemistry with the avidin–biotin–HRP visualizing system.

FIGURE 6. A 1 μm plastic section after staining with methylene blue.

FIGURE 7. A 5 μm cryostat section after incubation with rhodaminyl phalloidin for demonstration of F-actin.

(*Facing p.* 278)

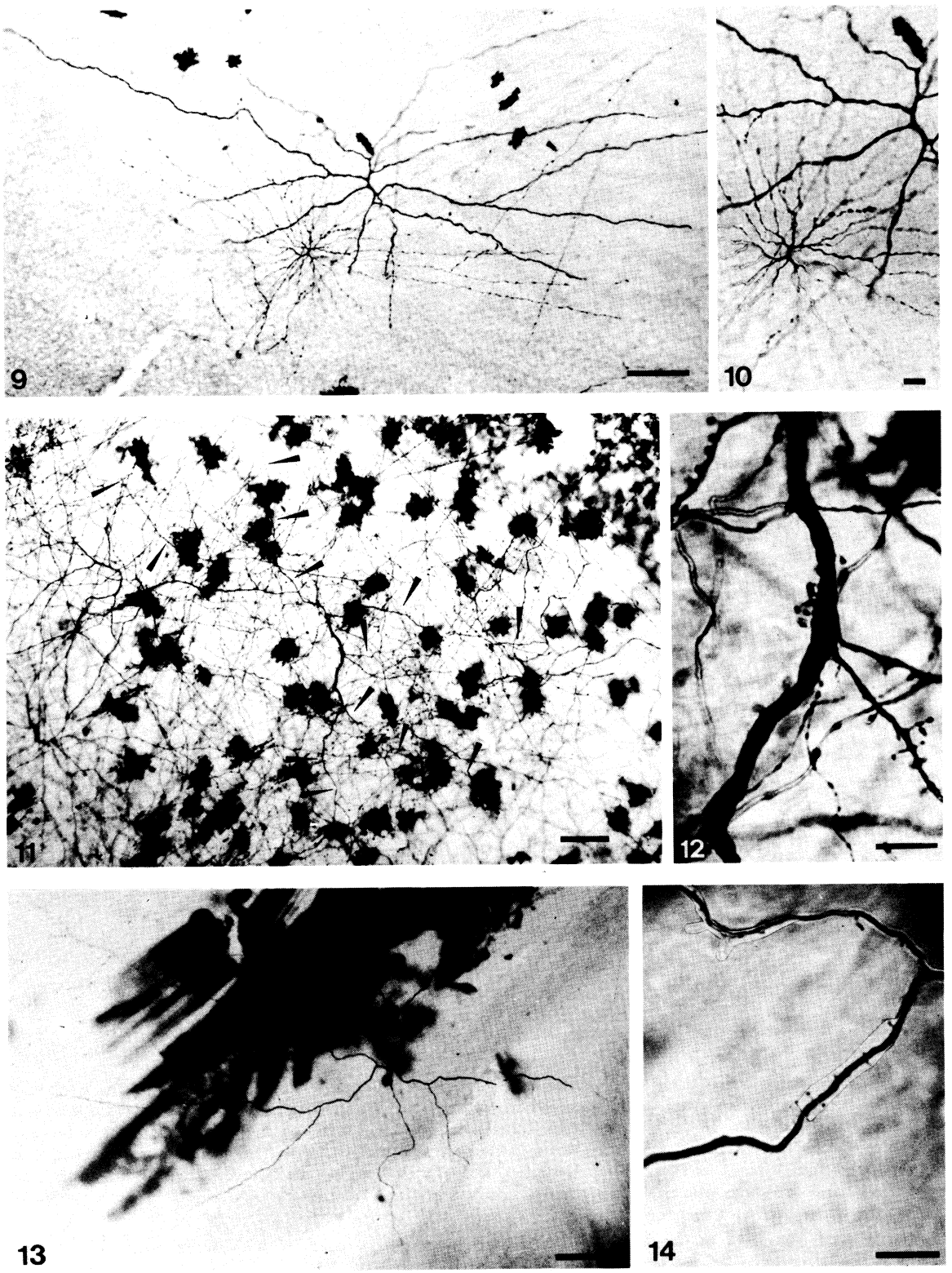

FIGURES 9–14. For description see facing plate 4.

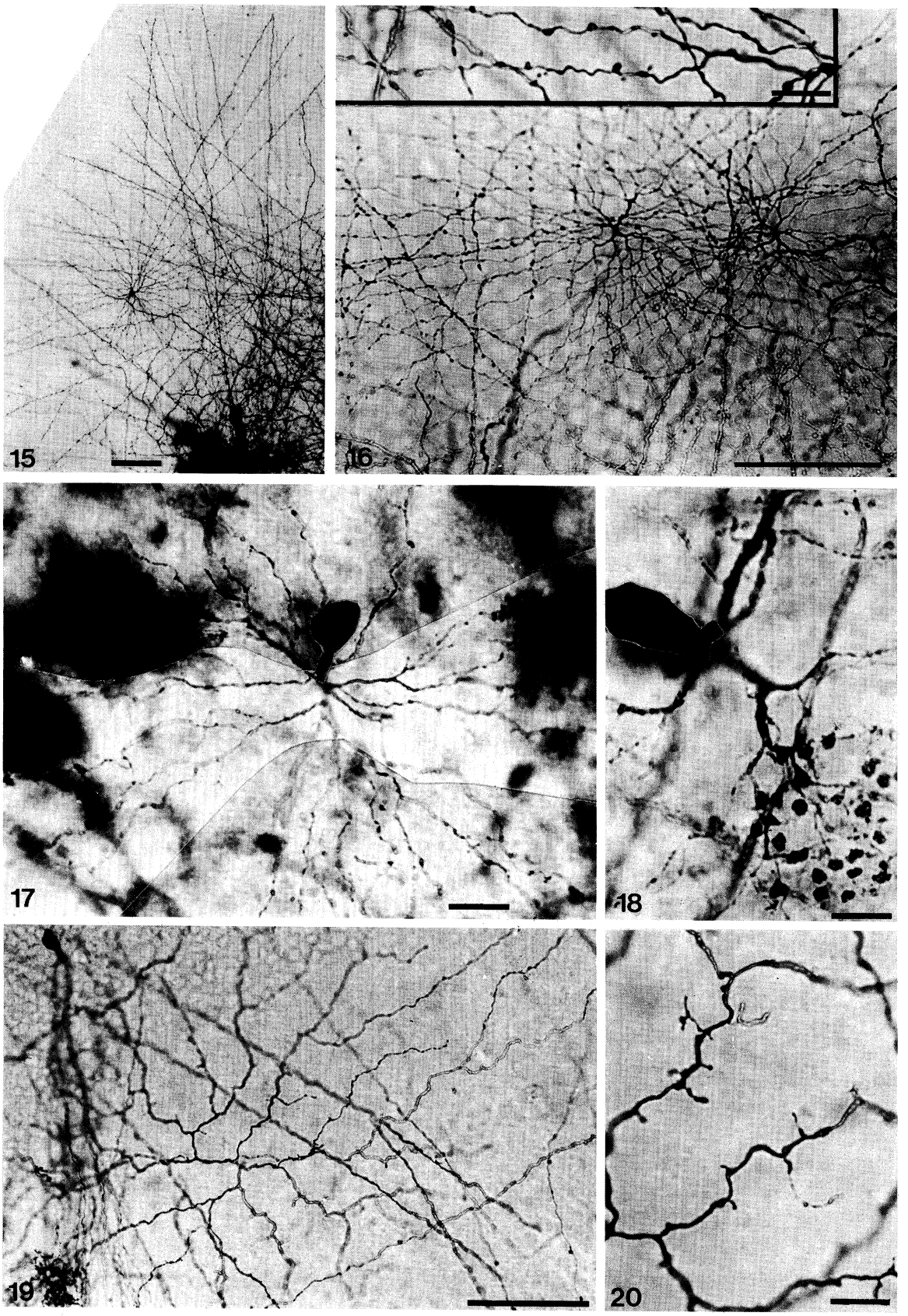

FIGURES 15–20. For description see facing plate 4.

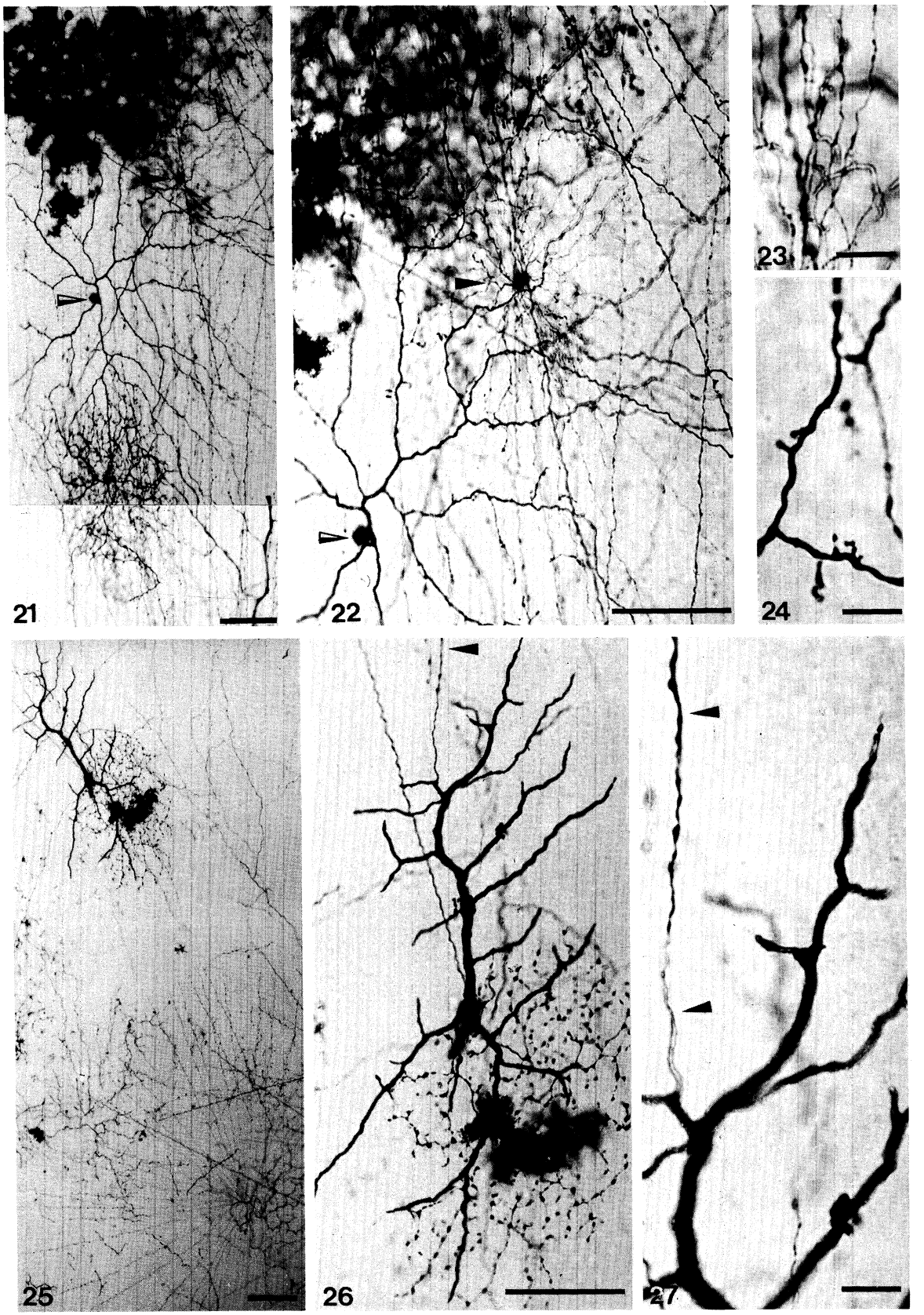

FIGURES 21–27. For description see opposite.

FIGURES 9–40. Light micrographs of amacrine cell types in 50 μm tangential sections. Calibration bars correspond to 50 μm in low-power views and 10 μm at high magnification.

DESCRIPTION OF PLATE 2

FIGURES 9 AND 10. Amacrine cell types 1 and 4; A1 is characterized by sparsely branched medium thick processes, whereas the A4 cell shows delicate processes with varicosities. The cell bodies are not included in this section; furthermore, some of the distal branches were found in neighbouring sections; therefore, the radial symmetry is not readily apparent.

FIGURES 11 AND 12. The dendrites of A2 cells are present among many Müller cells (dark, irregular dots) and are therefore marked by arrowheads. At high magnification (figure 12) numerous spines are observed on medium thick dendrites.

FIGURES 13 AND 14. Part of the A3 dendritic field is obscured by silver chromate crystals; it is polar-symmetric. Fine-structural details include numerous spines.

DESCRIPTION OF PLATE 3

FIGURES 15 AND 16. These specimens of A4 cells have their stem processes only 66 μm apart and are the most closely spaced of all A4 we have observed. Higher magnification (inset) shows that, in the distal parts, the dendrites bear numerous spines and varicosities.

FIGURE 17. The A9 cell has a uniformly radiate dendritic field; in contrast with A4 cells, varicosities are present also near the stem process.

FIGURE 18. Fine structure of an A13 cell showing the cluster of large, irregular varicosities in addition to delicate radiating dendrites.

FIGURES 19 AND 20. A42 (partly out of focus, on the left) and A11 with typical wavy dendrites including many spines and occasional varicosities.

DESCRIPTION OF PLATE 4

FIGURES 21–24. A1 (split arrows) and A15 (filled arrow) in addition to a ganglion-cell dendrite (unmarked in lower part). The A15 cell is characterized by a radial dendritic field, a peculiar, tortuous course of the delicate dendrites, many spinelike appendages and almost no varicosities (figure 23). By contrast, the fine structure of A1 cell dendrites (figure 24) shows medium-thick processes with occasional spines.

FIGURES 25–27. A26 (top) and A4 (bottom) in addition to ganglion-cell dendrites. Only one of the stratification levels of the A26 cell is included in this section; it demonstrates the thick dendrites with abrupt terminations and the beginning of a distal, 'd-type' dendrite (arrows).

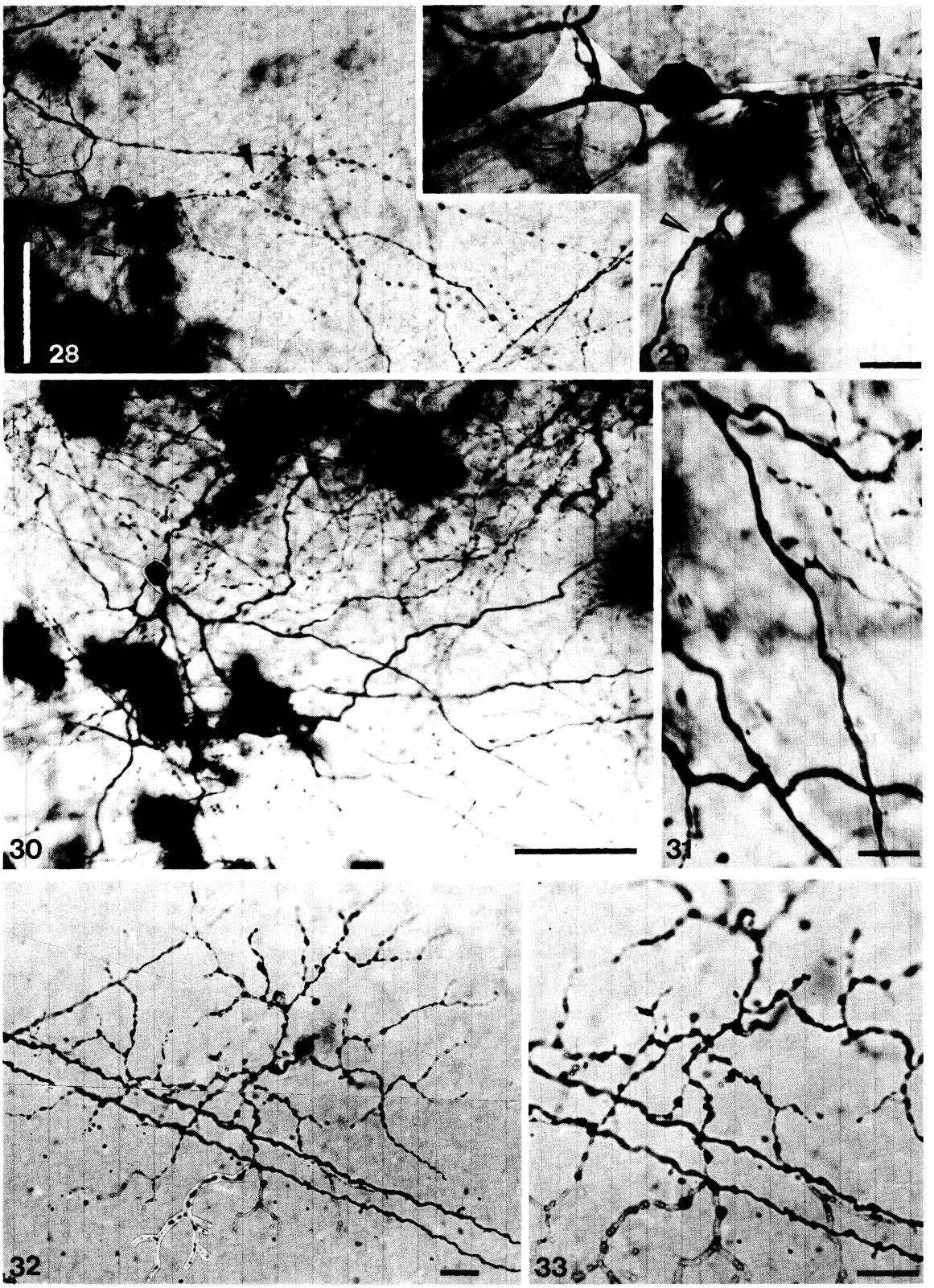

FIGURES 28–33. For description see opposite.

Description of plate 5

Figures 28 and 29. The A29 cell is characterized by a dendritic system with layer-specific differentiation. Filled arrows point to delicate, varicose processes in sublayer 2; split arrows mark medium-thick dendrites with irregular surface in sublayer 5.

Figures 30 and 31. A36 shows a slightly tortuous course of medium-thick dendrites. At higher magnification (figure 31), occasional spines and varicosities are seen.

Figures 32 and 33. Extensive branching of delicate dendrites and numerous small varicosities are typical of A37 cells.

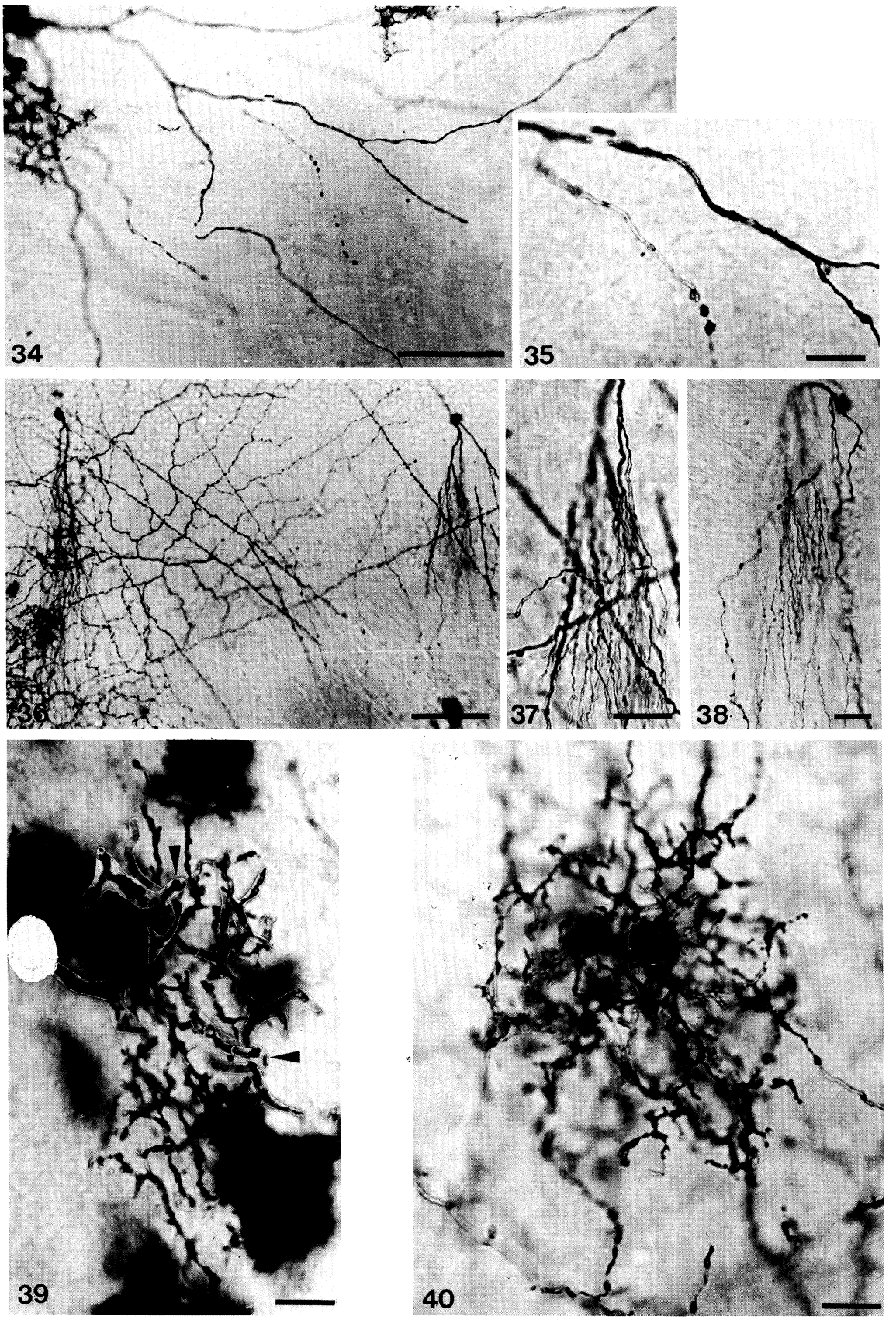

FIGURES 34–40. For description see opposite.

2.1. *Inventory*

Characteristic features of several cell types at low and medium magnification are shown in light micrographs as figures 9–40, plates 2–6. Furthermore, we have prepared, for each cell type, an identity (ID) chart which summarizes our quantitative and qualitative observations (see pp. 303–324).

2.1.1. *Stratified amacrine cells*

2.1.1.1. *Monostratified cells*

AC type 1 (A1). This widefield cell is characterized by medium thick processes, which become gradually thinner and show a few varicosities and occasional spines. It is sparsely branched with dendrites arranged essentially radially. We have observed subtypes in sublayers 1, 4, and 7 (figures 9, 10, 21, 22, and 24).

Amacrine cells with identical features have been described in the carp (Cajal 1894; Ammermüller & Weiler 1981), the bogue (Vallerga & Deplano 1984), and the catfish (Naka & Carraway 1975) as well as in the turtle (Kolb 1982), and mammals: cat (Kolb & Nelson 1981), rhesus monkey (Boycott & Dowling 1969) and man (Linberg *et al.* 1986). With such a wide distribution in the vertebrate retina, this cell type seems to be essential for retinal function. Electrophysiological studies in teleosts point to a sustained depolarization as typical light-evoked response (Murakami & Shimoda 1977; Chan & Naka 1976); hyperpolarizing responses have been recorded by Downing (1983). There are no indications as to the transmitter substance used by this cell type.

AC type 2 (A2). At first glance, this cell type is similar to the previous one, a widefield cell with medium thick tapering processes. With its overall bipolar symmetry there is no indication of a preferred orientation within the retina. The major difference is in the fine structure: in contrast with A1, there are numerous spines, most of which have distinct end-knobs and very rare varicosities (figures 11 and 12). A2 cells are found in sublayers 5 and 7; the subtype A2.5 had its perikaryon embedded in sublayer 4 and can thus be regarded as an interstitial cell.

Interspecific comparison shows an almost identical distribution to that of A1, with the exception of the rhesus monkey. For the cat, Freed *et al.* (1983) have shown that the corresponding types A19 and A20 have a rapid GABA uptake mechanism.

AC type 3 (A3). This is another sparsely branched, widefield amacrine cell with a more polar symmetry to its dendritic field. Again, it is the fine structure that distinguishes it from A1

DESCRIPTION OF PLATE 6

FIGURES 34 AND 35. The A41 cell has medium-thick, radiating processes in sublayer 2 with fine terminal branches bearing clusters of varicosities. Other fine processes leave sublayer 2 and continue (out of focus) in sublayer 7.

FIGURES 36–38. In low-power view, an A11 cell is seen flanked by two A42 cells. These diffuse cells are characterized by highly asymmetrical dendritic fields which are oriented parallelly. Their fine structure (figures 37 and 38) shows mostly unbranched dendrites with rare varicosities.

FIGURE 39. This small-field, diffuse A38 cell has most of its dendrite in sublayers 3 and 4; its perikaryon has been added in white. Its most striking features are two radial processes, which terminate with a discrete swelling in sublayer 7.

FIGURE 40. The 'cloud' of profusely branched diffuse processes belongs to an A43, a small-field cell with numerous varicosities.

and A2. In all specimens, even the proximal dendrites are thin, becoming delicate towards the periphery. Numerous spines are present all over the processes, whereas occasional varicosities occurred only in the distal parts (figures 13 and 14). Subtypes of A3 were present in sublayers 1, 5, 6, and 7.

Amacrine cells corresponding to A3 have been found in lower vertebrates: *Nannacara anomala* (cichlid) (Wagner 1973), carp (Ammermüller & Weiler 1981), catfish (Naka & Carraway 1975) and turtle (Kolb 1982). No information is available about their transmitter content and their physiology.

AC type 4 (A4). Widefield amacrine cells of this type are characterized by a uniformly radial symmetry and 28–33 delicate dendrites (figures 9, 10, 15, 16 and 25). From a primary stem dendrite arise 8–12 secondary processes, which branch once or twice close to their point of emergence; *ca.* 50 μm from this point the dendrites are unbranched. Their fine structure exhibits typical changes: initially they are *ca.* 0.3 μm thick and have smooth contours; after 250–300 μm their outline becomes irregular with numerous varicosities and spines (figure 16, inset). Type 4 cells are subdivided into two subtypes with stratification levels at sublayers 3 and 5.

A4 cells were the most common type in our Golgi preparations: in total, we found 51 specimens. For this reason we used this type to analyse the correlation between the maximal radius of their dendritic field and the distance from the optic nerve. Figure 2 indicates clearly that there is no systematic increase of the dendritic field size towards the ora serrata, the correlation coefficient being -0.144. In one case we observed a group of A4 cells in which the somata were situated closely together, with a minimal distance of 66 μm (figure 16). Although the statistical nature of the Golgi impregnation does not allow the evaluation of cell densities, we performed some calculations assuming that A4 cells are arranged in a square lattice of 66 μm distance. This results in a cell density of 255 A4 cells mm^{-2}. The mean area of dendritic field was determined by connecting the end points of the dendrites in six cells and found to be 0.674 mm^2 (s.d. ± 0.136). From these data a coverage factor of 151.6 can be calculated (according to Wässle *et al.* (1981)). Taking as effective zone for synaptic interactions only the parts of the dendrites comprising spines and varicosities, which constitute between 50 and 60 % of the total dendritic length (12.08 mm, s.d. ± 0.39; 55 % $\equiv$ 6.64 mm) the effective dendritic field overlap (Famiglietti 1985) amounts to a factor of 83.4.

A4 cells are commonly known as starburst amacrine cells. This descriptive term was introduced by Naka & Carraway (1975) for the catfish although similar cells had been previously observed in perch and carp (Cajal 1894), cichlids (Wagner 1973) and *Callionymus* (Vrabec 1966) and subsequently in the bogue (Vallerga & Deplano 1984), carp (Ammermüller & Weiler 1981) and turtle (Kolb 1982). In mammals, a kind of amacrine cell has been called 'starburst cell' by Famiglietti (1981) and Tauchi & Masland (1984); this is, however, not identical with our A4 cell. Major differences concern the size and size constancy: even large, peripheral starburst cells in the rabbit are half as wide as the average roach starburst cell. Furthermore, although the number of terminal branches is similar in both cases, branching points are distributed evenly over the entire length of the processes in mammals, whereas in fish, branching points are restricted to an area close (50 μm) to their origin from the stem process. This arrangement leads to a more homogeneous coverage of the dendritic field in the mammal starburst cell. Both mammal and roach starburst cells come in two subtypes, one for sublamina a and one for sublamina b; in mammals, these subtypes have a 'mirror

symmetric' arrangement (Famiglietti 1983*a*), with perikarya of 'type b' cells located in the GCL ('paramorphic pairs' (Kolb & Nelson 1981; Famiglietti 1983*b*)). By contrast, in fish, the cell bodies of both subtypes are situated in the INL. Compared with the morphometric data of roach starburst cells, rabbit starbursts have a total dendritic length of *ca.* 6 mm (at eccentricity $d = 8$) and a dendritic field area only 14% of the value found in the roach (Famiglietti 1985). On the other hand, their density is considerably higher and their dendritic overlap substantially lower in the rabbit than in the roach. It is possible that this is related to the differences in their branching pattern: in the roach the proximal branching leads to major gaps between individual dendrites in the periphery of the dendritic field, whereas in mammals the spacing of the processes is more homogeneous.

Finally, it is of interest to note some physiological and neurochemical properties of starburst cells. Masland & Tauchi (1986) have shown, by elegant double labelling experiments, that rabbit starburst cells contain acetylcholine, which is released maximally by flashing light stimuli driving both 'on' and 'off' cells alternatively. For the roach, direct evidence of such completeness is not available to date. Preliminary electrophysiological observations followed by intracellular HRP injection have shown A4.5 cells to respond with a sustained depolarization to the onset of a light flash (Downing 1983). In goldfish, Tumosa *et al.* (1984) have labelled two fibre plexi in sublayers 2 and 4 with anti-choline acetyltransferase, and Marc (1986) has reported two bands of radioactivity, after tritiated choline uptake, which were located at 33 and 57% of the IPL, respectively. These values correspond exactly to the stratification levels of the two subtypes of starburst cells in the roach, suggesting that in fish, too, A4 starburst cells may be cholinergic.

AC type 5 (A5). An asymmetrical dendritic field covering an angle of less than 150° is characteristic of this cell type. About ten medium thick, tapering dendrites are sparsely branched and carry large, irregular varicosities and numerous spines. There are two subtypes (A5.1 and A5.7) with stratification levels at the inner and outer border of the IPL.

Amacrine cells corresponding to our A5 have not, so far, been found in other retinae.

AC type 6 (A6). This cell type regularly occurs as an interstitial cell, the soma of which appears as a minor swelling in the same IPL sublayer as the dendrites. A6 cells appear to have a radial symmetry with, as a rule, 20 branches. These branches are remarkably thick and have smooth contours. Another regular feature is that their diameter is fairly constant, with rather abrupt terminations. At higher magnification one to three shorter branches of about 30 μm length continue as long, very delicate (0.2 μm) processes, which are very often lost in the tangle of other Golgi-impregnated dendrites. In the camera lucida drawing of the ID chart their full length is therefore underestimated. Most often these long branches run in opposite directions so that, in reality, A6 cells have a distinct bipolar symmetry. This type of interstitial cell occurs in two subtypes in the outer (A6.2) and inner (A6.5) part of the IPL.

In Golgi preparations, similar cells have been described in the carp by Cajal (1894) and in macaques by Boycott & Dowling (1969). With the refinement of intracellular recording and injection techniques A6 cells have been encountered more frequently, probably owing to the unusual calibre of their dendrites (Chan & Naka, 1976 (catfish); Murakami & Shimoda 1977 (carp); Sakai & Hashimoto 1983 (dace); Downing 1983 (roach)). In isolated HRP-injected cells the full extent of the two or three long delicate branches becomes especially apparent; they may occasionally give off other branches and reach lengths of more than 1 mm. In no case, however, was a morphologically distinct terminal apparent. Djamgoz *et al.* (1984) introduced

a terminological distinction between the thick and delicate processes of A6 cells, calling the thick ones proximal or p-type dendrites as opposed to the thin, distal or d-type dendrites. Analysing the orientation of the d-type dendrites, we found a clear preferential orientation orthogonal to the ganglion-cell axons. This orientation results in a ringlike arrangement of A6 cells around the optic nerve head. Similar observations have been made by Downing (1983).

Electrophysiological recordings have not yielded a uniform concept of A6 cell function. A6.5 cells had a light-evoked transient depolarization with a phasic component and signs of spectral selectivity (Sakai & Hashimoto 1983; Djamgoz *et al.* 1985), whereas most of the A6.2 cells showed sustained hyperpolarizations in accordance with the basic on–off subdivision of the IPL.

In ultrastructural studies of A6 cells, Zimmermann (1983) reported gap junctions occurring along the plasmalemma of p-type dendrites. This finding, which suggests electrotonic coupling, is supported by preliminary observations of extensive dye coupling among A6 cells after injection of fluorescent dyes (M. B. A. Djamgoz & H.-J. Wagner, unpublished).

AC type 7 (A7). In contrast to the previous type, A7 cells, which are also interstitial, are characterized by thick processes that become gradually thinner towards the periphery. In addition they bear small varicosities and occasional spines and are therefore not identical with d-type dendrites of A6 cells. Two main processes emerge in opposite directions from the soma. Together with the higher-order dendrites, A7 cells have a bipolar symmetry; as in A6 cells, their main orientation is at right angles to the optic fibres. The two subtypes observed stratify at sublayer 1 (A7.1) and sublayer 3 (A7.3).

Amacrine cells corresponding to our A7 cells have frequently been observed previously and described under various names in teleosts (Cajal 1894; Naka & Carraway 1975; Ammermüller & Weiler 1981) and mammals (West 1976). Their light-evoked membrane potential was either a sustained depolarization for a cell localized in sublamina a (carp (Teranishi *et al.* 1984)) or a transient on–off response (catfish (Chan & Naka 1976)). Extensive dye-coupling has been observed after intracellular injection of Lucifer Yellow, suggesting the presence of gap junctions (Teranishi *et al.* 1984).

AC type 8 (A8). This is another type with essentially bipolar symmetry, but on a smaller scale, as according to their largest radius these cells belong to the medium field type. The fine structure of the dendrites is irregular, comprising numerous spines and varicose swellings. The ramification levels of dendrites are linked by a stem process to the perikarya in the INL. Two subtypes have been observed: A8.4 and A8.6.

Only in teleosts have similar cell types been observed (bogue (Vallerga & Deplano 1984) and catfish (Naka & Carraway 1975)). Interestingly, owing to a different scheme of IPL subdivision in the bogue, two subtypes were discriminated, one between 20 and 40 % and the second between 40 and 60 %, which both correspond to our single A8.4 subtype occurring between 35 and 48 %. Correlation of immunocytochemistry and Golgi-impregnation indicates that A8 cells may contain somatostatin (Wagner & Zeutzius 1987).

AC type 9 (A9). Owing to their essentially radial symmetry and the straight course of their radiating dendrites (figure 17), this type has been included in starburst cells by some authors (Naka & Carraway 1975; Ammermüller & Weiler 1981). There are several features, however, that lead us to introduce a separate type for cells like A9. In the first place, there is a substantial difference in size, A9 cells ranging on the smaller side of medium-sized cells; furthermore,

branching occurs not only close to the stem process but up to 37 % of the total dendritic length; also, the course of the dendrites is more irregular, causing some of the branches to cross (which was never observed in A4 cells); finally, the numerous spines and occasional varicosities are distributed along the full length of the dendrites. Although all A9 cells observed had their level of stratification within sublayer 5 (A9.5), there were two groups of cells which had their dendrites separated by about 10 %, so that some cells had their processes at the inner and others at the outer border of sublayer 5.

AC type 10 (A10). This is another uniformly radiate cell of medium size. It differs from A9 cells in several aspects. Contrary to the previous type with continuously 'delicate' processes, the horizontal dendrites are 1–1.5 μm thick proximally, and become thinner (delicate) in the periphery. Furthermore, spines are the dominant feature, whereas varicosities are less frequent. Finally, branching points are found in the far periphery (75 % of maximal dendritic radius). A10 cells are present in sublayer 4 (A10.4) and 5 (A10.5). In the specimen recorded with the camera lucida, two of the secondary branches have been lost during thick sectioning so that the basic radial symmetry is not clearly apparent. A10-like cells have been observed in catfish (Naka & Carraway 1975) and in rat (Perry & Walker 1980).

The following monostratified cell types have been observed in a single sublayer only after Golgi impregnation. They are listed according to their dendritic field size.

AC type 11 (A11). A large dendritic field of radial symmetry and many branching points in the proximal half are characteristic of A11 cells (figures 19 and 20). Their dendrites show an irregular outline with a wavy course, including numerous spines and less frequent swellings. Their tortuous nature is also observed in the radial plane; this leads to a broad space (5 %) within sublayer 4 being occupied by A11 dendrites.

AC type 12 (A12). This incompletely recorded specimen was the only one of its type we found in Golgi preparations. However, another example of the same type was observed after HRP injection by M. B. A. Djamgoz & J. E. G. Downing (unpublished observation). A12 cells typically have only two or three secondary dendrites, which, however, are profusely branched with many lower-order processes branching at right angles. The medium thick proximal dendrites gradually taper and have 'delicate' terminals. Both varicosities and spines are frequent. The Golgi-impregnated cell had its ramification level at sublayer 5 (A12.5), whereas the HRP-stained cell stratified in sublayer 7 (A12.7).

Similar cells have previously been described in a cichlid species (Wagner 1973). The light-evoked response of the A12.7 cell was a sustained depolarization (M. B. A. Djamgoz & J. E. G. Downing, unpublished observation).

AC type 13 (A13). Starburst-like morphology is also typical of A13 cells. Unfortunately, its true size and the exact shape of the dendritic field could not be determined, because most of the very thin processes were lost *ca.* 150–200 μm from their origin. In contrast with A4 cells, four secondary processes, 50–70 μm long, emerge from the stem process and give off about 40 rather straight and unbranched dendrites. These have a diameter of 0.2–0.3 μm, which does not increase distally. Occasional short spines and small varicosities are found all along the dendrites. The most distinguishing feature of A13 cells is an accumulation of up to 20 prominent swellings in a small area of higher ramification at *ca.* 50 μm from the stem process (figure 18). This segregation of long straight dendrites and short processes with large irregular varicosities suggests a dual mode of information processing in this type of amacrine cell. A13 cells stratify in sublayer 5; in contrast with A4 cells they occupy the inner part at 65 %.

AC type 14 (A14). According to their radial symmetry, medium size, and ramification pattern, A14 cells come closest to mammal starburst cells (Famiglietti 1981; Tauchi & Masland 1985). They differ from rabbit starburst cells, however, in the distribution of varicosities and spines which, in our case, occur throughout the entire length of the dendrites. Interestingly, the fine structure of one particular dendrite differs from the remaining ones. Here, spines are much more frequent and the varicosities appear to have disappeared in a general increase of the dendritic diameter. One may speculate whether this reflects different functional states of individual processes.

The subtype of A14 cells observed in the roach stratifies in sublayer 2 (A14.2). A14-like cells have been previously described in cichlids (Wagner 1973) and macaques (Boycott & Dowling 1969).

AC type 15 (A15). The typical features of A15 cells are 35–40 radially orientated, delicate dendrites with a peculiar zigzag course (figures 21 and 22, arrowheads). In addition, there are many spine-like appendages lacking apical swellings, and almost no varicosities (figure 23). A15 cells have a radial symmetry and ramification points restricted to the proximal third of the dendritic field. They stratify in sublayer 4 (A15.4).

Cells corresponding to A15 have been observed in other cyprinids (Cajal 1894; Vallerga & Deplano 1984).

AC type 16 (A16). This cell type has a bipolar symmetry and is of intermediate size. As in A17 and A18, the orientation of the dendritic field is orthogonal to the optic nerve fibres. Its four main dendrites are medium thick and taper gradually from 3 to 1 μm. The characteristic features distinguishing A16 cells from the following two types are the thin dendritic terminals, occasional varicosities, and spines including terminal swellings. The only specimen observed had its stratification level in sublayer 2 (A16.2).

AC type 17 (A17). The bipolar symmetry of A17 cells is even more pronounced than in A16 cells, because the two primary dendrites leave the soma in opposite directions. They are of medium thickness and most of them do not become much thinner towards the periphery; they are virtually devoid of varicosities and bear few spines. We have observed a single specimen of A17 which ramifies in sublayer 1 (A17.1).

AC type 18 (A18). Contrary to the two previous types, A18 cells have thin and delicate dendrites; these bear numerous irregular varicosities and some spiny appendages. In Golgi preparations there was a single subtype in sublayer 1 (A18.1). After immunocytochemical staining and analysis of radial and tangential views, we found cells with identical morphological parameters with a positive reaction to anti-somatostatin (Wagner & Zeutzius 1987; see also Marshak *et al.* (1984) on goldfish).

AC type 19 (A19). This is another cell with an overall morphology reminiscent of starburst cells; it has been recognized as such by previous observers. It can, however, clearly be distinguished from 'true' A4 cells, as in this case we could trace all dendrites completely to their terminal so we are sure that A19 cells are of substantially smaller size and fall into the category of medium-field cells. Furthermore, there are numerous varicosities along the entire length of the dendrites; spines, on the other hand, are very rare. All six specimens observed had their level of stratification in sublayer 4 (A19.4).

Cells similar to A19 have been described only in teleosts (Cajal 1894; Wagner 1973; Naka & Carraway 1975; Ammermüller & Weiler 1981).

AC type 20 (A20). The asymmetrical, medium-field A20 cell is characterized by delicate,

slightly sinusoidal dendrites with many irregular varicosities and a few spines. Although secondary processes emerge close to the perikaryon, the main horizon of ramification is in sublayer 5 (A20.5).

AC type 21 (A21). Radial symmetry without strictly radiating processes is a typical feature of A21 cells. The irregularly branched dendrites are medium thick proximally and gradually taper towards the periphery. Swellings of various size and spiny appendages are found mostly on the terminal processes. We have observed a single subtype at 62% in sublayer 5 (A21.5). In the bogue, an A21-like cell has also been described (Vallerga & Deplano 1984).

AC type 22 (A22). This medium-size cell has an essentially circular dendritic field which is formed by three major, moderately branched dendrites. Important fine-structural features are the irregular process diameter with alternating thin and medium thick portions, varicosities and short delicate spines. Horizontal branches also stratify in sublayer 5 (A22.5).

A comparison with neurotensin-positive cells in roach after immunocytochemistry suggests that A22 cells contain this neuropeptide (Wagner & Zeutzius 1987). A similar cell which is also neurotensin-positive has been observed in turtle (Brecha *et al.* 1984).

AC type 23 (A23). The most prominent characteristic of this smallfield cell are the meandering, moderately branched processes. Fine structurally, the dendrites are less than 0.4 μm thick, with occasional small varicosities. We have observed a single specimen branching at 37% in sublayer 4 (A23.4).

AC type 24 (A24). This is among the smallest amacrine cells encountered in roach, its largest diameter being about 80 μm. The delicate dendrites are arranged radially and form a roughly circular dendritic field. Varicosities are absent and spines occur only rarely. The stratification level of A24 cells is in sublayer 5 (A24.5). Vallerga & Deplano (1984) have observed cells corresponding to A24 in the bogue.

2.1.1.2. *Amacrine cells with more than one level of stratification*

AC type 25 (A25). At two levels of the IPL, radiating dendrites originate from a radial stem process. In sublayer 2, the resulting dendritic field is asymmetrical, whereas in sublayer 5 it is more circular. The dendrites have a fairly irregular outline; their medium thick calibre decreases gradually distally. There are no varicosities but many spines. The perikaryon of our A25.2/5 cell is situated in the IPL and appears as a swelling in the outer part of the stem process.

AC type 26 (A26). The individual levels of stratification of A26 cells closely resemble those of A6 cells: a similar branching pattern, thick dendrites with abrupt terminations; occasional spines originating from these proximal dendrites; and two or three long, 'distal' dendrites (figures 25–27). The planes of stratification are linked by a stout radial stem process, which often contains the perikaryon. In one case, the radial process continued to link the dendrites to a cell body at the inner border of the INL. In Golgi preparations, we found bi- or tristratified cells with a constant dendritic plane in sublayer 5 and another one in either sublayer 1 or 2.

Golgi-impregnated A26 cells have been observed in catfish (Naka & Carraway 1975) and encountered several times after intracellular penetrations. In addition to the bistratified cells described above, specimens with four levels of stratification were observed; a constant feature is again the occurrence of dendrites in both the 'off' and the 'on'-space of the IPL. The light-evoked responses recorded of A26 cells are unusually diverse: Teranishi *et al.* (1984) observed on–off reactions; Sakai & Hashimoto (1983) reported both transient and sustained

components, whereas Chan & Naka (1976) and Downing (1983) described transient answers. It may be speculated that this divergence is caused by the micropipette's picking up local signals from a single dendritic level under certain stimulation conditions.

AC type 27 (A27). A mostly radial, medium-sized dendritic field with sparsely branched, tapering dendrites characterizes this type of amacrine cell. Fine structural details include irregular swellings and a general lack of spines. The two specimens of A27 cells observed both have three levels of stratification which, however, are only identical in sublayer 1 and differ more proximally. Furthermore, in one case (A27.1/3/7), there is only a single stem process, whereas in the other (A27.1/4/5), the inner sublayers are reached by four different secondary or tertiary dendrites.

A bistratified subtype with fine-structural detail and ramification pattern similar to A27 cells has been shown in the carp by Cajal (1894). Radial micrographs of immunostained material in turtles suggest that A27 cells may contain glucagon (Brecha *et al.* 1984). In the catfish, A27-like cells had transient responses (Chan & Naka 1976).

AC type 28 (A28). This is a bistratified version of the monostratified A7 cell. Two to four medium thick processes emerge from a perikaryon in the outer part of the IPL. In each sublayer the dendrites branch sparsely and taper gradually; in the outer stratification level in sublayer 2, there are two branches that descend to sublayer 4 where they form a second dendritic field of identical symmetry.

A28-like cells have been found in other teleosts (Naka & Carraway 1975; Ammermüller & Weiler 1981). Transient light-evoked responses have been recorded from similar Procion Yellow injected cells by Murakami & Shimoda (1977). Interestingly, in all cells the sublayers subserved are identical.

AC type 29 (A29). The distinguishing feature of A29 cells is a differential dendritic fine structure in the two sublayers occupied (figures 28 and 29). The dendrites in sublayer 2 are of medium thickness and have fairly smooth contours with occasional spiny appendages; in the periphery, however, where they have tapered to 'delicate' diameters, they bear numerous varicose swellings. By contrast, the two delicate branches that extend to sublayer 5 are devoid of such surface specializations.

In the catfish, A29-like cells give sustained depolarizing responses (Chan & Naka 1976).

AC type 30 (A30). Two primary processes emerge from the perikaryon of this cell type, each of which ramifies at different levels of the IPL. In sublayer 1, there is a long, sparsely branched dendrite. Remarkably, four short secondary processes originate from the long dendrite which extends proximally and distally without leaving sublayer 1. The other processes which reach sublayer 7 are more extensively branched. A regular feature of this part of the dendritic field is that one dendrite forms an ascending loop to sublayer 5 where it runs for a distance of *ca.* 100 μm before returning to the inner border of the IPL. No preferential orientation of this asymmetrical cell was observed.

AC type 31 (A31). Thick, short, and rarely branching processes with abrupt, medium thick terminations are characteristic of this cell type. In one case, a long d-type dendrite was observed. The soma is situated in the distal part of the IPL. The processes terminate in three different sublayers, which, however, are not identical in the two specimens recorded. A31 cells differ from A26 cells because their processes are shorter and have substantially less branching points.

A bistratified subtype corresponding to our A31 cell has been described in the carp by Cajal (1894).

2.1.2. *Diffuse amacrine cells*

AC type 32 (A32). This radially symmetrical cell bears some similarities to A14 in its branching pattern. There are, however, two major differences. (i) The proximal dendrites are of medium thickness and, in general, completely lack spines; in the distal part, some small varicosities are found. (ii) The dendrites are not restricted to a single sublayer. The proximal portion stratifies in sublayer 1; after about a third of their total length they bend 'downwards' and continue in sublayer 2.

AC type 33 (A33). In this cell, the radially orientated dendrites are characterized by numerous varicosities of quite irregular shape and size; they also bear occasional spines. The branching point of the stem processes is localized in the inner part of sublayer 5. Some processes extend at this level for their entire length; others leave this sublayer and terminate in sublayer 6. Ammermüller & Weiler (1981) have observed a cell with a similarly broadened level of stratification.

AC type 34 (A34). Radial symmetry of the medium-size dendritic field, and wavy processes with diameters of about 0.5 μm are typical of A34 cells. The dendrites show extensive branching and numerous varicose swellings of various sizes. Owing to their irregular course, the dendrites cover a radial sheet of 16%; this corresponds exactly to the extent of sublayer 5. In our specimen of A34 the perikaryon could not unequivocally be discriminated and was therefore added and drawn stippled.

AC type 35 (A35). This is a cell with three sparsely branched secondary dendrites originating from a stem process at the level of sublayer 4 where they extend laterally and give off occasional branches that reach vitread into sublayer 6. Fine-structurally, A35 dendrites are characterized by numerous large, irregular swellings.

AC type 36 (A36). The long axis of this large cell with a bipolar dendritic field extends mostly parallel to the orientation of ganglion cell axons (figures 30 and 31). The initially medium thick dendrites taper distally; they bear some spines and varicosities. Characteristically, the dendrites have a widely meandering course in the radial plane, covering a radial area of 23–34%. Two subtypes have been found in A36 cells, one in the 'off-space' (A36.1–4) and one in the 'on-space' (A36.5–6) of the IPL.

In the bogue, Vallerga & Deplano (1984) have observed a similar cell type.

AC type 37 (A37). A radially symmetric, small dendritic field, sometimes with a soma located eccentrically, characterizes A37 cells (figures 32 and 33). The delicate dendrites are extensively branched and show numerous large and small varicosities. In radial view, the diffuse dendritic field extends over 15–18%. We have observed two subtypes occupying either sublayers 2–3 or 5–6.

A37-like cells have not yet been described in teleost retinae; by contrast, in the turtle (Kolb 1982) and ground squirrel (West 1976) similar cell types do occur.

AC type 38 (A38). This type of amacrine cell has an elliptical dendritic field with a long tangential diameter of *ca.* 120 μm and a radial width of *ca.* 15% (figure 39). The dendrites that emerge from the stem process in the sublayers 3 and 4 have a very irregular course and fine structure; they are profusely branched. The most characteristic feature of A38 cells are two or three radial processes which originate from the main dendritic field and terminate with a discrete swelling near the ganglion cell bodies in sublayer 7. In none of the four specimens observed did those processes continue into the optic fibre layer; we could therefore exclude the

possibility that A38 were displaced ganglion cells. In the pigeon, a similar cell type has been found (A. P. Mariani, personal communication).

AC type 39 (A39). Two broad levels of meandering processes (sublayers 2–3 and 5–6) are characteristic of this cell type with a medium sized, radially organized dendritic field. Not all processes are restricted to either of the ramification levels; instead, even in the periphery there are radial dendrites connecting the two strata. The fine structure of A39 cells shows medium thick, tapering dendrites with small varicosities distally. A39-like cells have been studied in the cat; according to Freed *et al.* (1983) they take up tritiated GABA and have sustained depolarizing light-evoked responses (Kolb & Nelson 1981).

AC type 40 (A40). These are large, all-diffuse cells, the thin or delicate branches of which run through all sublayers of the IPL without any preferential distribution. A single, 'd-type' dendrite is orientated orthogonal to the ganglion-cell axons and is localized in sublayer 1. The processes are characterized by occasional long spinelike appendages and small varicosities.

Similar cells have been observed in carp (Cajal 1894).

AC type 41 (A41). This cell seems to consist of two different dendritic systems. There are medium thick radiating processes extending laterally in sublayer 2 with some fine terminal branches bearing clusters of varicosities. From these dendrites in the outer IPL originate numerous thin branches, which cross the IPL radially and terminate mostly in sublayer 7 where they continue tangentially, give off occasional branches and form irregular varicosities (figures 34 and 35).

A41-like cells have previously been described in carp (Cajal 1894); cichlids (Wagner 1973); and turtle (Kolb 1982). Furthermore, Weiler & Marchiafava (1981) recorded sustained depolarizing responses from these cells in turtles.

AC type 42 (A42). These striking cells are frequently encountered in Golgi preparations both in our material and in previous studies of teleosts (Cajal 1894; Wagner 1973; Ammermüller & Weiler 1981; Vallerga & Deplano 1984). A42 cells are characterized by a very asymmetrical dendritic field which covers only 20–35% in tangential view with a maximal dendritic radius of about 600 μm (figures 36–38). There are two stem processes that give off long delicate processes, which are virtually unbranched and only rarely bear varicosities. We have observed a number of subtypes that share this general appearance in tangential view but differ in their radial distribution of dendrites (figure 8*a*, *b*). Two subtypes with broad diffuse dendritic fields covered 33–39% of the IPL and were essentially restricted to either the 'off-space' (A42.1–4) or the 'on-space' (A42.4–7). The orientation of these cells with respect to the ganglion cell axons (0°) was roughly orthogonal (55–95°). Two other subtypes had their dendrites organized across the 'on–off' border, one being broad-diffuse (A42.3–5), and the other all-diffuse (A42.1–7). By contrast to the former the dendritic field of these subtypes was mostly parallel to the optic fibres (160–190°) with the dendrites always pointing away from the optic papilla.

AC type 43 (A43). This is another cell type which is often stained in Golgi material. It has been described in almost every retina studied: carp (Cajal 1894; Ammermüller & Weiler 1981); cichlid (Wagner 1973); bogue (Vallerga & Deplano 1984); turtle (Kolb 1982); rat (Perry & Walker 1980); ground squirrel (West 1976); cat (Kolb & Nelson 1981); and man (Linberg *et al.* 1986). Its processes are profusely branched, have a narrow winding course, and bear many small varicosities (figure 40). The overall impression of the A43 dendritic field is that of a dense cloud of branches and terminals filling a cylindrical 'cartridge' of the IPL. In our

TABLE 3. SUMMARY OF MORPHOLOGICAL CRITERIA USED FOR THE CLASSIFICATION OF AMACRINE CELL TYPES

(Broad vertical bars indicate the radial extension of diffuse cells; in stratified cells with more than one level of stratification, the positions of the individual dendritic systems are indicated by crosses connected by thin vertical lines.)

	1	2	3	4	5	6	7	8	9	10	11	12	13	14	15	16	17	18	19	20	21	22	23	24	25	26	27	28	29	30	31	32	33	34	35	36	37	38	39	40	41	42	43
fine structure																																											
diameter of primary dendrite																																											
thick (4–7 μm)	.	.	.	.	.	+	.	.	.	.	.	.	.	.	.	.	.	.	.	.	.	.	.	.	.	+	.	.	.	.	+	.	.	.	.	.	.	.	.	.	.	.	.
medium thick (2–3 μm)	+	+	.	.	+	.	+	.	.	.	.	+	.	.	.	+	+	.	.	.	+	.	.	.	+	.	+	+	+	+	.	+	+	.	+	+	.	+	+	+	+	+	.
thin (1–1.5 μm)	.	.	+	.	.	.	.	+	.	+	+	.	+	+	.	.	.	+	.	.	.	+	.	.	.	.	.	.	.	.	.	.	.	.	.	.	+	.	.	.	.	.	.
delicate (<0.5 μm)	.	.	.	+	.	.	.	.	+	.	.	.	.	.	+	.	.	.	+	+	.	.	+	+	.	.	.	.	.	.	.	.	.	+	.	.	.	.	.	.	.	.	+
diameter of terminal dendrite																																										
medium thick (2–3 μm)	.	.	.	.	.	+	.	.	.	.	.	.	.	.	.	.	+	.	.	.	.	.	.	.	.	+	.	.	.	.	+	.	.	.	.	.	.	.	.	.	.	.	.
thin (1–1.5 μm)	.	+	+	+	.	.	.	.	.	.	+	.	.	.	.	+	.	.	.	.	+	.	.	.	+	.	+	.	.	+	.	.	.	.	.	.	.	+	+	.	.	.	.
delicate (<0.5 μm)	+	.	+	+	+	+	+	+	+	+	.	+	+	+	+	.	.	+	+	+	.	+	+	+	.	+	+	+	+	+	+	+	+	+	+	+	+	.	+	+	+	+	+
varicosities																																										
many	+	.	.	+	+	.	.	.	+	.	.	+	+	+	.	.	.	+	+	+	+	+	+	.	.	.	.	.	+	.	.	+	+	+	+	+	+	+	+	.	+	.	+
few	.	+	+	.	.	+	+	+	.	+	+	.	.	.	+	+	+	.	.	.	.	.	.	+	+	+	+	+	.	+	+	.	+	.	.	.	.	.	.	+	.	+	.
spines																																										
many	.	+	+	+	.	.	.	+	.	+	+	+	.	.	+	.	.	.	.	.	+	.	+	.	+	.	.	.	.	.	.	.	.	+	.	.	+	+	.	.	.	.	+
few	+	.	.	.	+	+	+	.	+	.	.	.	+	+	.	+	+	+	+	+	.	+	.	+	.	+	+	+	+	+	+	+	+	.	+	+	+	.	+	+	+	+	.
location of soma																																										
INL	+	+	+	+	+	.	.	+	+	+	+	+	+	+	+	+	+	+	+	+	+	+	+	+	+	.	+	+	+	+	.	+	+	+	+	+	+	+	+	+	+	+	+
IPL	.	.	.	.	.	+	+	.	.	.	.	.	.	.	.	.	.	.	.	.	.	.	.	.	.	+	.	.	.	.	+	.	.	.	.	.	.	.	.	.	.	.	.
dendritic field pattern																																										
degree of ramification																																										
high	.	.	.	+	.	.	.	.	+	.	+	+	+	+	+	.	.	.	+	.	+	.	.	+	+	+	.	+	.	.	.	+	+	+	.	+	+	+	+	+	+	+	+
low	+	+	+	.	+	+	+	+	.	+	.	.	.	.	.	+	+	+	.	+	.	+	+	.	.	.	+	.	+	.	+	+	.	.	+	.	.	.	.	.	.	.	.
orientation																																										
radial	+	.	+	+	.	.	.	.	+	+	+	+	+	+	+	.	.	.	+	.	+	+	+	+	.	.	+	.	.	.	.	.	+	+	.	+	+	.	.	.	.	.	+
polar	.	+	.	.	.	+	+	+	.	.	.	.	.	.	.	+	+	+	.	+	.	.	.	.	.	+	.	+	+	+	+	+	.	.	+	.	.	.	.	.	.	.	.
asymmetrical	.	.	.	.	+	.	.	.	.	.	.	.	.	.	.	.	.	.	.	.	.	.	.	.	+	.	.	.	.	.	.	.	.	.	.	.	.	+	+	+	+	+	.
radius																																										
wide (>450 μm)	+	+	.	+	.	.	.	.	.	.	+	.	.	.	.	.	.	.	.	.	.	.	.	.	+	+	.	.	.	.	.	.	.	.	.	+	.	.	+	+	+	+	.
medium (100–450 μm)	.	.	+	.	+	+	+	+	.	+	.	+	+	+	+	+	+	+	+	+	+	+	.	.	.	.	+	+	+	+	+	+	+	+	+	.	.	.	.	.	.	.	.
small (<100 μm)	.	.	.	.	.	.	.	.	+	.	.	.	.	.	.	.	.	.	.	.	.	.	+	+	.	.	.	.	.	.	.	.	.	.	.	.	+	+	.	.	.	.	+
sublayers (radial distribution of dendrites in IPL sublayers)																																										
1	+	.	+	.	+	.	+	.	.	.	.	.	.	.	.	.	+	+	.	.	.	.	.	.	.	+	+	.	.	+	.	+	.	.	.	.	.	.	.	.	.	.	.
2	.	.	.	.	.	+	.	.	.	.	.	.	.	+	.	+	.	.	.	.	.	.	.	.	+	+	+	+	.	.	.	.	.	.	.	.	.	.	.	.	.	.	.
3	.	.	.	+	.	.	+	.	.	.	.	.	.	.	.	.	.	.	.	.	.	.	.	.	.	+	+	+	+	+	+	.	.	.	.	.	.	.	.	.	.	.	.
4	+	.	.	.	.	.	.	+	.	+	+	.	.	.	+	.	.	.	+	.	.	.	+	.	.	+	+	+	+	+	+	.	.	.	.	.	.	.	.	.	.	.	.
5	.	+	.	+	.	+	.	.	+	+	.	+	+	.	.	.	.	.	.	+	+	+	.	+	+	+	+	+	+	+	+	.	.	.	.	.	.	.	.	.	.	.	.
6	.	.	.	.	.	.	.	+	.	.	.	.	.	.	.	.	.	.	.	.	.	.	.	.	.	+	+	+	+	+	+	.	.	.	.	.	.	.	.	.	.	.	.
7	+	+	+	.	+	.	.	.	.	.	.	+	.	.	.	.	.	.	.	.	.	.	.	.	.	.	+	+	+	+	+	.	.	.	.	.	.	+	.	.	.	.	.

TABLE 4. SYNOPSIS OF AMACRINE CELL TYPES IN ROACH AND IN OTHER SPECIES

species...	roach (*Rutilus rutilus*)	perch (*Box salpa*)	carp (*Cyprinus carpio*)	bogue (*Boops boops*)	*Nannacara anomala*	carp (*Cyprinus carpio*)	catfish (*Ictalurus punctatus*)	turtle (*Pseudemys scripta elegans*)	rat	ground squirrel (*Citellus m.*)	cat	rhesus (*Macaca mulatta*)	man (*Homo sapiens*)
reference...	own observations	Cajal (1894)	Cajal (1894)	Vallerga & Deplano (1984)	Wagner (1973)	Ammermüller & Weiler (1981)	Nara & Carraway (1975)	Kolb (1982)	Perry & Walker (1980)	West (1976)	Kolb & Nelson (1981)	Boycott & Dowling (1969)	Linberg *et al.* (1986)
no. of types...	43	14	5	10	5	3	27	9	5	22	8	19
focus...	t/r	tang.	radial	t/r	r	t/r	t	t/r	t	r	t/r		t/r
	1	—	giant 5th level	1WC	—	radiate	starburst asymmetr. (fig. 5*c*)	A18, A22	—	—	A20, A21	Sa1	A20 (cat)
	2	—	giant 4th level large 5th level	5WC	—	radiate	starburst asymmetr. (fig. 5*d*)	A19, A20	—	—	A19, A22	—	A19 (cat)
	3	—	—	—	i	radiate	starburst symmetr. (fig. 5*b*)	A25, A26	—	—	—	—	—
	4	larger polygonal stratified cell 2nd level	larger polygonal stratified cell 2nd level	4WR	k	starburst A	—	A23, (A24)	—	A2	—	—	—
	5	—	—	—	—	—	—	—	—	—	—	—	—
	6	—	cell of the IPL	—	—	—	—	—	—	—	—	intra-plexiform cell	...
	7	—	hemi-spherical strat. cell 1st level	—	—	spindle-shaped soma	spaghetti (fig. 6 e–h)	—	—	A5	—	—	—
	8	—	—	2MV, 3MV	—	—	starburst asymmetr. (fig. 5*d*)	—	—	—	—	—	—
	9	—	—	—	—	starburst A	starburst symmetr. (fig. 5*a*)	—	—	—	—	—	—
	10	—	—	—	—	—	starburst symmetr. (fig. 5*b*)	—	narrowfield unistratified type b	—	—	—	—

11	—	—	—	j	—	—	—	—	—	—	—	—	
12	—	—	—	j	—	—	—	—	—	—	—	—	
13	—	—	—	(k)	—	—	—	—	—	—	—	—	
14	—	—	—	j	—	—	—	—	—	—	Sa2	—	
15	—	small 3rd level	INC	—	—	—	—	—	—	—	—	—	
16	—	—	—	—	—	—	—	—	—	—	—	—	
17	—	—	—	—	—	—	—	—	—	—	—	—	
18	—	—	—	—	—	—	—	—	—	—	—	—	
19	—	small 3rd level	—	(k)	starburst A	starburst (fig. 5*a*)	—	—	—	—	—	—	
20	—	—	—	j		—	—	—	—	—	—	—	
21	—	—	3SC	j	—	—	—	—	—	—	—	—	
22	—	—	—	j	—	—	—	—	—	—	—	—	
23	—	—	—	—	—	—	A3	—	—	—	—	—	
24	—	—	5SV	—	—	—	—	—	—	—	—	—	
25	—	—	—	n	—	—	—	—	—	—	—	—	
26	—	—	—	n	—	spindle	—	—	—	—	—	—	
27	—	bistratified	—	—	—	—	—	—	—	—	—	—	
28	—	—	—	—	spindle-shaped soma	spindle	—	—	—	—	—	—	
29	—	—	—	—	—	—	—	—	—	—	—	—	
30	—	—	—	—	—	—	—	—	—	—	—	—	
31	—	bistratified cell of the IPL	—	n	—	—	—	—	—	—	—	—	
32	—	—	—	—	—	—	—	—	—	—	—	—	
33	—	—	—	—	radiate	—	—	—	—	—	—	—	
34	—	—	—	—	—	—	—	—	—	—	—	—	
35	—	—	—	—	—	—	—	—	—	—	—	—	
36	—	—	45WT	—	—	—	—	—	—	—	—	—	
37	—	—	—	—	—	—	A2	—	(A3)	—	—	—	
38	—	—	—	—	—	—	—	—	—	—	—	—	
39	—	—	—	—	—	—	—	—	—	—	—	—	
40	—	multipolar diffuse	—	—	—	—	—	—	—	—	—	—	
		multipolar 5th level	—	—	—	—	—	—	—	—	—	—	
41	—	multipolar 5th level	—	q	—	—	A15	—	—	—	—	—	
42	—	diffuse	AWB	m	—	—	—	—	—	—	—	—	
43	—	pyriform diffuse	DNB	p, r	small diffuse	—	A4, A6, A10	diffuse A1	A13	—	—	A13 (cat)	

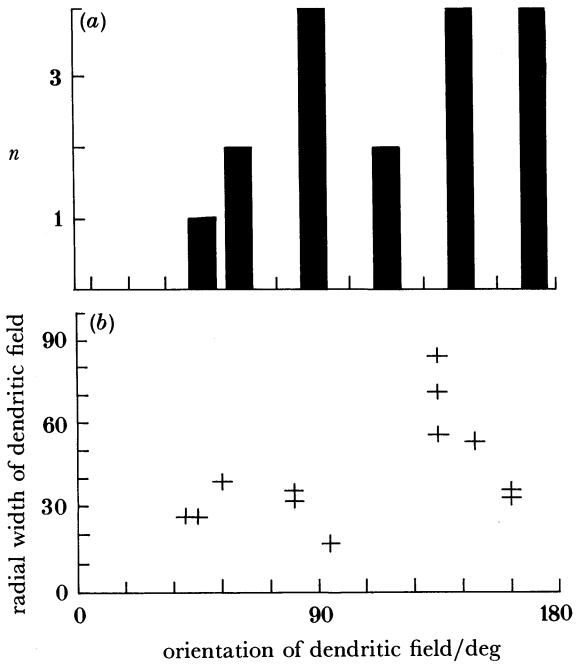

FIGURE 8. Analysis of dendritic-field orientation of various subtypes of A42 cells. Frequency distribution of main dendritic-field axis orientation with respect to the direction of optic nerve fibres (0°). One group of cells extends its dendritic field parallel to these axons; a second group is at right angles and a third one runs the dendrites obliquely to the ganglion-cell axons. (*b*) Correlation between the dendritic-field orientation and the width of radial extension. Two groups of cells are clearly distinguished: broad-diffuse cells orient their dendrites roughly at right angles, and all-diffuse cells have their dendrites almost parallel to the direction of ganglion-cell axons.

material, we could distinguish two different subtypes: A43.1–7 is a typical all-diffuse cell extending through the entire IPL, whereas A43.5–6 cells have their dendritic field restricted to the inner half of the IPL.

In the cat, this type of diffuse cell has been found to accumulate [^{3}H]GABA (Freed *et al.* 1983); its light-evoked response is a sustained hyperpolarization (Kolb & Nelson 1981).

In addition to the presentation of the individual cell types in ID charts, we have assembled the various features of each type in table 3. Table 4 summarizes the comparison of the amacrine cell types according to our classification with amacrine cells identified previously in different species.

DISCUSSION

3. *Aspects of basic amacrine-cell function*

Within the basic network of the IPL, amacrine cells provide elements for modifying the transmission from bipolar terminals to ganglion-cell dendrites by establishing radially and horizontally orientated local circuits. Thus, they contribute to shaping the geometrical and dynamic properties of ganglion-cell receptive fields. Understanding of their specific functions is fairly vague and is in sharp contrast to the amount of information available concerning their morphology, transmitter content and light-evoked membrane-potential changes. From the few successful studies in which electrophysiology was correlated with a structural analysis emerged such divergent properties as selectively coding for movement and direction information (catfish

(Naka 1980)), involvement in the formation of the receptive field of off-centre beta cells (cat (Kolb & Nelson 1984)), local adaptation effects of rod bipolar cells (cat (Kolb & Nelson 1984)), and serving as interneurons for the rod on-centre pathway (cat (Kolb & Nelson 1984)). It therefore appears difficult to propose a homogeneous function for this class of retinal neuron.

To judge from their synaptology, amacrine cells are capable of functioning at three different levels.

(i) Gap junctions between amacrine cell dendrites (Dowling 1979) provide lateral pathways and can create multicellular aggregates with coupled membrane potential. Transcellular transport of intracellularly injected dyes has been shown to link identical types of amacrine cell (homologous coupling) (Naka & Christensen 1981; Zimmermann 1983; Teranishi *et al.* 1984). In this way, functional effects similar to those at horizontal cells in the outer plexiform layer can be achieved (for review, see Djamgoz & Wagner (1987)).

(ii) Individual amacrine cells may act as functional entities. Their intricate patterns of chemical synapses, involving single pre- and postsynapses, serial and reciprocal synapses, imply that the nature of the amacrine dendritic field determines at the same time the 'view of the world' and its 'field of action' (Palay & Chan-Palay 1975). Electrophysiological recordings have clearly shown a correlation between the radial extent of the dendritic field and the time course and duration of the light evoked responses (Marchiafava & Weiler 1982).

(iii) Electro-anatomical modelling of rabbit starburst cells (Bloomfield & Miller 1982) has revealed that the function of amacrine cells as cellular units is supplemented by a mode of action where isolated parts of the dendritic field act as functional units creating multiple independent microcircuits. Dendritic varicosities in cat amacrine cells comprise both pre- and postsynaptic elements (Elias & Stevens 1980) and thus constitute examples of individual input–output systems with intervaricose segments allowing passive current spread along limited dendritic segments but only to a negligible degree into inactive branches. Miller (1979) proposed that activation of the entire dendritic tree may only be achieved by stimulation involving somatic spikes and that in the subthreshold mode portions of the dendritic tree may function independently of each other. Especially from the two last modes of action it is evident that any attempt to categorize amacrine cells on morphological criteria must take into account both 'gross-anatomical' features, such as size and shape of the dendritic field in the tangential plane, and fine-structural elements like dendritic calibre and the occurrence of varicosities and spines. The third major key parameter is then the radial position and extent of the dendritic tree within the IPL.

4. *Evaluation of parameters for classification*

4.1. *Functional relevance*

The criteria used in the present study have also been applied by previous investigators; however, often only a limited combination of parameters has been examined, and attempts towards quantification have been even more rare. The size of amacrine dendritic fields can be correlated with the size of their receptive fields (Kolb & Nelson 1981). Together with the radial distribution of processes, dendritic field size is the most widely used feature (Cajal 1893; Boycott & Dowling 1969; West 1976; Perry & Walker 1980; Kolb *et al.* 1981; Kolb 1982; Vallerga & Deplano 1984; Ammermüller & Weiler 1981). Naka (1980) presented

physiological evidence that direction-selective responses could be recorded from amacrine cells with asymmetrical or polarly organized dendritic fields; on morphological grounds, similar implications have been made by Ammermüller & Weiler (1981), Mariani (1982) and Vallerga & Deplano (1984). Because inhibitory synapses are preferentially localized near branching points (Koch *et al.* 1982) the pattern and, more important, the frequency of ramification may be correlated with the density of synapses impinging on a given dendritic field. Wagner (1973), Naka & Carraway (1975), West (1976) and Kolb (1982) have also used this criterion.

As regards fine structure, it is obvious that the diameter of a dendrite or an intervaricose segment determines the velocity of signal propagation (Rall 1962). Consequently, West (1976), Kolb *et al.* (1981), Kolb (1982) and Vallerga & Deplano (1984) have adopted this criterion for their classifications. Furthermore, the occurrence of varicosities, which have been recognized as specialized elements of synaptic input and output (Ellias & Stevens 1980), or as accumulations of mitochondria (Weiler & Zettler 1979), and of spines, which constitute elaborate postsynapses with high-resistance coupling to the main dendrite (Coss & Perkel 1985) has been taken into account in more recent analyses of retinal-cell morphology (Naka & Carraway 1975; Kolb *et al.* 1981; Kolb 1982; Vallerga & Deplano 1984; Vallerga & Ratto 1985).

By contrast, the importance of the radial aspect of dendritic arborization for defining types of retinal cells has been realized long before the functional characterization of sublamina a and b as off- and on-'spaces' had been introduced by Famiglietti & Kolb (1976) (Cajal 1894; Boycott & Dowling 1969; Wagner 1973; West 1976). At present, the precise localization of the stratification within the IPL is attempted in every study dealing with structure and function of neural elements of the inner retina (for review, see Djamgoz & Wagner (1987)).

4.2. *Validity in view of morphological plasticity*

Another essential prerequisite for the validity of our classification approach is the stability and reproducibility of the parameters used. This, in turn, is related to methodological and biological properties of our preparations.

Biological stability implies that neither the overall structure and differentiation nor the detailed morphology of the dendritic field is subject to changes due to development or adaptive modification in response to different functional states. Also, the regional position within the retina should ideally be without major influence on the morphology of the cell.

Teleost retinae are characterized by continual growth, which is manifest to a minor degree throughout the fundus and more pronounced in the periphery (Scholes 1976; Johns 1977; Johns & Easter 1977). This entails a continuous remodelling of the connectivity, as has been demonstrated in the goldfish for b1 bipolar cells (Kock & Stell 1985) and for ganglion cells (Macy & Easter 1981; Kock 1982*a*, *b*). Modification of dendritic fields, which was observed in these cases over a period of several years, can also occur over a shorter time span (e.g. three months) as regular events in superior cervical ganglion cells of adult mice (Purves *et al.* 1986). Fine-structural adaptation to increased stimulation has been widely observed in spines. Marked enlargement of spine heads has been found, after only nine minutes of induced escape behaviour, in tectal interneurons of jewel fish (Burgess & Coss 1980). In the cone pedicles of teleosts, horizontal cell terminals expand their surface by 25–30% by growing numerous 'spinules' within 30 min after the onset of illumination; at dusk, these structures disappear within the same period (Wagner 1980). Similar structural changes in the IPL have not yet been reported; however, in view of the above examples it can by no means be taken for granted that

the morphology of amacrine cells is static. For this reason, we have based our observations on specimens of roughly equal body and eye size; furthermore, we included only cells whose perikarya were closer than 0.5 mm to the periphery. To provide a homogeneous functional state, preparation took place under identical conditions after at least two hours of dark-adaptation and shortly before noon.

The absolute size of the dendritic field cannot, *a priori*, be taken as a significant feature of a given amacrine type. In the cat's AII cells and rabbit 'starburst' cells the diameter of dendritic fields is twice as high in the periphery as in the centre (Kolb *et al.* 1981; Tauchi & Masland 1984). For α (Y) and β (X) ganglion cells in the cat the difference is even more striking (a factor of 100 (Boycott & Wässle 1974)). These differences are obviously related to differences in ganglion cell density and to the differentiation of an area centralis in these mammals. In species with a more homogeneous distribution of ganglion cells and photoreceptors (rat (Perry & Walker 1980), bogue (Vallerga & Deplano 1984) and carp (Ammermüller & Weiler 1981)) no correlation of dendritic-field size and eccentricity has been observed; this is in good agreement with our evaluation of A4 starburst cell sizes in various locations of the roach retina.

4.3. *Reliability of staining methods*

On the methodological side, the rapid Golgi impregnation is certainly far from being a well-controlled, reproducible tool for visualizing nerve cells. Along with microinjection techniques it has the essential advantage of staining only individual cells, which can then be analysed with all their processes. Two major drawbacks must, however, be mentioned in the present context.

First, doubts have been raised as to the completeness of the silver chromate filling (Perry & Walker 1980; Kolb 1982). Intracellular injections with HRP or, especially, Lucifer Yellow have resulted in a more reliable staining of terminal branches or very delicate processes (Saito *et al.* 1985; M. B. A. Djamgoz, personal communication). In d-type dendrites it may be assumed that they are connected to an as yet unknown terminal structure which was not filled. On the other hand, the Golgi method has proved reproducible enough to form the basis for most of our current concepts about morphological differentiation of neurons and glial cells. For the present investigation, we most often found two or more cells with similar morphological features which, according to our criteria, could be grouped as a specific type. For this reason, we feel confident that even where only a single specimen was recorded the classification of separate types was justified.

The second critical point about this technique concerns the statistical nature with which cells are stained. Contrary to preparations with reduced silver stains, which rely on the affinity of neurofilaments for silver and therefore stain cytological features quantitatively, or immunocytochemistry which marks neuron populations according to their content of a specific molecule, no reliable information can be derived from Golgi preparations about the density of cell types or dendrites. Furthermore, even with a sample of 250 recorded cells after Golgi impregnation there is no reason to assume that the 43 cell types and 70 subtypes as defined in the present study represent the complete population of roach amacrine cell types. Rather, because in immunocytochemical observations we have observed cells with somatostatin-like immunoreactivity which we have not been able to find in the Golgi material (Wagner & Zeutzius 1987) we feel that the present catalogue may eventually need to be expanded.

5. *Principles of morphological organization of amacrine-cell dendritic fields*

The structural diversity of amacrine cells is essentially determined by the organization of bipolar terminals and ganglion-cell dendrites which are engaged in synaptic communication. The specificity of their interactions may be supposed to be the cause of the large number of dendritic-field patterns and surface specializations, such as spines and varicosities, which we used to identify the cell types. Yet, disregarding the fine structural details, some basic principles of organization of amacrine dendritic fields become apparent.

Among the monostratified cells, the most common pattern of arborization in roach is that of secondary dendrites radiating from a common point of origin at the end of a single primary or stem process (A3, 4, 9, 11, 13, 14, 15, 19, 23, 24). Depending on the number and location of branching points, different degrees of coverage of the dendritic field are achieved. The absence of asymmetry in these types suggests that their main function is to provide a homogeneous density of synaptic interactions. The various sizes of dendritic fields may either reflect differences in receptive-field sizes, or must be regarded in the context of the spacing of their somas, or possible functional non-equivalences of different parts of the processes, as in the case of A4 cells. The assumed homogeneity of synaptic site densities would make these radiate cells candidates for the processing of local-contrast and chromatic information.

By contrast, cells with asymmetrical or polar dendritic fields and a more irregular branching pattern (A2, 5, 8, 12, 16, 17, 18, 20) may serve more specialized functions, such as mediating motion- and direction-sensitivity (Naka 1980).

The third group of stratified cells with some common features are those amacrine types with stout dendrites, some of which have been shown to be electrically coupled (A6, 7, 26, 28, 31). Information about further connectivity suggests that they receive their main input from bipolar cells, whereas their output is as yet unclear (Sakai & Hashimoto 1983; H.-J.W. & E.W., personal observations). In view of their coarse structure and their coupling by gap junctions, it is tempting to speculate that the function of these cells may consist in influencing the resting potential of neighbouring cells over large distances and that they may thus control the threshold of a given sublayer.

Some of these considerations may apply not only to monostratified but also to multistratified and diffuse cells. In these latter cells, however, additional functional properties must be assumed if they are activated as a whole. More specifically, they may be assigned either transfer roles between individual sublayers, or simultaneous activation of different combinations of sublayers. They may also collect information from (for example) sublayers a and b and relay them to a specific class of ganglion cell in only one sublayer (cat A8 cells (Kolb & Nelson 1985); A17 cells (Nelson & Kolb 1985)). In this context, cell types appear especially interesting which have different dendritic fine structures in different sublayers (A13, 29, 38, 42). These cell types may therefore be supposed to have differential functions in the individual sublayers. Electron microscopic analysis of cat amacrine cells has shown that similar layer-specific differences are also found in cat AII cells (Kolb & Nelson 1984).

6. *Functional aspects of* IPL *stratification: role of amacrine cells*

The major characteristic of IPL organization is its subdivision into a zone where 'off-centre' ganglion cells receive their bipolar input (sublamina a) and a second zone where the dendrites of 'on-centre' ganglion cells are located (sublamina b) (Famiglietti & Kolb 1976; Famiglietti

et al. 1977). Morphologically, a number of examples have been found for cell types with essentially identical features in each of these sublayers. Such 'paramorphic' pairs may have antagonistic functions, as in cat beta ganglion cells, which have their cell bodies in the ganglion-cell layer and differ only in the level of their dendritic stratification (Wässle *et al.* 1981*a*, *b*). Cholinergic amacrine cells in rabbits have a mirror symmetric arrangement which includes not only their processes but also their perikarya (Vaney *et al.* 1981; Vaney 1984; Tauchi & Masland 1984). In the cat, it has been possible to define the physical border between sublamina a and b: the lobular appendages of AII cells are the structures which contact the most proximal terminal of presumed 'off-centre' bipolar cells and are therefore taken as definition landmarks.

Unfortunately, in species lacking AII cells the exact limit of the 'on'- and the 'off'-space is much less clear. It may be speculated that it coincides with one of the sublayers as defined either by bipolar terminals (Scholes 1975; Haesendonck & Missotten 1983; Deplano & Vallerga 1983), by amacrine-cell dendrites (this paper) or by banding systems due to optical or neurochemical properties (Marc 1986).

If we take a closer look at the widths of the a and b sublaminae, and of the other sublayers, a simple mirror symmetry is not apparent. Rather, sublayers of various thickness and complexity are characteristic of all species analysed and with all techniques used. This suggests that, in addition to complementary functions, specific functions may be localized in the IPL which supplement the basic 'on–off' subdivision. Such a conclusion is further substantiated if one examines the dendritic morphology of the various amacrine types and subtypes found in the roach. Although we cannot exclude the possibility that additional subtypes are still to be observed, it is evident that each cell type has a specific combination of subtypes. Some types are restricted to the proximal half of the IPL (A7, A12), some are found only in the distal half (A7, A28), and others have their dendrites both distal and proximal, sometimes with a preference for the intermediate sublayers 4 and 5 (A1, A3). Only in the asymmetrical A5 cell have we observed a strict mirror symmetry with subtypes in sublayers 1 and 7. On the other hand, the supposedly cholinergic A4 cell, which is the classic example of mirror symmetry in the rabbit, occurs only in sublayers 3 and 5 in the roach.

The differentiation of amacrine subtypes in the various sublayers may be regarded as a special case of paramorphism. It has been previously observed in a number of species after Golgi-impregnation (Cajal 1894; Wagner 1973; Vallerga & Deplano 1984) and after immunocytochemical staining for somatostatin (Marshak *et al.* 1984; Wagner & Zeutizus 1987). Supposing that other morphological subtypes also share the same neurotransmitter or neuropeptide, one may speculate that subtypes fulfil similar, if not identical, tasks in the respective sublayers. This, in turn, would mean that each IPL sublayer, composed of a specific combination of bipolar terminals, amacrine subtypes and ganglion cell types or subtypes, has a clearly defined functional role and thus constitutes a biological entity.

For certain kinds of visual information, parallel processing in each sublamina might be required and in this way might lead to the differentiation of multiple subtypes. Such as mode of signal transmission may be envisioned for chromatic information, where colour channels could be processed separately in both the 'on'- and the 'off'-sublamina. Consequently, amacrine and also ganglion cell types would be required with several subtypes. Although physiological support for such a model is not available, at present, two additional morphological observations are in accordance with the above interpretation. Comparison of the overall IPL

thickness in mono- and tetrachromatic species indicates that in the tetrachromatic roach the IPL is about three times as thick (40 μm) as in the monochromatic catfish (13 μm). Furthermore, somatostatin-immunoreactive amacrine cells in the catfish are represented by a single type, whereas in the roach two different types of somatostatin-positive cell have been identified, each with several subtypes (Wagner & Zeutzius 1987).

In conclusion, we feel that substantial progress in our understanding of retinal information processing has resulted recently from correlative work linking light- and electron-microscopic morphology, electrophysiology of light-evoked responses to appropriate stimuli, and cytochemical data about the transmitters used. The present detailed description is intended to simplify the identification of amacrine cell types, thus providing a reference for future intracellular and neurochemical work.

For stimulating discussions and critical reading of the manuscript, we thank M. B. A. Djamgoz, R. H. Douglas and R. Weiler. The Deutsche Forschungsgemeinschaft provided financial support. D. Drenckhahn kindly made available the fluorescent rhodamine-labelled phalloidin.

REFERENCES

Ammermüller, J. & Weiler, R. 1981 The ramification pattern of amacrine cells within the inner plexiform layer of the carp retina. *Cell Tiss. Res.* **220**, 699–723.

Avery, J. A., Bowmaker, J. K., Djamgoz, M. B. A. & Downing, J. E. G. 1982 Ultra-violet sensitive receptors in a freshwater fish. *J. Physiol., Lond.* **334**, 23.

Bloomfield, S. A. & Miller, R. F. 1982 A physiological and morphological study of the horizontal cell types of the rabbit retina. *J. comp. Neurol.* **208**, 288–303.

Boycott, B. B. & Dowling, J. E. 1969 Organization of the primate retina: light microscopy *Phil. Trans. R. Soc. Lond.* B **255**, 109–184.

Boycott, B. B. & Wässle, H. 1974 The morphological types of ganglion cells of the domestic cat's retina. *J. Physiol., Lond.* **240**, 397–419.

Brecha, N. C., Sharma, S. C. & Karten, H. J. 1981 Localization of substance P-like immunoreactivity in the adult and developing goldfish retina. *Neuroscience* **6**, 2737–2746.

Brecha, N. C., Eldred, W., Kuljis, R. O. & Karten, H. J. 1984 Identification and localization of biologically active peptides in the vertebrate retina. *Prog. retinal Res.* (ed. N. Osborne & G. Chader) **3**, 185–226.

Burgess, J. W. & Coss, R. G. 1980 Crowded jewel fish show changes in dendritic spine density and spine morphology. *Neurosci. Lett.* **17**, 277–281.

Cajal, S. R. y 1894 *Die Retina der Wirbelthiere: übersetzt von R. Greef.* Wiesbaden: Bergmann-Verlag.

Cattaneo, D. 1922 La struttura della retina nei vertebrati. *Ann. Ottal. clin. Ocul.* **50**, 349–390.

Chan, R. Y. & Naka, K.-I. 1976 The amacrine cell. *Vision Res.* **16**, 1119–1129.

Coss, R. G. & Perkel, D. H. 1985 The function of dendritic spines: a review of theoretical issues. *Behav. neur. Biol.* **44**, 151–185.

Deplano, S. & Vallerga, S. 1983 Quantitative morphology of amacrine cells in teleost retina. In *Photoreceptors* (ed. A. Borsellino & L. Cervetto), pp. 295–318. New York: Plenum Press.

Djamgoz, M. B. A. 1984 Electrophysiological characterization of spectral sensitivities of horizontal cells in cyprinid fish retina. *Vision Res.* **24**, 1677–1687.

Djamgoz, M. B. A. & Downing, J. E. G. 1983 A quantitative analysis of cone photoreceptor–horizontal cell connectivity patterns at ribbon synapses in a cyprinid fish (roach) retina. *J. Physiol., Lond.* **341**, 75*P*.

Djamgoz, M. B. A. & Ruddock, K. H. 1983 Spectral characteristics of transient amacrine cells in a cyprinid fish (roach) retina in vitro. *J. Physiol., Lond.* **339**, 19*P*.

Djamgoz, M. B. A., Downing, J. E. G. & Wagner, H.-J. 1984 The dendritic fields of functionally identified amacrine cells in a cyprinid fish retina. *J. Physiol., Lond.* **349**, 21*P*.

Djamgoz, M. B. A., Downing, J. E. G., Wagner, E., Wagner, H.-J. & Zeutzius, I. 1985 Functional organization of amacrine cells in the teleost fish retina. In *Neurocircuitry of the retina* (ed. A. Gallego & P. Gouras), pp. 188–204. New York: Elsevier.

Djamgoz, M. B. A. & Wagner, H.-J. 1987 Intracellular staining of retinal neurones: applications to studies of functional organization. In *Progress in retinal research* (ed. N. Osborne & J. Chader), pp. 85–150. Oxford: Pergamon Press.

Djamgoz, M. B. A., Downing, J. E. G. & Wagner, H.-J. 1987 Retinal neurones of cyprinid fish: Intracellular marking with horseradish peroxidase and correlative morphological analysis. *Expl Biol.* **46**, 203–216.

Dogiel, A. 1888 Über das Verhalten der nervösen Elemente in der Retina der Ganoiden, Reptilien, Vögel und Säugethiere. *Anat. Anz.* **3**, 133–143.

Dowling, J. E. 1979 Information processing by local circuits: the vertebrate retina as a model system. In *The neurosciences: fourth study program* (ed. F. O. Schmitt & F. G. Warden), pp. 163–181. Cambridge, Massachusetts: MIT Press.

Dowling, J. E. & Ehinger, B. 1975 Synpatic organisation of the amine-containing interplexiform cells of the goldfish and cebus monkey. *Science, Wash.* **188**, 270–273.

Dowling, J. E. & Werblin, F. S. 1969 Organisation of the retina of the mudpuppy, *Necturus maculosus*. I. Synaptic structure. *J. Neurophysiol.* **32**, 315–338.

Downing, J. E. G. 1983 Functionally identified interneurons in the vertebrate (fish) retina: electrophysiological, ultrastructural and pharmacological studies. Ph.D. thesis, University of London.

Drenckhahn, D. & Kaiser, H.-W. 1983 Evidence for the concentration of F-actin and myosin in synapses and in the plasmalemmal zone of axons. *Eur. J. Cell Biol.* **31**, 235–240.

Drenckhahn, D. & Wagner, H.-J. 1985 Relation of retinomotor responses and contractile proteins in vertebrate retinas. *Eur. J. Cell Biol.* **37**, 156–168.

Dunn-Meynell, A. A. & Sharma, S. C. 1986 The visual system of the channel catfish (*Ictalurus punctatus*). I. Retinal ganglion cell morphology. *J. comp. Neurol.* **247**, 32–55.

Ellias, S. A. & Stevens, J. K. 1980 The dendritic varicosity: a mechanism for electrically isolating the dendrites of cat retinal amacrine cells? *Brain Res.* **196**, 365–372.

Famiglietti, E. V. Jr 1981 Starburst amacrines: 2 mirror-symmetric retinal networks. *Invest. Ophthal. vis. Sci.* suppl. 20, p. 204.

Famiglietti, E. V. Jr 1983*a* 'Starburst' amacrine cells and cholinergic neurons: mirror-symmetric on and off amacrine cells of rabbit retina. *Brain Res.* **261**, 138–144.

Famiglietti, E. V. Jr 1983*b* On and off pathways through amacrine cells in mammalian retina: the synaptic connections of 'starburst' amacrine cells. *Vision Res.* **23**, 1265–1279.

Famiglietti, E. V. Jr 1985 Starburst amacrine cells: morphological constancy and systematic variation in the anisotropic field of rabbit retinal neurons. *J. Neurosci.* **5**, 562–577.

Famiglietti, E. V. Jr & Kolb, H. 1976 Structural basis for 'on' and 'off'-center responses in retinal ganglion cells. *Science, Wash.* **194**, 193–195.

Famiglietti, E. V. Jr, Kaneko, A. & Tachibana, M 1977 Neuronal architecture of on and off pathways to ganglion cells in carp. *Science, Wash.* **198**, 1267–1269.

Famiglietti, E. V. Jr & Vaughn, J. E. 1981 Golgi-impregnated amacrine cells and GABAergic retinal neurons: a comparison of dendritic, immunocytochemical and histochemical stratification in the inner plexiform layer of rat retina. *J. comp. Neurol.* **197**, 129–139.

Fifkova, E. & Delay, R. J. 1982 Cytoplasmic actin in neuronal processes as a possible mediator of synaptic plasticity. *J. Cell Biol.* **95**, 345–350.

Freed, M. A., Nakamura, Y. & Sterling, P. 1983 Four types of amacrine cells in the cat retina that accumulate GABA. *J. comp. Neurol.* **219**, 295–304.

Haesendonck, E. van & Missotten, L. 1983 Stratification and square pattern arrangement in the dorsal inner plexiform layer in the retina of *Callionymus lyra* (L.). *J. ultrastruct. Res.* **83**, 296–302.

Harris, R. M. 1985 Light microscopic depth measurements of thick sections. *J. Neurosci. Meth.* **14**, 97–100.

Holmgren-Taylor, I. 1983 Synapses of the inner plexiform layer in the retina of a cyprinid fish. *Cell Tiss. Res.* **229**, 337–350.

Hughes, A. 1977 The pigmented rat optic nerve: fibre count and fibre diameter spectrum. *J. comp. Neurol.* **176**, 263–268.

Hughes, A. 1981 Population magnitudes and distribution of major modal classes of cat retinal ganglion cell as estimated from HRP filling and a systematic survey of soma diameter spectra for classical neurons. *J. comp. Neurol.* **197**, 303–339.

Hughes, A. & Wieniawa-Narkiewicz, E. 1980 A newly identified population of presumptive microneurones in the cat retinal ganglion cell layer. *Nature, Lond.* **284**, 468–470.

Ishida, A. T., Stell, W. K. & Lightfoot, D. O. 1980 Rod and cone inputs into bipolar cells in goldfish retina. *J. comp. Neurol.* **191**, 315–335.

Johns, P. R. 1977 Growth of the adult goldfish eye. III. Source of new retinal cells. *J. comp. Neurol.* **176**, 343–358.

Johns, P. R. & Easter, S. S. Jr 1977 Growth of the adult goldfish eye. II. Increase in retinal cell number. *J. comp. Neurol.* **176**, 331–342.

Kaneko, A. 1973 Receptive field organization of bipolar and amacrine cells in the goldfish retina. *J. Physiol, Lond.* **235**, 133–153.

Koch, C., Poggio, T. & Torre, V. 1982 Retinal ganglion cells: functional interpretation of dendritic morphology. *Phil. Trans. R. Soc. Lond.* B **298**, 227–264.

Kock, J.-H. 1982*a* Neuronal addition and retinal expansion during growth of the crucian carp eye. *J. comp. Neurol.* **209**, 264–274.

Kock, J.-H. 1982*b* Dendritic tree structure and dendritic hypertrophy during growth of the crucian carp eye. *J. comp. Neurol.* **209**, 275–286.

Kock, J.-H. & Stell, W. K. 1985 Formation of new rod photoreceptor synapses onto differentiated bipolar cells in goldfish retina. *Anat. Rec.* **211**, 69–74.

Kolb, H. 1982 The morphology of bipolar cells, amacrine cells and ganglion cells in the retina of the turtle *Pseudemys scripta elegans*. *Phil. Trans. R. Soc. Lond.* B **298**, 355–393.

Kolb, H. & Nelson, R. 1981 Amacrine cells of the cat retina. *Vision Res.* **21**, 1625–1633.

Kolb, H., Nelson, R. & Mariani, A. 1981 Amacrine cells, bipolar cells and ganglion cells of the cat retina: A Golgi study. *Vision Res.* **21**, 1081–1114.

Kolb, H. & Nelson, R. 1984 Neural architecture in the cat retina. In *Progress in retinal research* (ed. N. Osborne & J. Chader), vol. 3, pp. 21–60. Oxford: Pergamon Press.

Kolb, H. & Nelson, R. 1985 Functional neurocircuitry of amacrine cells in the cat. In *Neurocircuitry of the retina: A Cajal memorial* (ed. A. Gallego & P. Gouras), pp. 215–232. New York: Elsevier.

Lam, D. M.-K., Su, Y.-Y. T. & Watt, C. B. 1986 The self-regulating synapse: a functional role for the co-existence of neuroactive substances. *Brain Res. Rev.* **11**, 249–257.

Levine, J. S. & McNichol, E. F. 1979 Visual pigments in teleost fishes: effects of habitat, microhabitat and behaviour on visual system evolution. *Sensory Processes* **3**, 95–131.

Linberg, K. A., Fisher, S. K. & Kolb, H. 1986 A Golgi study of amacrine cells in the human retina. *Invest. Ophthal. vis. Sci.* **27** (suppl.), 203.

Macy, A. & Easter, S. S. Jr 1981 Growth-related changes in the size of receptive field centers of retinal ganglion cells in goldfish. *Vision Res.* **21**, 1497–1504.

Marc, R. E. 1986 Neurochemical stratification in the inner plexiform layer of the vertebrate retina. *Vision Res.* **26**, 223–238.

Marchiafava, P. L. 1976 Centrifugal actions on amacrine and ganglion cells in the retina of the turtle. *J. Physiol., Lond.* **255**, 137–155.

Marchiafava, P. L. & Weiler, R. 1982 The photoresponses of structurally identified amacrine cells in the turtle retina. *Proc. R. Soc. Lond.* B **214**, 403–415.

Mariani, A. P. 1982 Association amacrine cells could mediate directional selectivity in pigeon retina. *Nature, Lond.* **298**, 654–655.

Marshak, D. W. & Dowling, J. E. 1984 Chemical synapses of cone horizontal cell axons in the goldfish retina. *Soc. Neurosci. Abstr.* **10**, 21.

Marshak, D. W., Yamada, T. & Stell, W. K. 1984 Synaptic contacts of somatostatin-immunreactive amacrine cells in goldfish retina. *J. comp. Neurol.* **225**, 44–52.

Masland, R. H. & Mills, J. W. 1979 Autoradiographic identification of actylcholine in the rabbit retina. *J. Cell Biol.* **83**, 159–178.

Masland, R. H. & Tauchi, M. 1986 The cholinergic amacrine cell. *Trends Neurosci.* **95**, 218–223.

McGuire, B. A., Stevens, J. K. & Sterling, P. 1984 Microcircuitry of bipolar cells in cat retina. *J. Neurosci.* **4**, 2920–2938.

Miller, R. F. 1979 The neuronal basis of ganglion cell receptive field organization and the physiology of amacrine cells. In *The neurosciences: fourth study program* (ed. F. O. Schmitt & F. G. Warden), pp. 227–245. Cambridge, Massachusetts: MIT Press.

Mitarai, G., Goto, T. & Tagaki, S. 1978 Receptive field arrangement of colour-opponent bipolar and amacrine cells in the carp retina. *Sensory Processes* **2**, 375–382.

Murakami, M. & Shimoda, Y. 1977 Identification of amacrine and ganglion cells in the carp retina. *J. Physiol., Lond.* **264**, 801–818.

Naka, K.-I. 1976 Neuronal circuitry in the catfish retina. *Invest. Ophthal. vis. Sci.* **15**, 926–935.

Naka, K.-I. 1980 A class of catfish amacrine cells responds preferentially to objects which move vertically. *Vision Res.* **20**, 961–965.

Naka, K.-I. & Carraway, N. R. G. 1975 Morphological and functional identification of catfish retinal neurons: I. Classical morphology. *J. Neurophysiol.* **38**, 53–71.

Naka, K.-I. & Christensen, B. N. 1981 Direct electrical connections between transient amacrine cells in the catfish retina. *Science, Wash.* **214**, 462–464.

Nelson, R. & Kolb, H. 1985 A17: a broad-field amacrine cell in the rod system of the cat retina. *J. Neurophysiol.* **54**, 592–614.

Palay, S. L. & Chan-Palay, V. 1975 Cell form as an expression of neuronal function. In *Proceedings of the Golgi centennial symposium* (ed. M. Santini), pp. 51–60. New York: Raven Press.

Perry, V. H. & Walker, M. 1980 Amacrine cells, displaced amacrine cells and interplexiform cells of the rat. *Proc. R. Soc. Lond.* B **208**, 415–431.

Pierantoni, R. L. & Ogden, T. E. 1982 Mosaic of bipolar axon terminals in the retina of a teleost. *Invest. Ophthal. vis. Sci.* suppl. **22**, 112.

Purves, D., Hadley, R. D. & Voyvodic, J. T. 1986 Dynamic changes in the dendritic geometry of individual neurons visualized over periods of up to three months in the superior cervical ganglion of living mice. *J. Neurosci.* **6**, 1051–1060.

Rall, W. 1962 Electrophysiology of a dendritic neuron model. *Biophys. J.* **2**, 145–167.

Rodieck, R. W. & Brening, R. K. 1982 On classifying retinal ganglion cells by numerical methods. *Brain Behav. Evol.* **21**, 42–46.

Saito, T., Kujiraoka, T., Yonaha, T. & Chino, Y. 1985 Reexamination of photoreceptor-bipolar connectivity patterns in carp retina: HRP-EM and Golgi-EM studies. *J. comp. Neurol.* **236**, 141–160.

Sakai, H. & Hashimoto, Y. 1983 Rod input to amacrine cells in dace retina. *Brain Res.* **270**, 345–349.

Sasaki-Sherrington, S., Jacobs, J. R. & Stevens, J. K. 1984 Intracellular control of axial shape in non-uniform neurites: a serial electron microscope analysis of organelles and microtubules in AI and AII retinal amacrine neurites. *J. Cell Biol.* **98**, 1279–1290.

Scholes, J. H. 1975 Colour receptors, and their synaptic connexions in the retina of a cyprinid fish. *Phil. Trans. R. Soc. Lond.* B **270**, 61–118.

Scholes, J. H. 1976 Neural connections and cellular arrangement in the fish retina. In *Neural principles in vision* (ed. F. Zettler & R. Weiler), pp. 63–93. Berlin: Springer-Verlag.

Schwassmann, H. O. 1968 Visual projection upon the optic tectum in foveate marine teleosts. *Vision Res.* **8**, 1337–1348.

Stell, W. K. 1975 Horizontal cell axons and axon terminals in goldfish retina. *J. comp. Neurol.* **159**, 503–520.

Stell, W. K. & Harosi, F. 1976 Cone structure and visual pigment content in the retina of the goldfish. *Vision Res.* **16**, 647–657.

Tauchi, M. & Masland, R. H. 1984 The shape and arrangement of the cholinergic neurons in the rabbit retina. *Proc. R. Soc. Lond.* B **223**, 101–119.

Tauchi, M. & Masland, R. H. 1985 Local order among the dendrites of an amacrine cell population. *J. Neurosci.* **5**, 2494–2501.

Teranishi, T., Negishi, K. & Kato, S. 1984 Dye coupling between amacrine cells in carp retina. *Neurosci. Lett.* **51**, 73–78.

Toyoda, J., Hashimoto, H. & Ohtsu, K. 1973 Bipolar–amacrine transmission in the carp retina. *Vision Res.* **13**, 295–307.

Tumosa, N., Eckenstein, F. & Stell, W. K. 1984 Immunocytochemical localization of putative cholinergic neurons in the goldfish retina. *Neurosci. Lett.* **48**, 255–259.

Vallerga, S. & Deplano, S. 1984 Differentiation, extent and layering of amacrine cell dendrites in the retina of a sparid fish. *Proc. R. Soc. Lond.* B **221**, 465–477.

Vallerga, S. & Ratto, G. M. 1985 Are dendritic beads related to synaptic loci? In *Neurocircuitry of the retina: a Cajal memorial* (ed. A. Gallego & P. Gouras), pp. 265–269. New York: Elsevier.

Vaney, D. I. 1980 A quantitative comparison between the ganglion cell populations and axonal outflows of the visual streak and the periphery of the rabbit retina. *J. comp. Neurol.* **176**, 263–268.

Vaney, D. I. 1984 'Coronate' amacrine cells in the rabbit retina have 'starburst' dendritic morphology. *Proc. R. Soc. Lond.* B **220**, 501–508.

Vaney, D. I., Peichl, L. & Boycott, B. B. 1981 Matching populations of amacrine cells in the inner nuclear and ganglion cell layers of the rabbit retina. *J. comp. Neurol.* **199**, 373–391.

Vrabec, F. 1966 A new finding in the retina of a marine teleost *Callionymus lyra*. L. *Folia morphol.* **14**, 143–147.

Wagner, H.-J. 1973 Die nervösen Netzhautelemente von *Nannacara anomala* (Cichlidae, Teleostei). I. Darstellung nach Silberimprägnation. *Z. Zellforsch. mikrosk. Anat.* **137**, 63–86.

Wagner, H.-J. 1980 Light-dependent plasticity of the morphology of horizontal cell terminals in cone pedicles of fish retinas. *J. Neurocytol.* **9**, 573–590.

Wagner, H.-J. & Speck, P. T. 1985 Computer graphics in neurobiology. *Eur. J. Cell Biol.* suppl. **36**, 70.

Wagner, H.-J. & Zeutzius, I. 1987 Amacrine cells with neurotensin- and somotostatin-like immunoreactivity in three species of teleosts with different colour vision. *Cell Tiss. Res.* **248**, 663–673.

Wässle, H., Boycott, B. B. & Illing, R. B. 1981 Morphology and mosaic of on- and off-beta cells in the cat retina and some functional considerations. *Proc. R. Soc. Lond.* B **212**, 177–195.

Weiler, R. & Marchiafava, P. L. 1981 Physiological and morphological study of the inner plexiform layer in the turtle retina. *Vision Res.* **21**, 1635–1638.

Weiler, R. & Zettler, F. 1979 The axon bearing horizontal cells in the teleost retina are functional as well as structural units. *Vision Res.* **19**, 1261–1268.

Weiler, R. & Ball, A. K. 1984 Co-localization on neurotensin-like immunoreactivity and ^{3}H-glycine uptake system in sustained amacrine cells of the turtle retina. *Nature, Lond.* **311**, 759–761.

Werblin, F. S. 1970 Response of retinal cells to moving spots: intracellular recordings in *Necturus maculosus*. *J. Neurophysiol.* **33**, 342–350.

West, R. W. 1972 Superficial warming of epoxy blocks for cutting of 25–150 μm sections resectioned in the 40–90 nm range. *Stain Technol.* **47**, 201–204.

West, R. W. 1976 Light and electron microscopy of the ground squirrel retina: functional considerations. *J. comp. Neurol.* **168**, 355–378.

West, R. W. & Dowling, J. E. 1972 Synapses onto different morphological types of retinal ganglion cells. *Science, Wash.* **178**, 510–512.

Witkovsky, P. & Dowling, J. E. 1969 Synaptic relationships of the plexiform layers of carp retina. *Z. Zellforsch. mikrosk. Anat.* **100**, 60–82.

Zimmerman, R. P. 1983 Bar synapses and gap junctions in the inner plexiform layer: synaptic relationships of the interstitial amacrine cell of the retina of the cichlid fish *Astronotus ocellatus*. *J. comp. Neurol.* **218**, 471–479.

Description of pullout 1

Figure 41. Summary diagram of amacrine types and subtypes in the roach. Each cell type is shown in tangential view (according to the camera lucida drawing) and in its semischematic radial aspect (as reconstructed from focus readings or radial sections). The following groups can be recognized: (i) Monostratified cells with several subtypes: A1–A10. (ii) Monostratified cells with only a single subtype: A11–A24. (iii) Stratified cells with more than one level of stratification: A25–A31. (iv) Diffuse amacrine cells: A32–A43. Within these groups, the cells are arranged in order of decreasing size of dendritic field. (Bar 100 μm.)

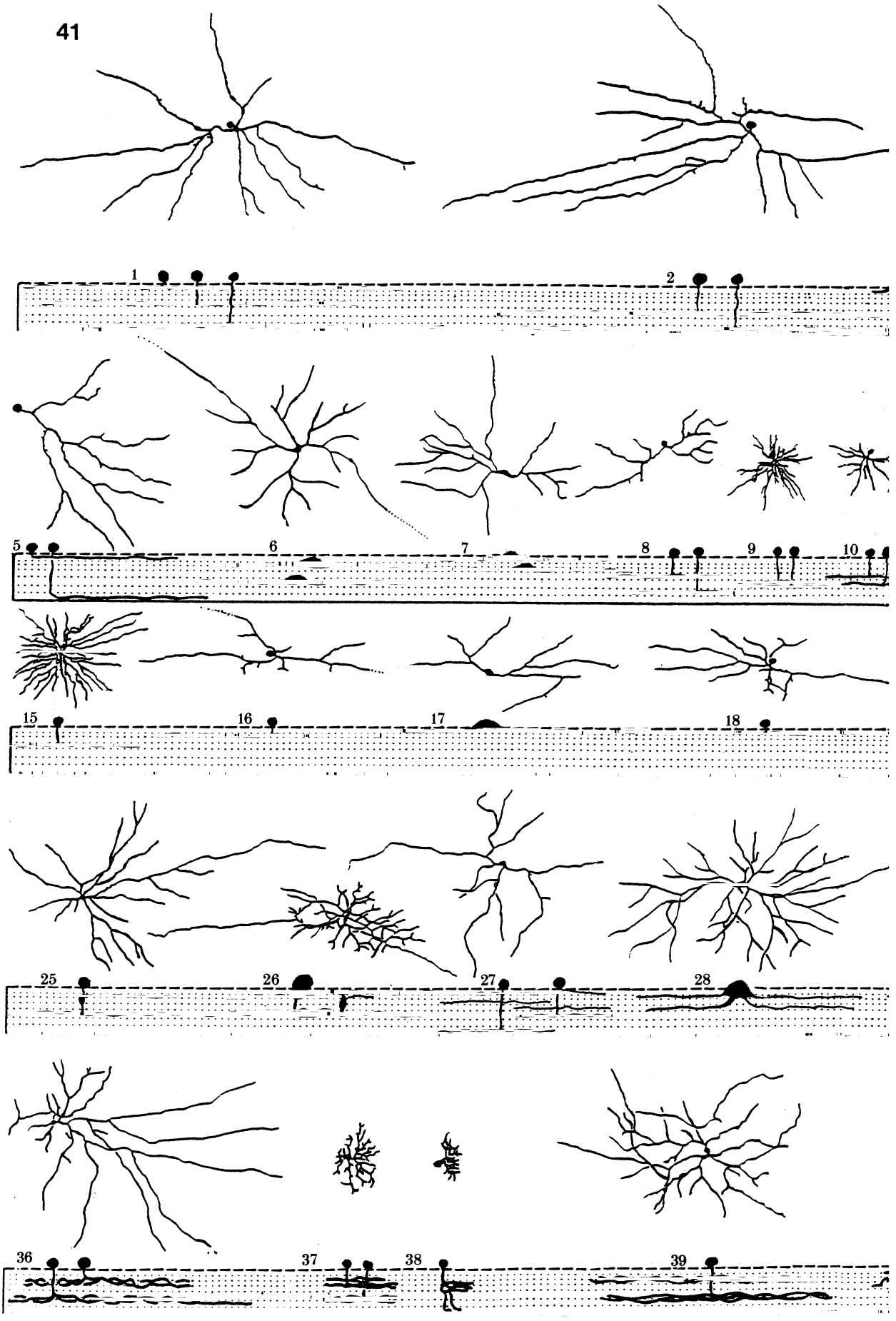

FIGURE 41. For descri

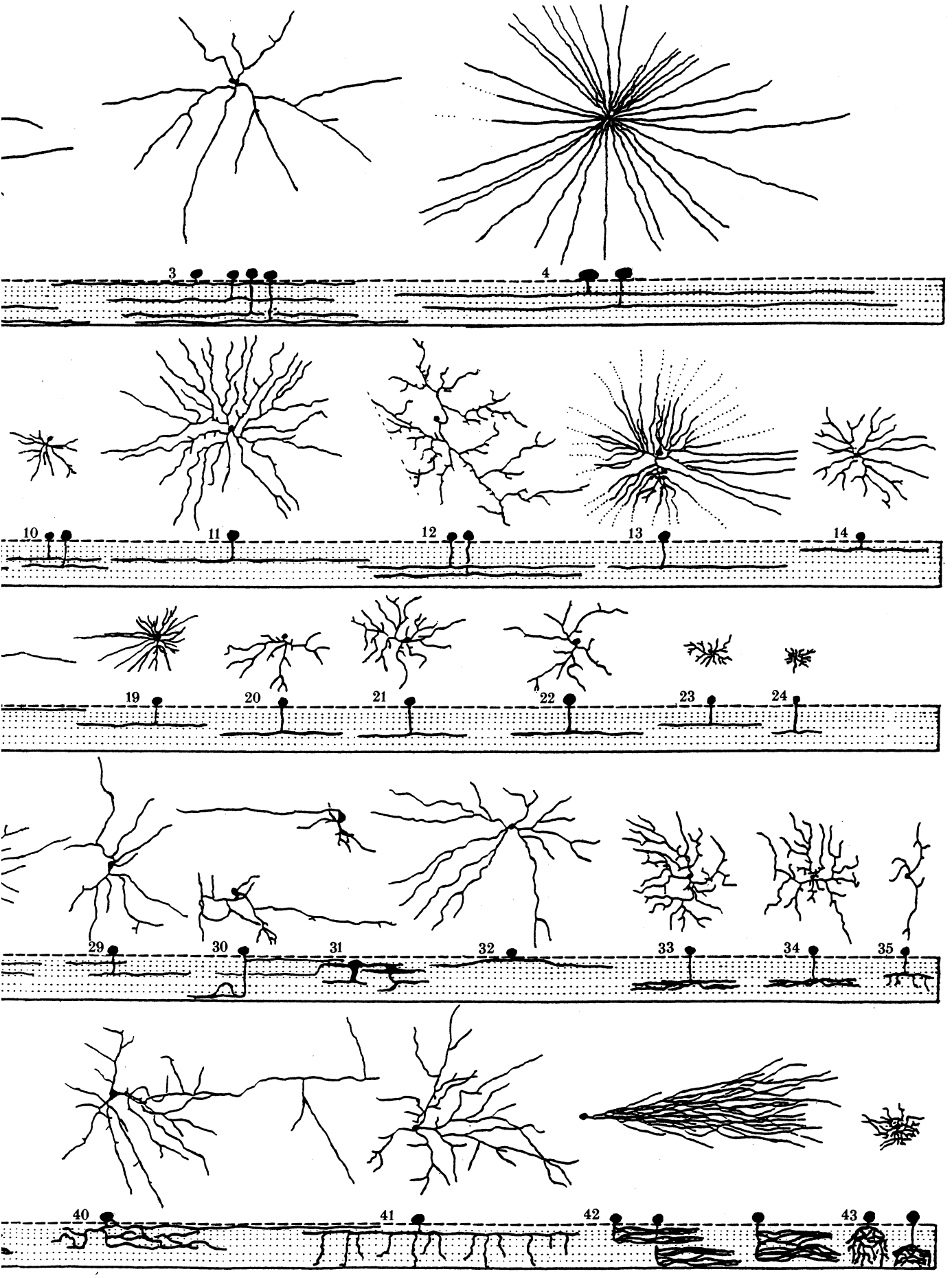

For description see opposite.

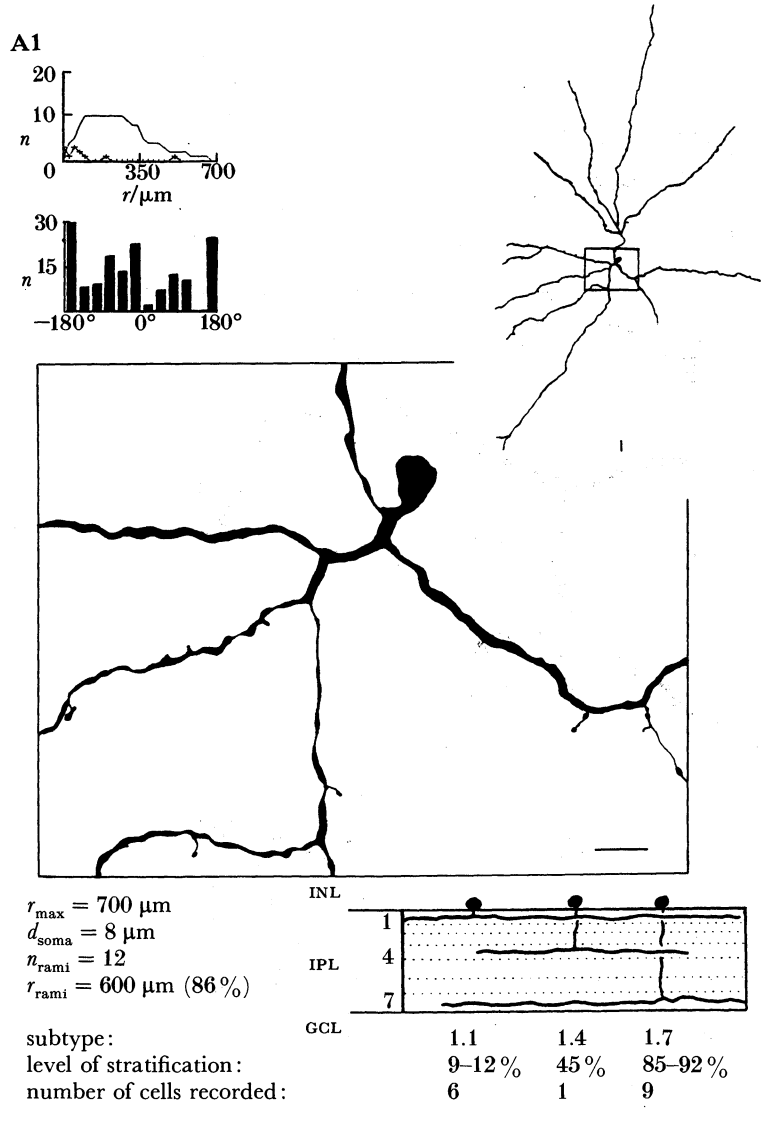

r_{max} = 700 μm
d_{soma} = 8 μm
n_{rami} = 12
r_{rami} = 600 μm (86 %)

subtype:	1.1	1.4	1.7
level of stratification:	9–12 %	45 %	85–92 %
number of cells recorded:	6	1	9

Explanation of the ID charts of amacrine cell types

ID charts are referred to by their type number (1–43) in the top left-hand corner.

A *low-power tangential view* of a camera lucida drawing of a representative specimen occupies the upper right-hand corner. The length of the horizontal bar corresponds to 50 μm; the vertical bar indicates the direction of the optic disc, and serves to illustrate the orientation of the cell.

A *high-power view* with the essential fine-structural details of the area indicated by the box in the overview is shown in the centre panel (scale bar 10 μm).

The *semischematic drawing* in the lower right-hand corner gives the position of the soma and the location of the dendrites (in the seven sublayers of the IPL) of the respective subtypes.

In the *graph* (top left) we plotted the number of dendritic processes (continuous line) and the number of branching points (crosses) with respect to the soma or the stem process.

The *histogram*, below, indicates the number of dendrites within 30° sectors of the dendritic field; 0° gives the orientation of the optic nerve fibres. The values were obtained by counting the intersections of processes with concentric circles spaced at 17 μm intervals.

A *summary* of the basic numerical data is found at the bottom of each panel. The largest radius (r_{max}), largest diameter of perikaryon in whole mount view (d_{soma}), total number of ramification points (n_{rami}), and absolute and relative distance between the last ramification point and the soma (r_{rami}) are recorded. The values represent the maximal readings of all specimens recorded of each type.

A *list of subtypes* indicates the level(s) of stratification and the number of specimens recorded.

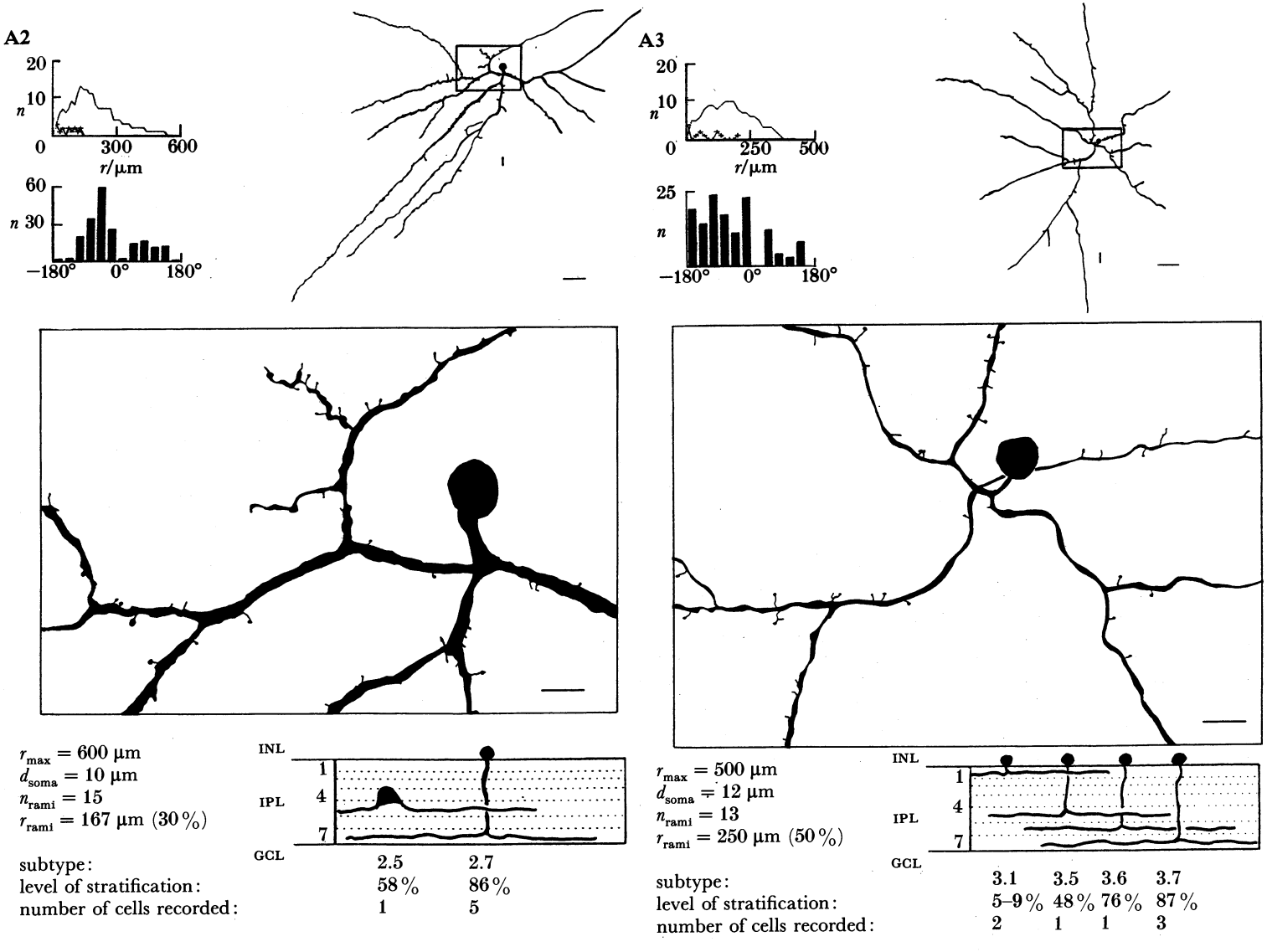

$r_{max} = 600$ µm
$d_{soma} = 10$ µm
$n_{rami} = 15$
$r_{rami} = 167$ µm (30 %)

subtype:
level of stratification:
number of cells recorded:

$r_{max} = 500$ µm
$d_{soma} = 12$ µm
$n_{rami} = 13$
$r_{rami} = 250$ µm (50 %)

subtype:
level of stratification:
number of cells recorded:

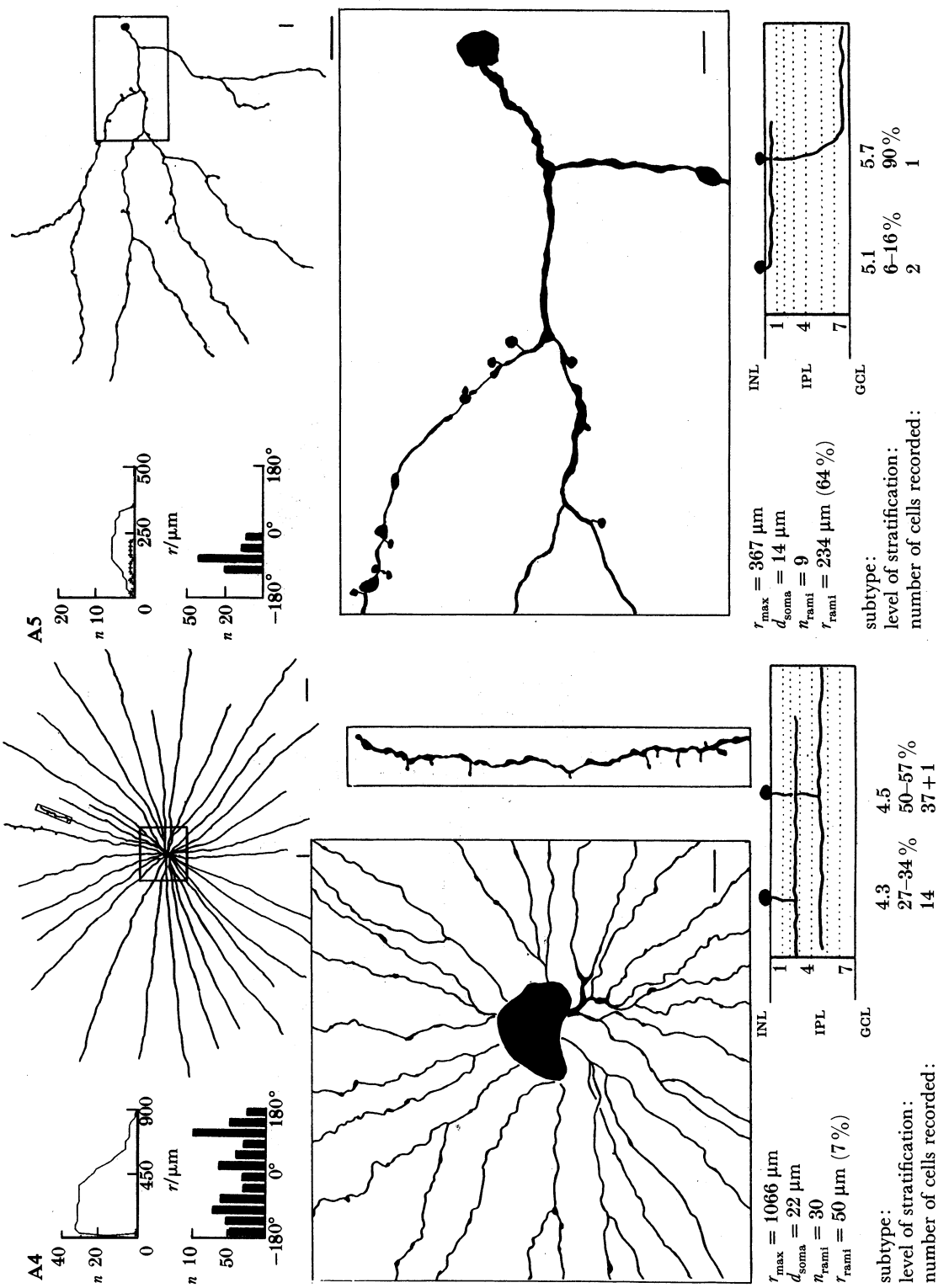
A4
A5
n
r/µm
−180°
0°
180°
INL
IPL
GCL
r_{max} = 1066 µm
d_{soma} = 22 µm
n_{rami} = 30
r_{rami} = 50 µm (7%)
subtype: 4.3 4.5
level of stratification: 27–34% 50–57%
number of cells recorded: 14 37+1
r_{max} = 367 µm
d_{soma} = 14 µm
n_{rami} = 9
r_{rami} = 234 µm (64%)
subtype: 5.1 5.7
level of stratification: 6–16% 90%
number of cells recorded: 2 1

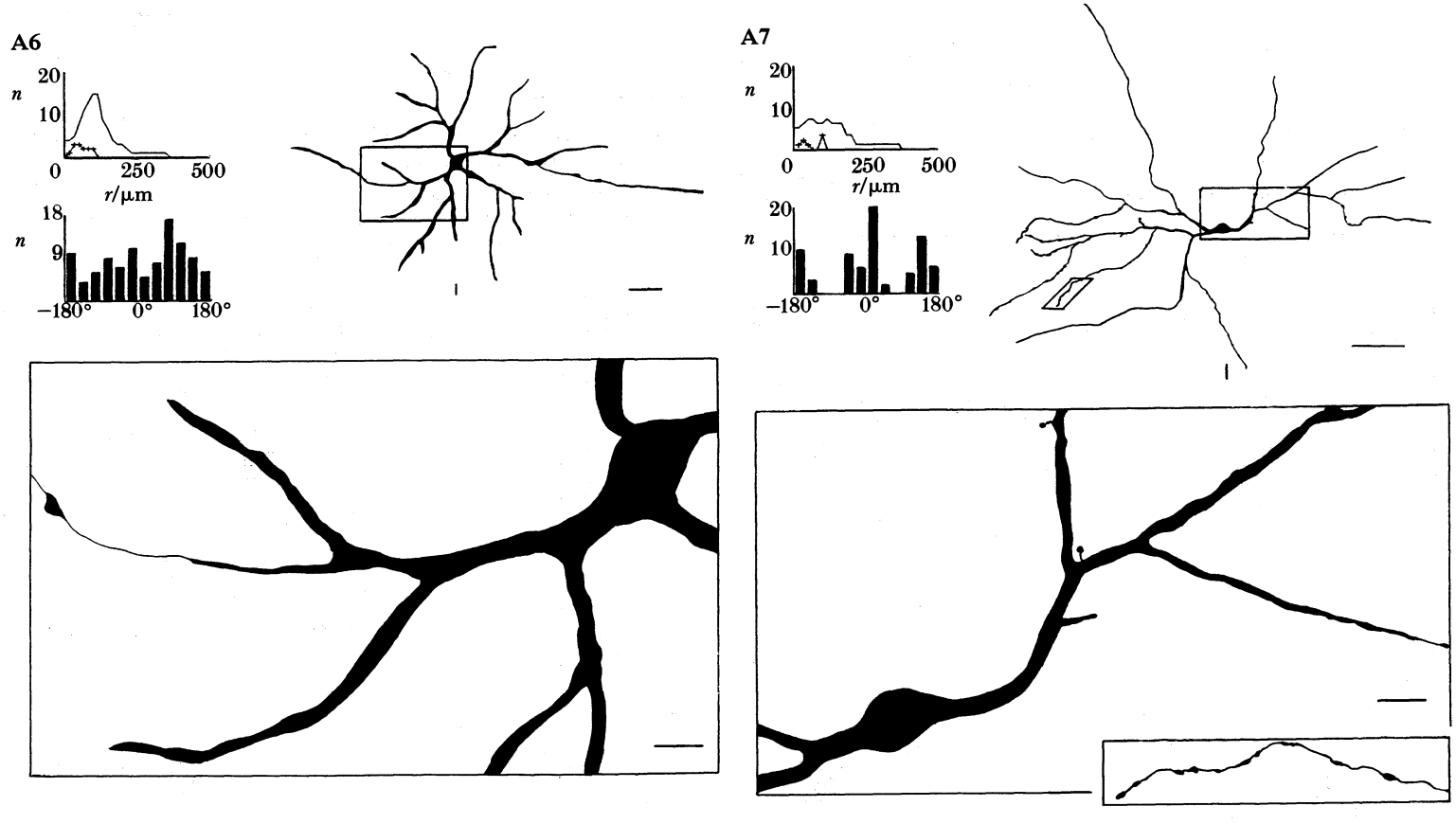

r_{max} = 350 µm
d_{soma} = 15 µm
n_{rami} = 14
r_{rami} = 117 µm (33 %)

subtype:	6.2	6.5
level of stratification:	22 %	58–67 %
number of cells recorded:	1	8

r_{max} = 400 µm
d_{soma} = 13 µm
n_{rami} = 13
r_{rami} = 225 µm (69 %)

subtype:	7.1	7.3
level of stratification:	8–10 %	27–28 %
number of cells recorded:	3	2

A8

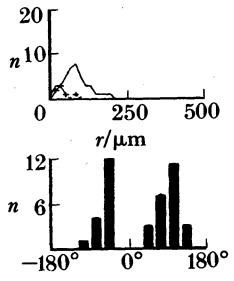

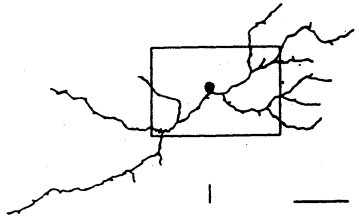

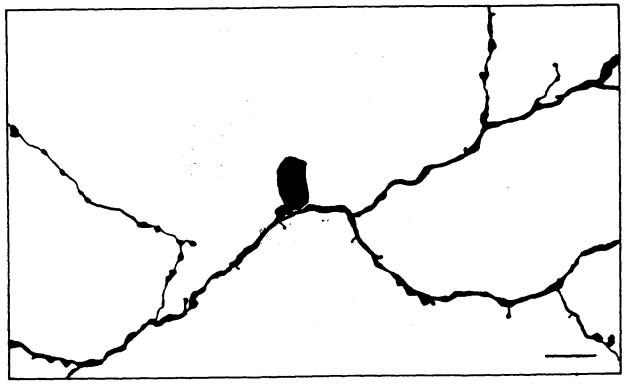

r_{max} = 217 µm
d_{soma} = 8 µm
n_{rami} = 9
r_{rami} = 117 µm (54 %)

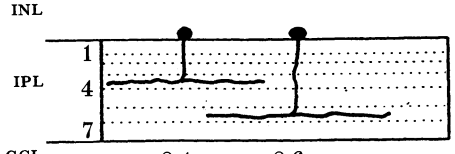

subtype:	8.4	8.6
level of stratification:	37 %	82 %
number of cells recorded:	1	1

A9

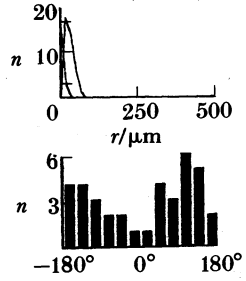

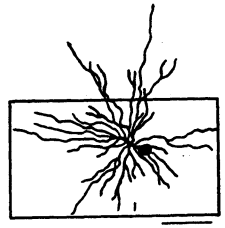

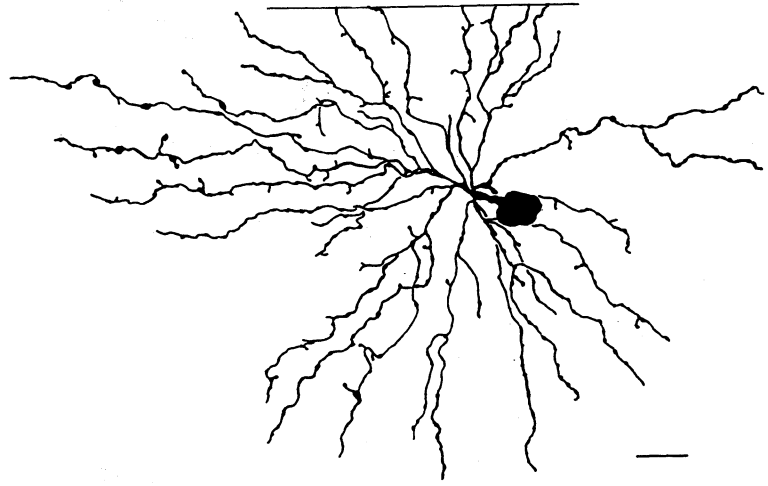

r_{max} = 134 µm
d_{soma} = 8 µm
n_{rami} = 20
r_{rami} = 50 µm (37 %)

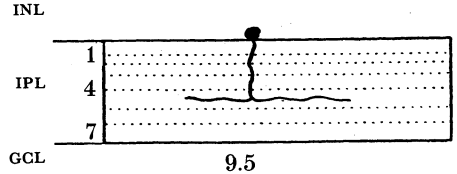

subtype:	9.5
level of stratification:	53–57 %/66 %
number of cells recorded:	5

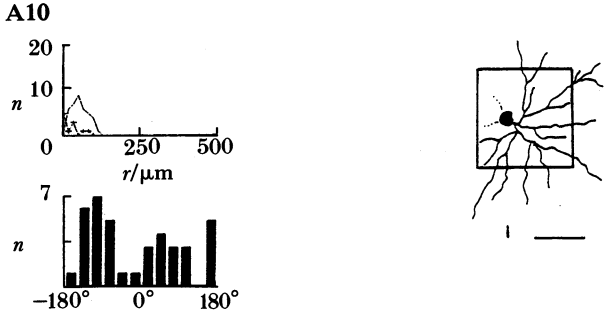

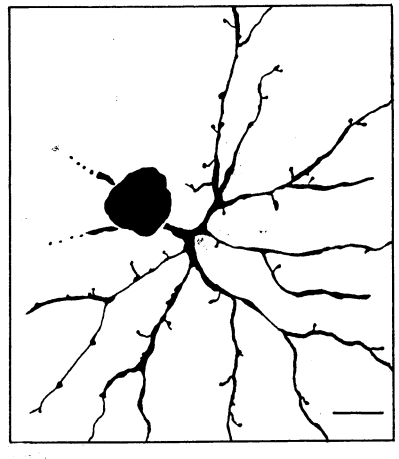

r_{max} = 134 µm
d_{soma} = 10 µm
n_{rami} = 15
r_{rami} = 100 µm (75%)

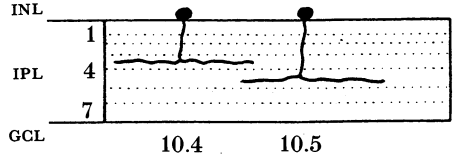

subtype:	10.4	10.5
level of stratification:	42%	60%
number of cells recorded:	1	1

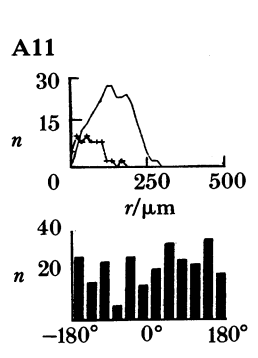

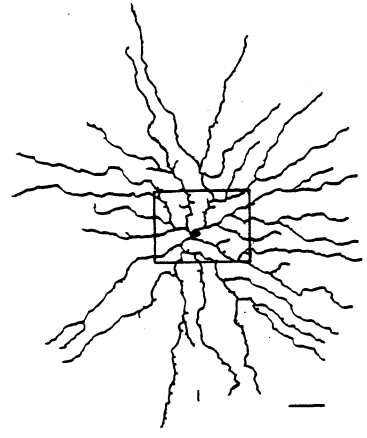

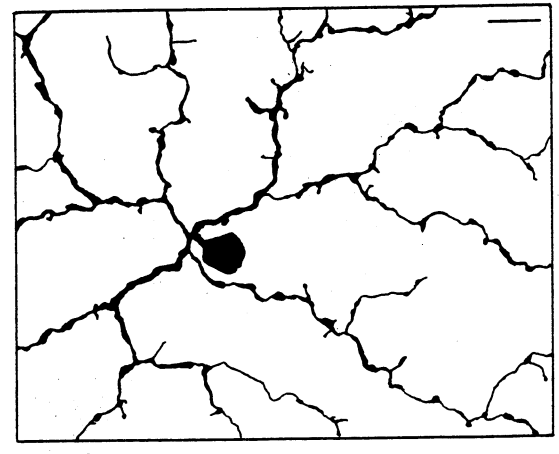

r_{max} = 500 µm
d_{soma} = 8 µm
n_{rami} = 24
r_{rami} = 250 µm (50%)

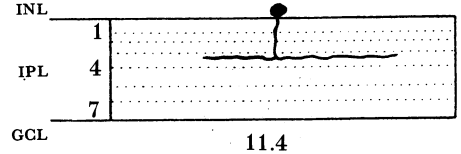

subtype:	11.4
level of stratification:	35–40%
number of cells recorded:	3

A12

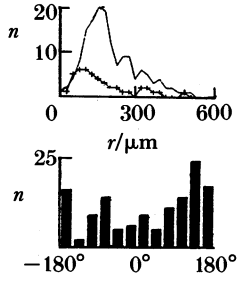

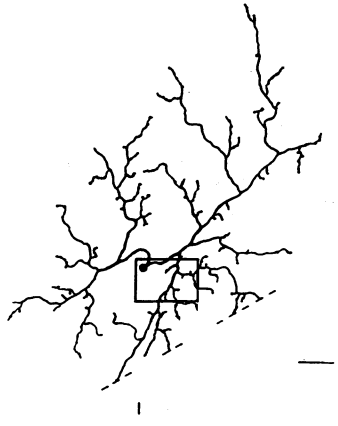

r_{max} = 550 µm
d_{soma} = 11 µm
n_{rami} = 44
r_{rami} = 525 µm (95 %)

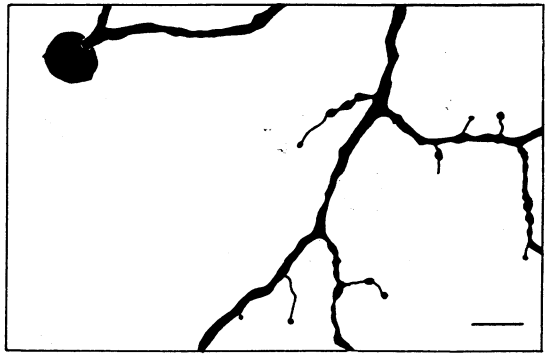

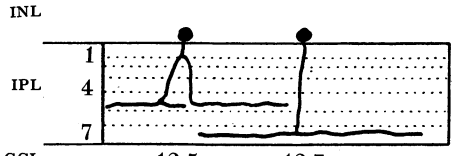

subtype:	12.5	12.7
level of stratification:	55–60 %	85 %
number of cells recorded:	1	1

A13

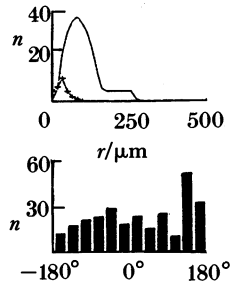

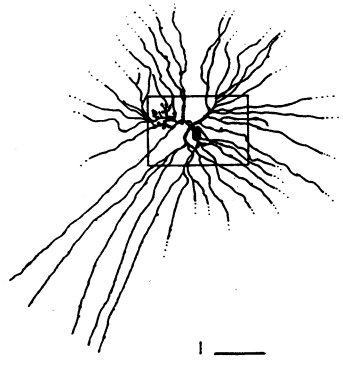

r_{max} = 300 µm
d_{soma} = 11 µm
n_{rami} = 29
r_{rami} = 70 µm (23 %)

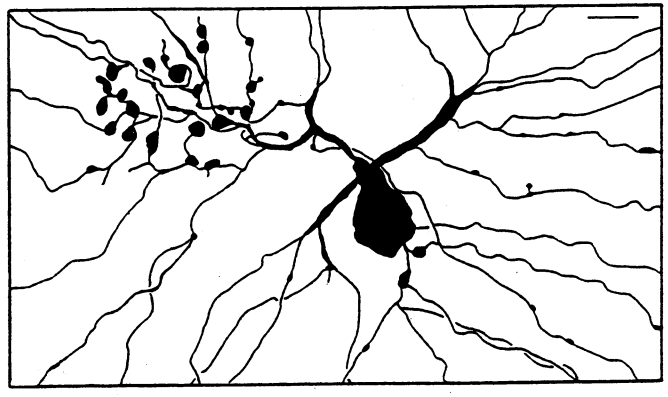

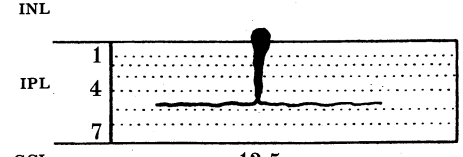

subtype:	13.5
level of stratification:	65 %
number of cells recorded:	2

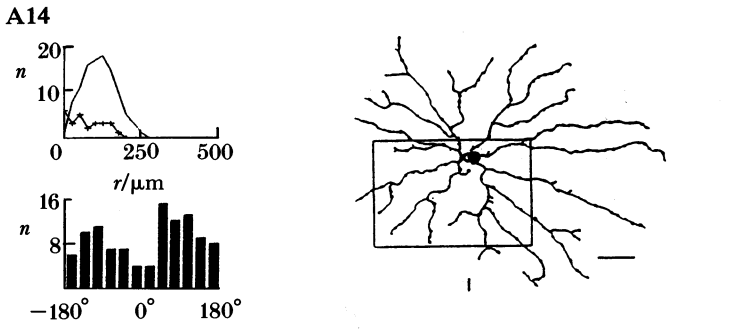

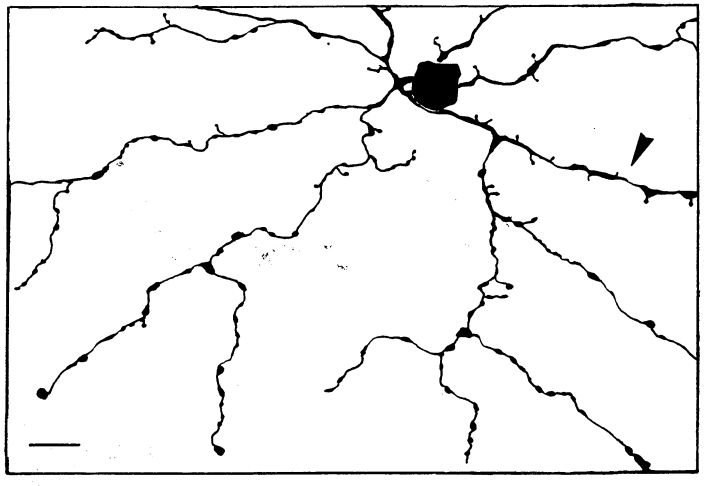

$r_{max} = 275$ µm
$d_{soma} = 8$ µm
$n_{rami} = 22$
$r_{rami} = 200$ µm (73%)

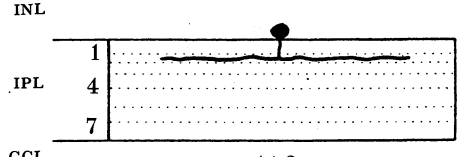

subtype: 14.2
level of stratification: 19–24%
number of cells recorded: 8

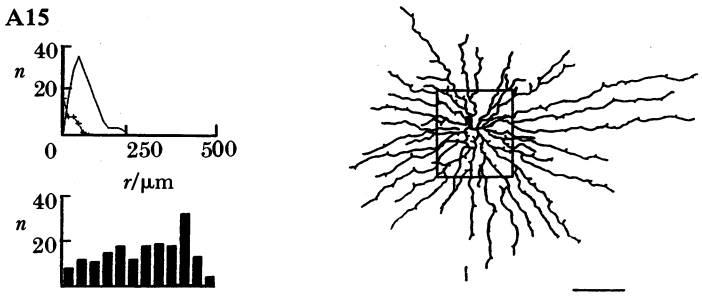

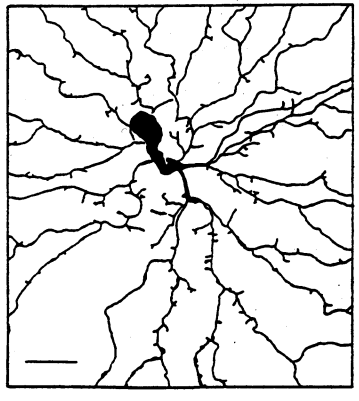

$r_{max} = 217$ µm
$d_{soma} = 5$ µm
$n_{rami} = 38$
$r_{rami} = 84$ µm (39%)

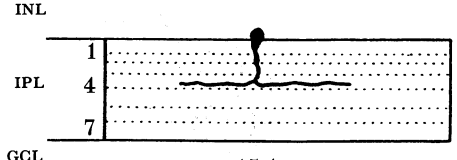

subtype: 15.4
level of stratification: 45%
number of cells recorded: 2

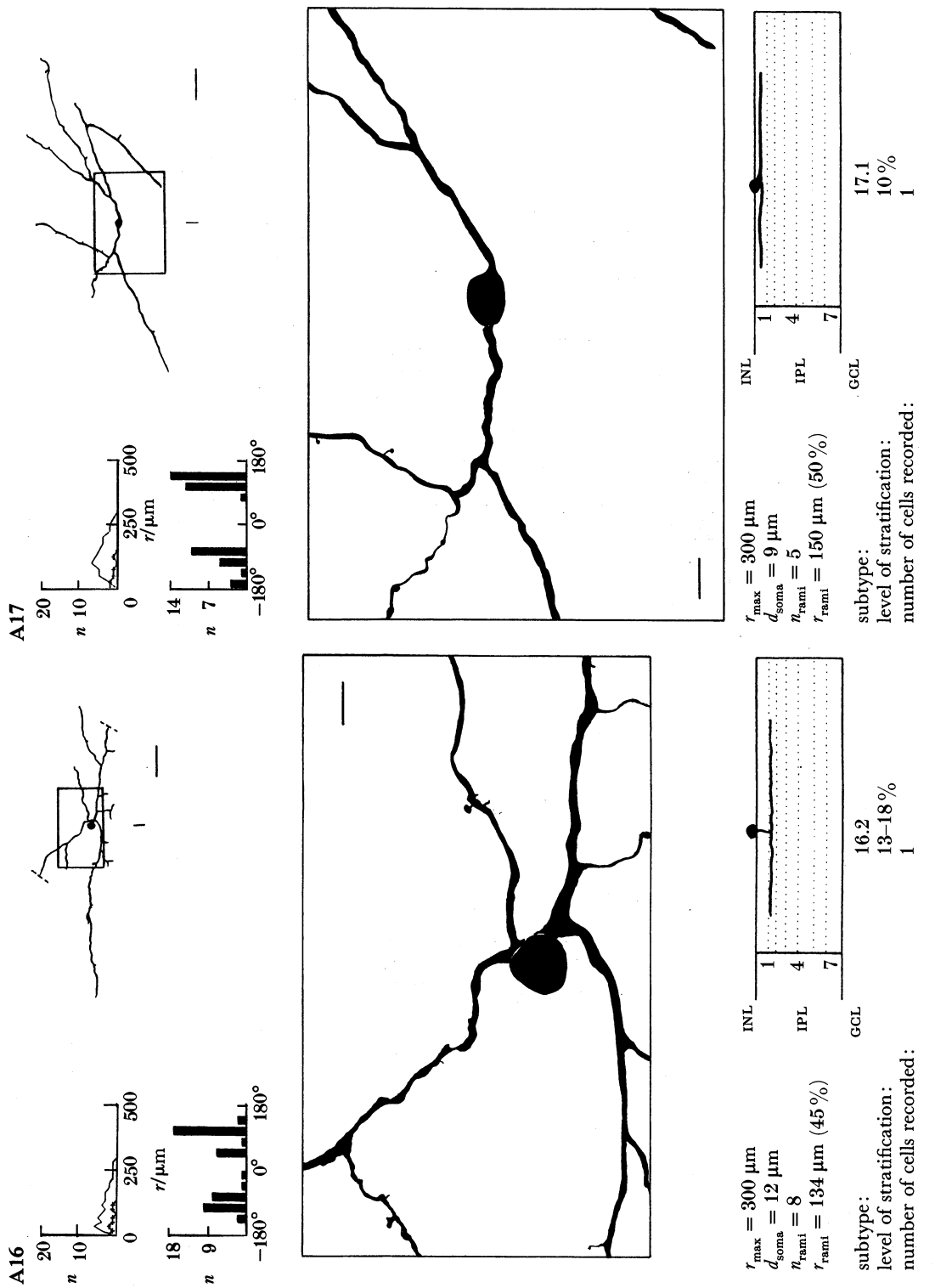
A16
A17
n
r/μm
0
250
500
−180°
0°
180°
INL
IPL
GCL
r_{max} = 300 μm
d_{soma} = 12 μm
n_{rami} = 8
r_{rami} = 134 μm (45%)
subtype: 16.2
level of stratification: 13–18%
number of cells recorded: 1
r_{max} = 300 μm
d_{soma} = 9 μm
n_{rami} = 5
r_{rami} = 150 μm (50%)
subtype: 17.1
level of stratification: 10%
number of cells recorded: 1

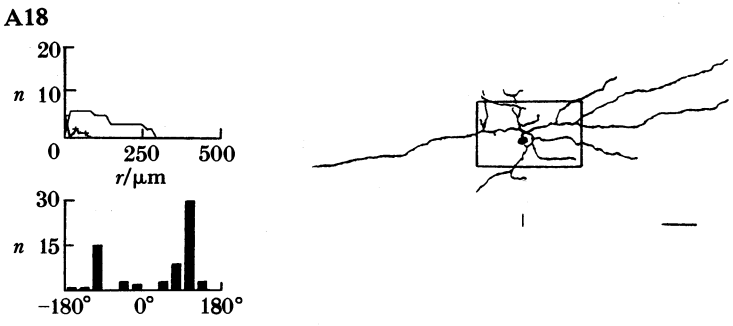

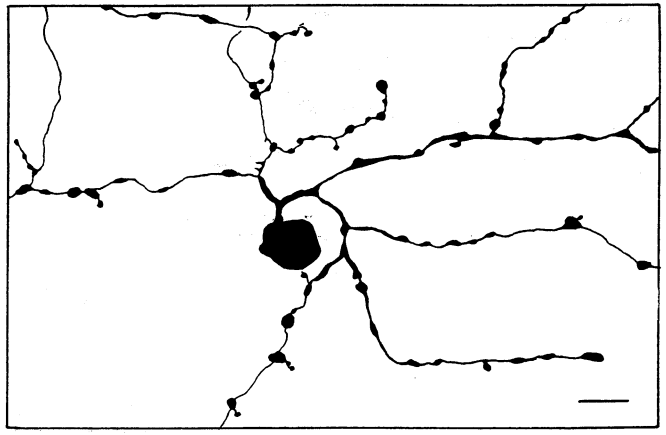

r_{max} = 300 µm
d_{soma} = 10 µm
n_{rami} = 9
r_{rami} = 84 µm (28 %)

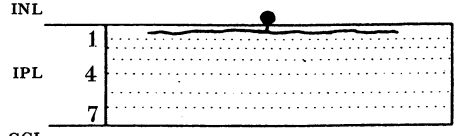

subtype: 18.1
level of stratification: 5 %
number of cells recorded: 1

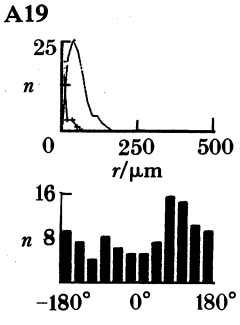

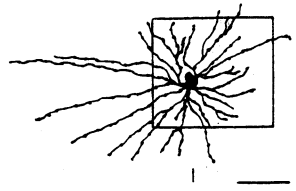

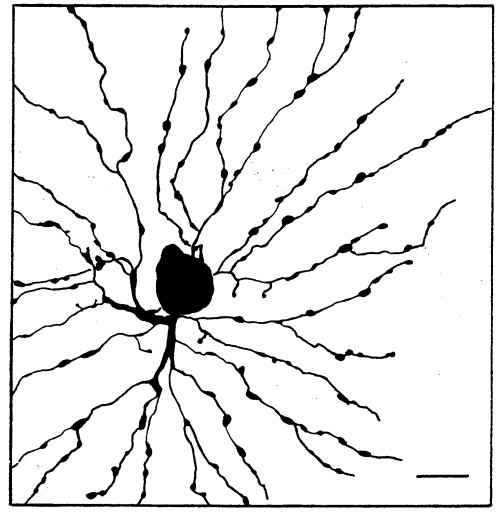

r_{max} = 167 µm
d_{soma} = 11 µm
n_{rami} = 26
r_{rami} = 67 µm (40 %)

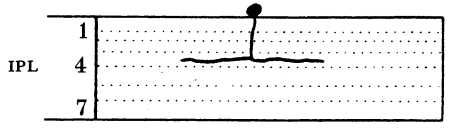

subtype: 19.4
level of stratification: 42–46 %
number of cells recorded: 6

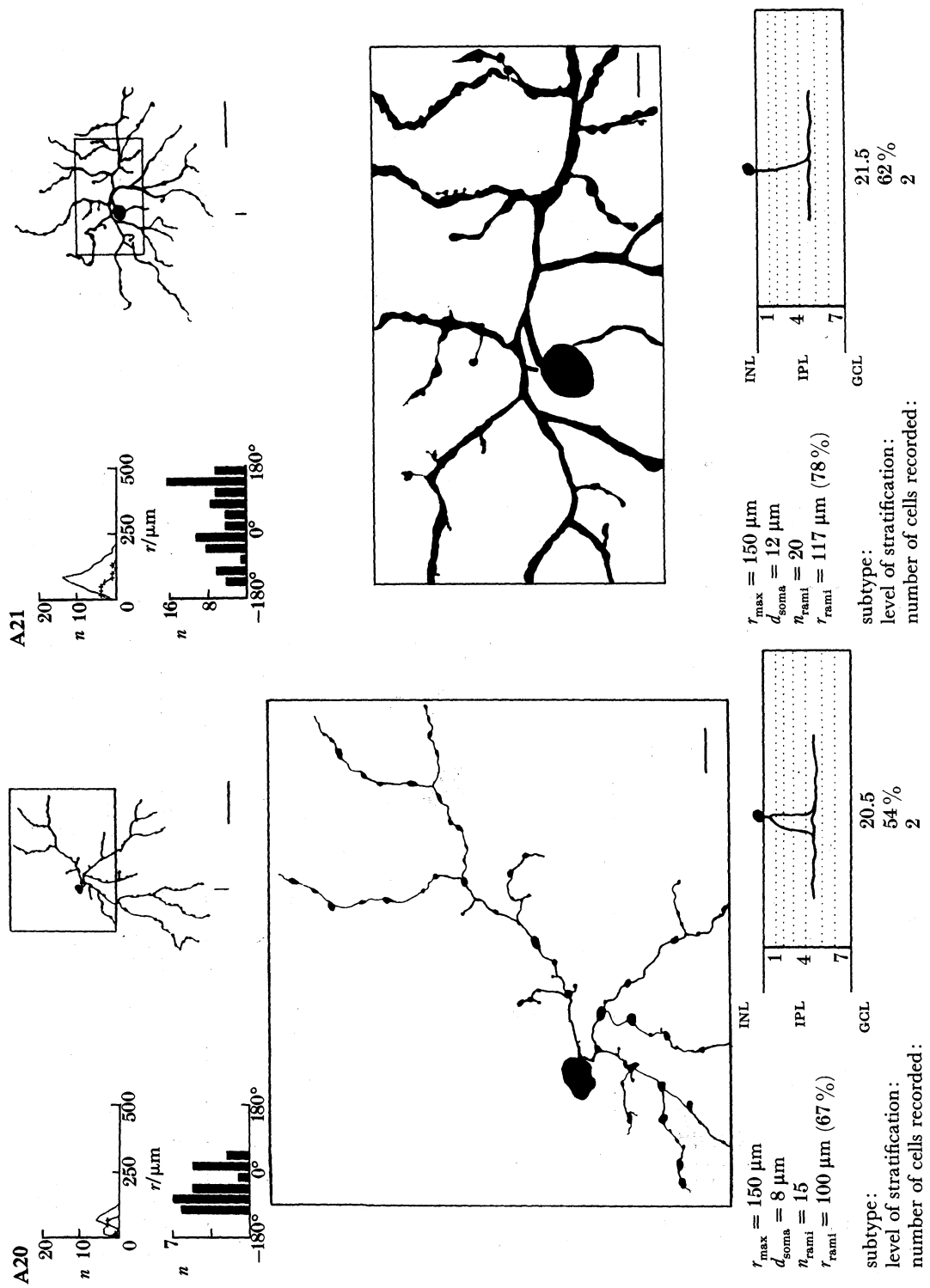
A20
A21
n
r/µm
−180°
0°
180°
INL
IPL
GCL
r_{max} = 150 µm
d_{soma} = 8 µm
n_{rami} = 15
r_{rami} = 100 µm (67%)
subtype: 20.5
level of stratification: 54%
number of cells recorded: 2
r_{max} = 150 µm
d_{soma} = 12 µm
n_{rami} = 20
r_{rami} = 117 µm (78%)
subtype: 21.5
level of stratification: 62%
number of cells recorded: 2

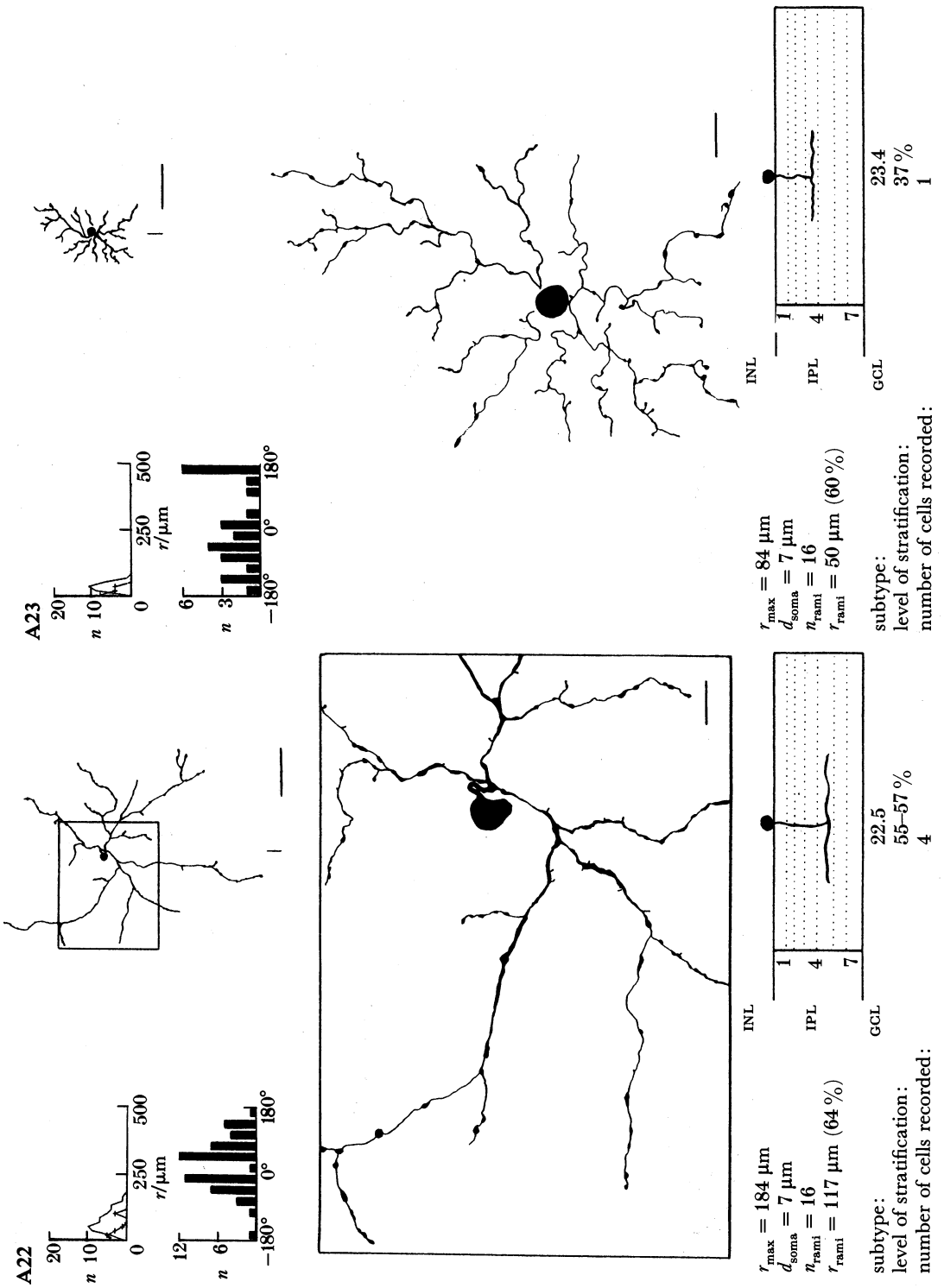
A22
A23
n
r/µm
0
250
500
20
10
12
6
3
−180°
0°
180°
INL
IPL
GCL
1
4
7
r_{max} = 184 µm
d_{soma} = 7 µm
n_{rami} = 16
r_{rami} = 117 µm (64 %)
subtype: 22.5
level of stratification: 55–57 %
number of cells recorded: 4
r_{max} = 84 µm
d_{soma} = 7 µm
n_{rami} = 16
r_{rami} = 50 µm (60 %)
subtype: 23.4
level of stratification: 37 %
number of cells recorded: 1

A24

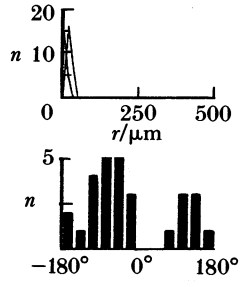

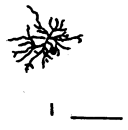

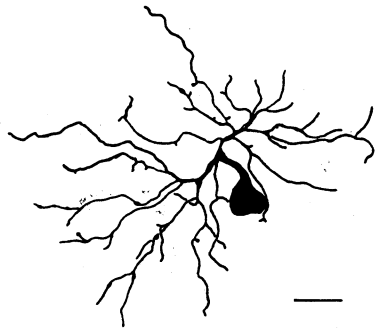

$r_{max} = 50$ µm
$d_{soma} = 7$ µm
$n_{rami} = 20$
$r_{rami} = 34$ µm (68 %)

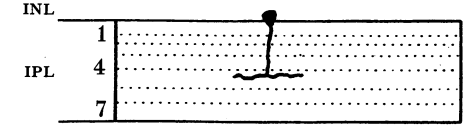

subtype: 24.5
level of stratification: 52 %
number of cells recorded: 1

A25

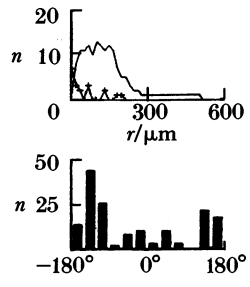

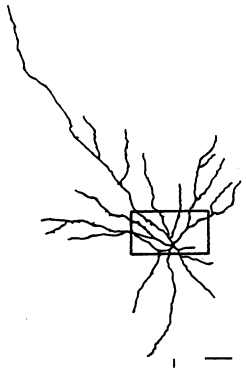

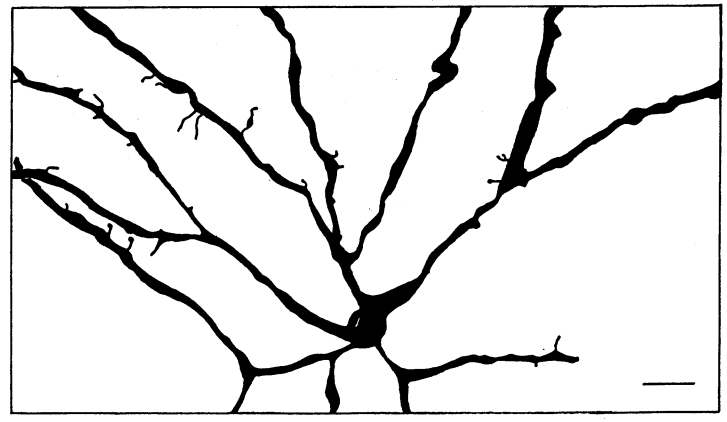

$r_{max} = 534$ µm
$d_{soma} = 7$ µm
$n_{rami} = 18$
$r_{rami} = 200$ µm (37 %)

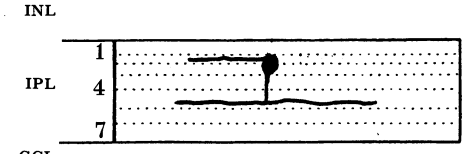

subtype: 25.2/5
level of stratification: 22/59–64 %
number of cells recorded: 1

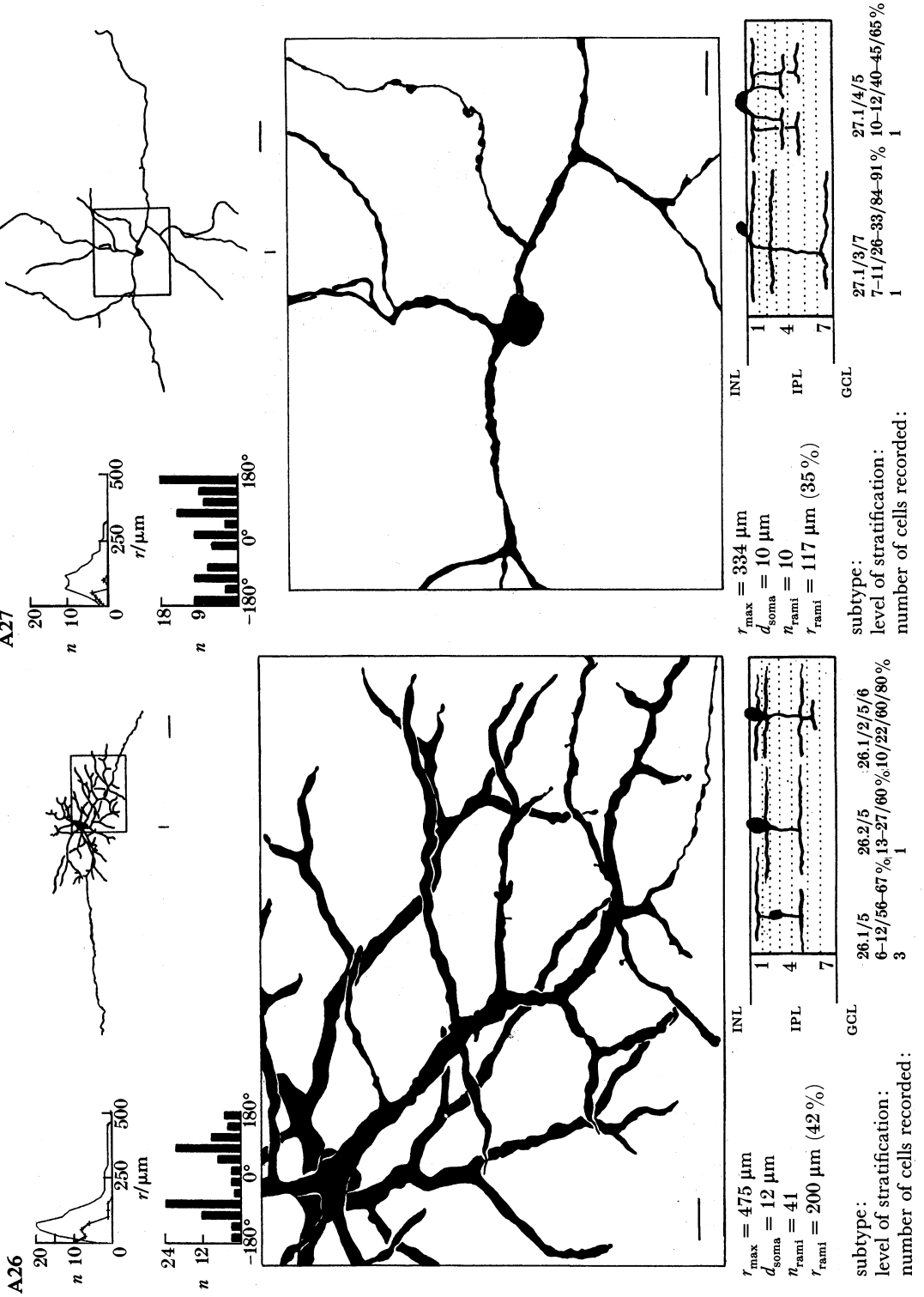
A26
A27
n
r/µm
−180° 0° 180°
INL
IPL
GCL
r_{max} = 475 µm
d_{soma} = 12 µm
n_{rami} = 41
r_{rami} = 200 µm (42 %)
r_{max} = 334 µm
d_{soma} = 10 µm
n_{rami} = 10
r_{rami} = 117 µm (35 %)
subtype:
level of stratification:
number of cells recorded:
26.1/5
6–12/56–67 %
3
26.2/5
13–27/60 %
1
26.1/2/5/6
10/22/60/80 %
27.1/3/7
7–11/26–33/84–91 %
1
27.1/4/5
10–12/40–45/65 %
1

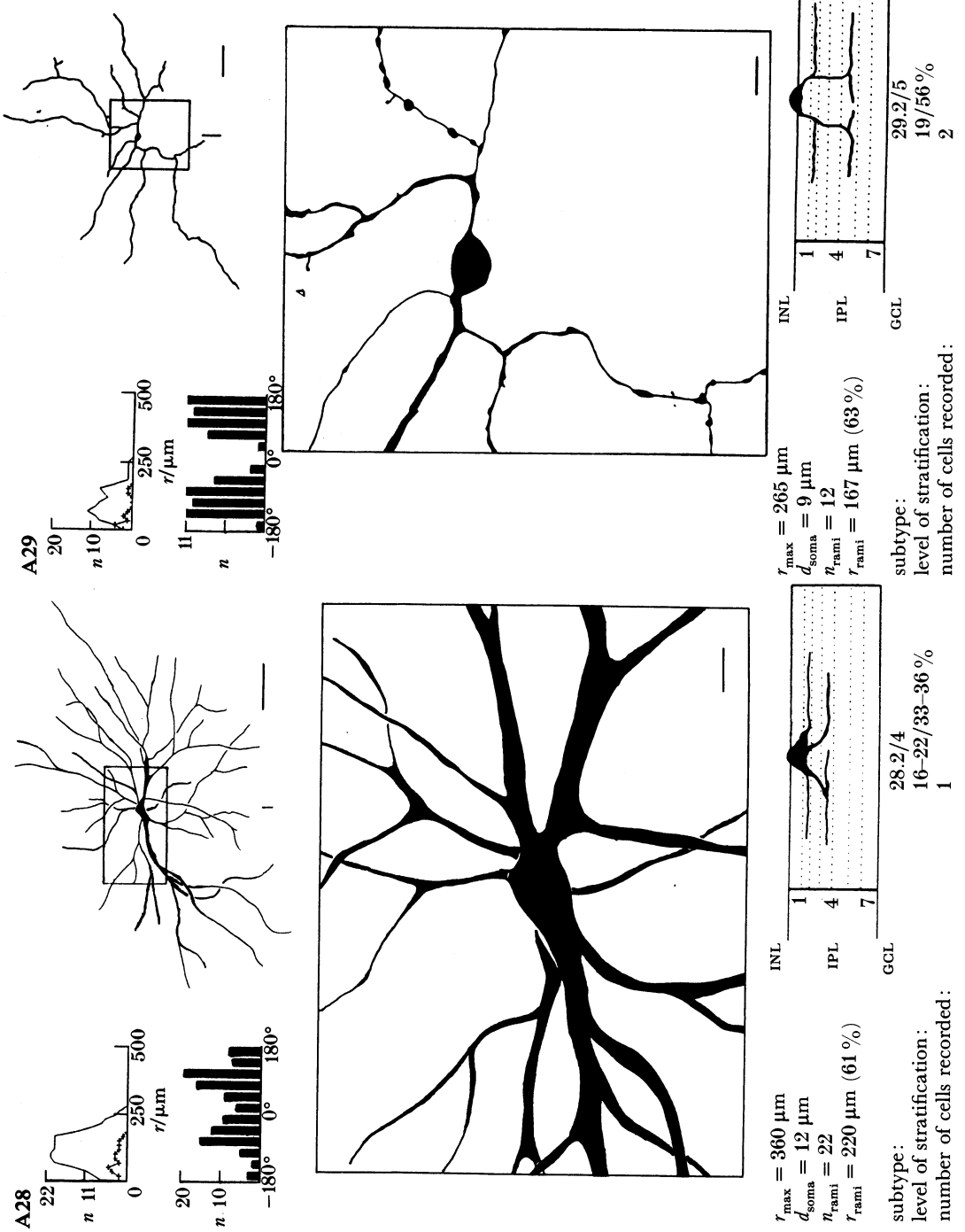
A28
A29
n
r/µm
−180°
0°
180°
INL
IPL
GCL
1
4
7
r_{max} = 360 µm
d_{soma} = 12 µm
n_{rami} = 22
r_{rami} = 220 µm (61 %)
subtype: 28.2/4
level of stratification: 16–22/33–36 %
number of cells recorded: 1
r_{max} = 265 µm
d_{soma} = 9 µm
n_{rami} = 12
r_{rami} = 167 µm (63 %)
subtype: 29.2/5
level of stratification: 19/56 %
number of cells recorded: 2

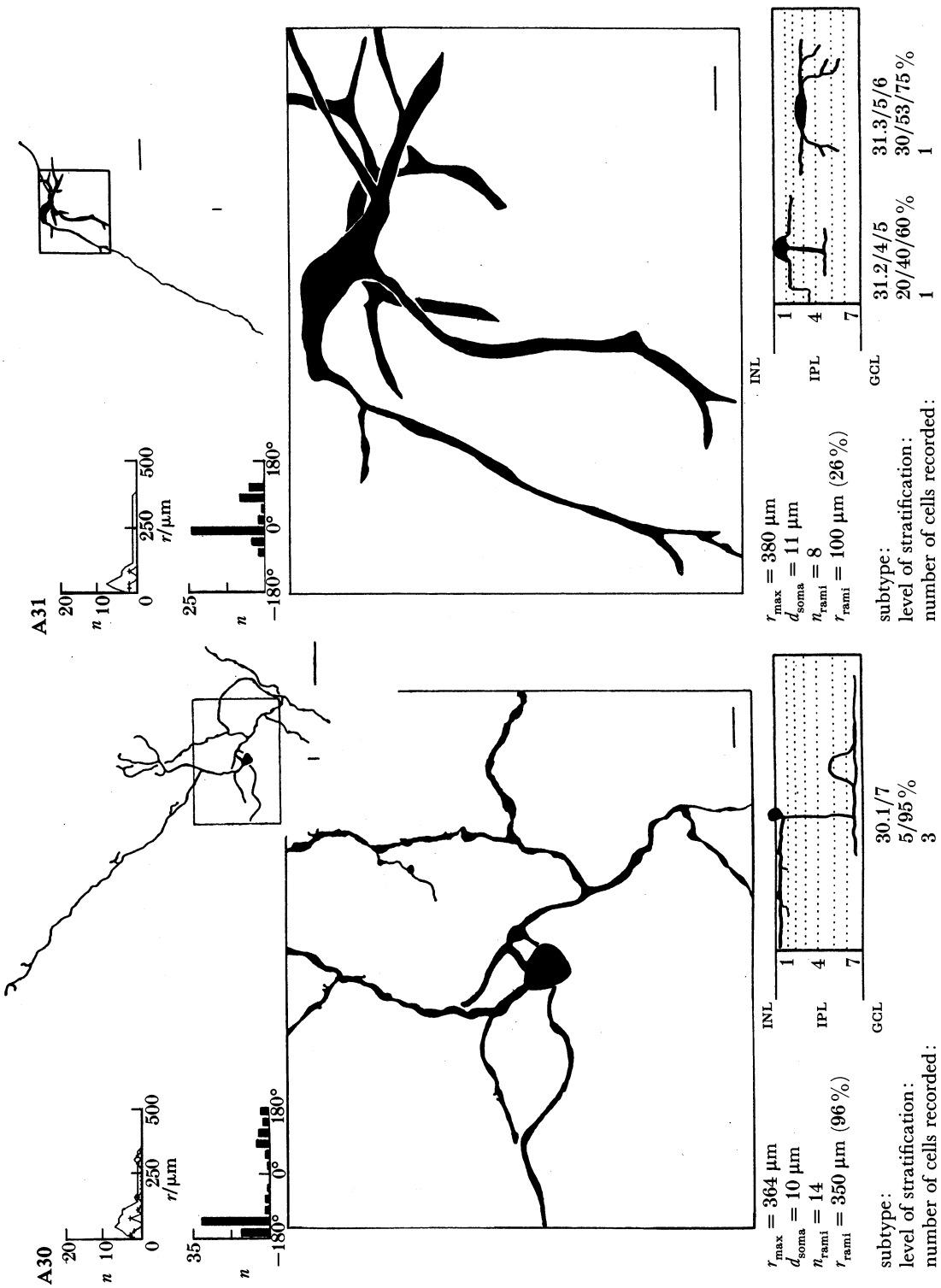
A30
A31
n
r/µm
0
250
500
20
10
35
25
−180°
0°
180°
INL
IPL
GCL
1
4
7
r_{max} = 364 µm
d_{soma} = 10 µm
n_{rami} = 14
r_{rami} = 350 µm (96 %)
subtype: 30.1/7
level of stratification: 5/95 %
number of cells recorded: 3
r_{max} = 380 µm
d_{soma} = 11 µm
n_{rami} = 8
r_{rami} = 100 µm (26 %)
subtype: 31.2/4/5
level of stratification: 20/40/60 %
number of cells recorded: 1
31.3/5/6
30/53/75 %
1

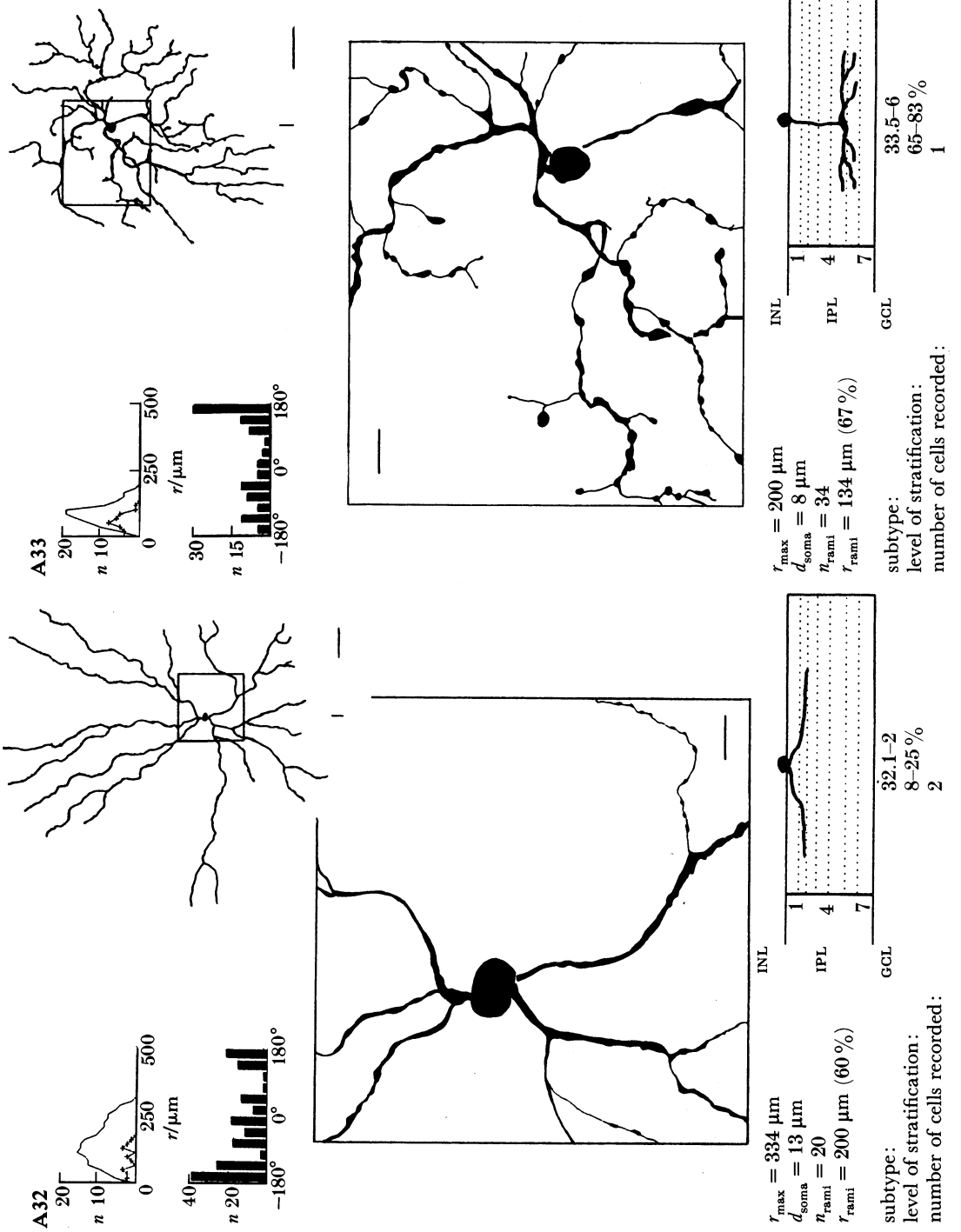
A32
A33
n
r/µm
−180°
0°
180°
INL
IPL
GCL
1
4
7
r_{max} = 334 µm
d_{soma} = 13 µm
n_{rami} = 20
r_{rami} = 200 µm (60%)
subtype: 32.1–2
level of stratification: 8–25%
number of cells recorded: 2
r_{max} = 200 µm
d_{soma} = 8 µm
n_{rami} = 34
r_{rami} = 134 µm (67%)
subtype: 33.5–6
level of stratification: 65–83%
number of cells recorded: 1

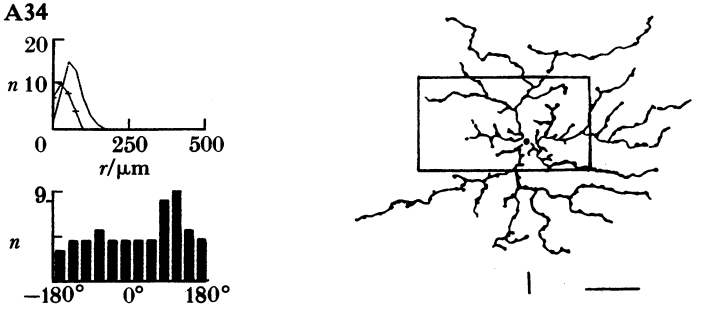

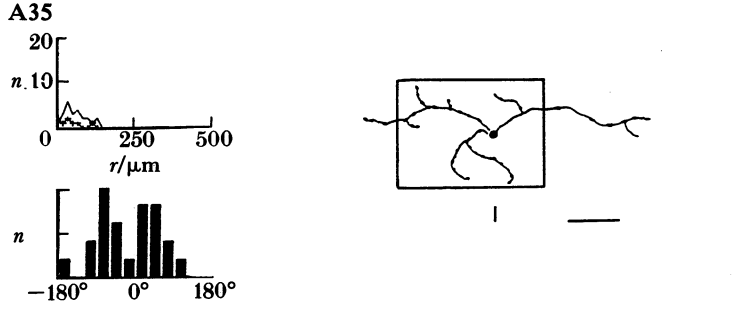

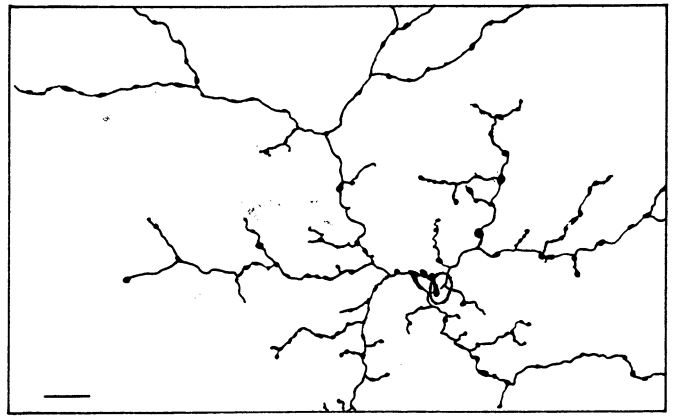

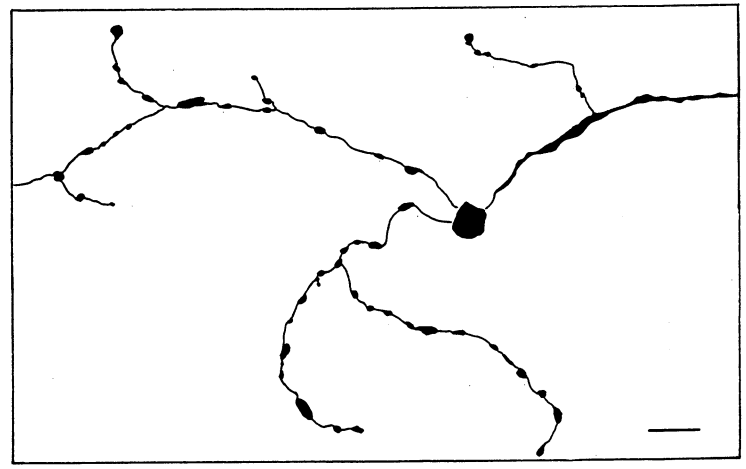

r_{max} = 175 µm
d_{soma} = /
n_{rami} = 29
r_{rami} = 100 µm (57 %)

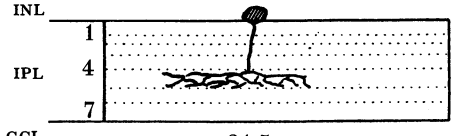

subtype: 34.5
level of stratification: 48–64 %
number of cells recorded: 1

r_{max} = 150 µm
d_{soma} = 9 µm
n_{rami} = 8
r_{rami} = 134 µm (89 %)

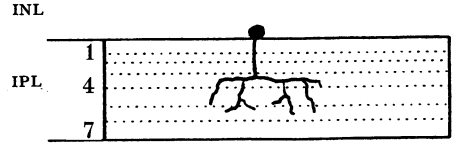

subtype: 35.4–6
level of stratification: 39–72 %
number of cells recorded: 4

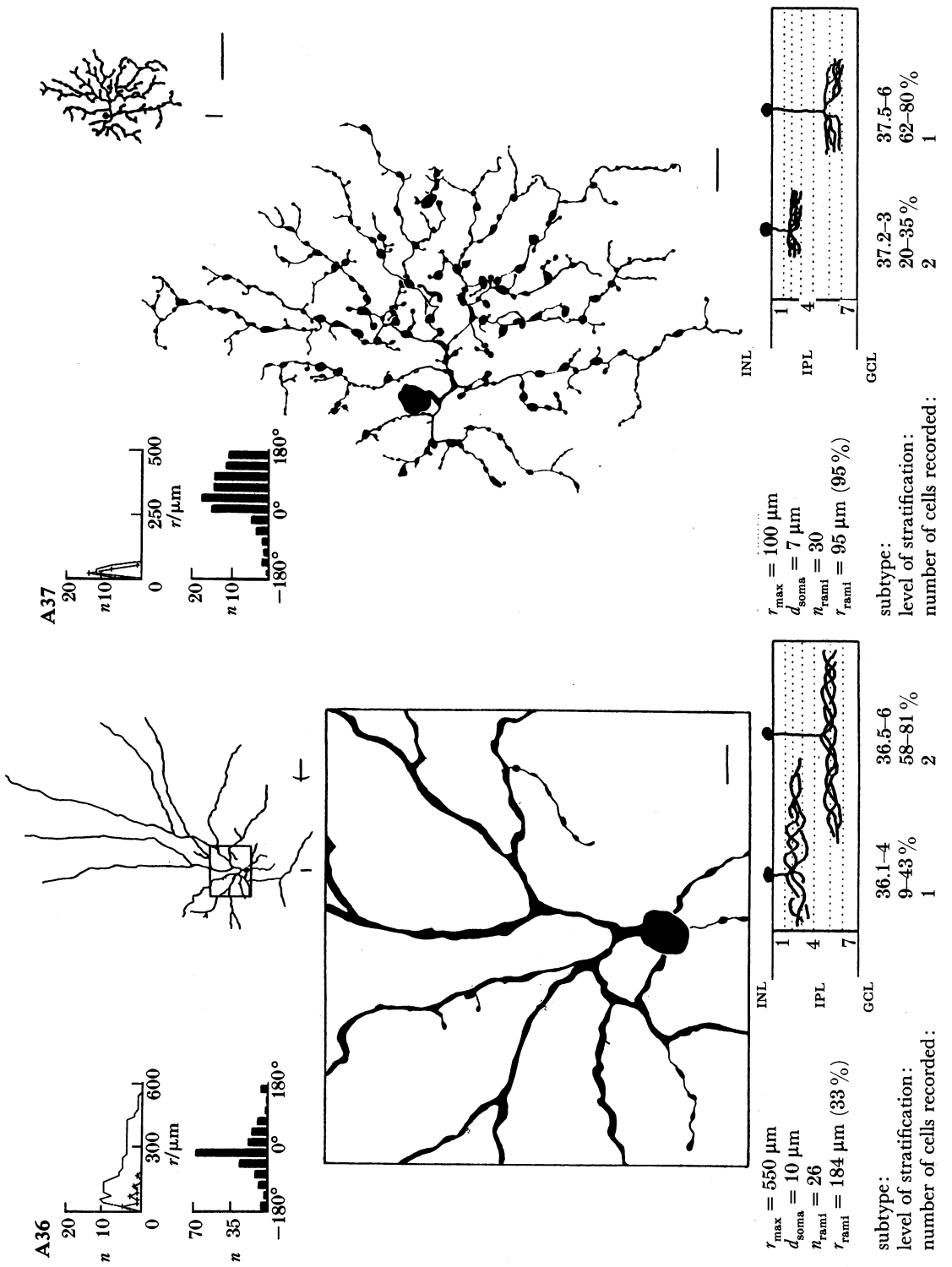
A36
A37
n
r/µm
−180°
0°
180°
INL
IPL
GCL
1
4
7
r_{max} = 550 µm
d_{soma} = 10 µm
n_{raml} = 26
r_{raml} = 184 µm (33 %)
r_{max} = 100 µm
d_{soma} = 7 µm
n_{raml} = 30
r_{raml} = 95 µm (95 %)
subtype: 36.1–4 36.5–6 37.2–3 37.5–6
level of stratification: 9–43 % 58–81 % 20–35 % 62–80 %
number of cells recorded: 1 2 2 1

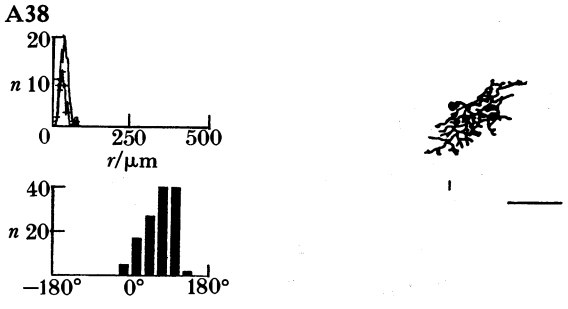

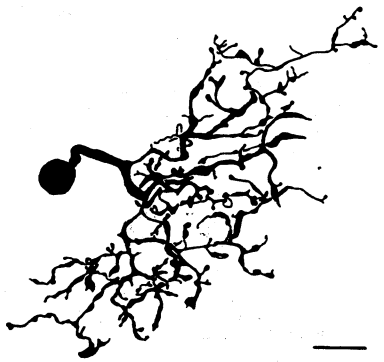

r_{max} = 83 µm
d_{soma} = 10 µm
n_{rami} = 71
r_{rami} = 80 µm (96 %)

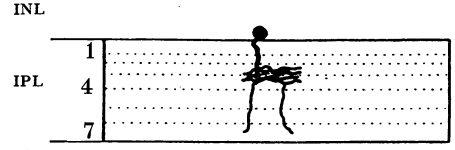

subtype: 38.3–4/7
level of stratification: 28–43/91 %
number of cells recorded: 4

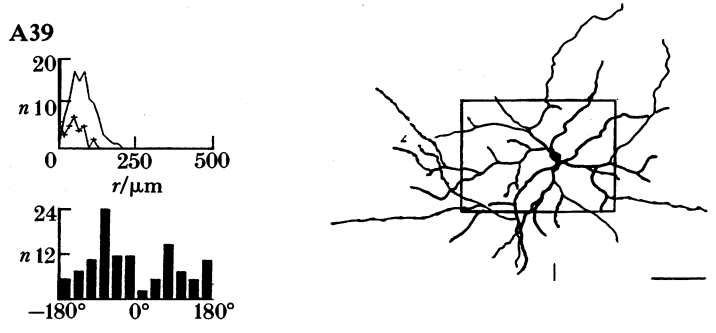

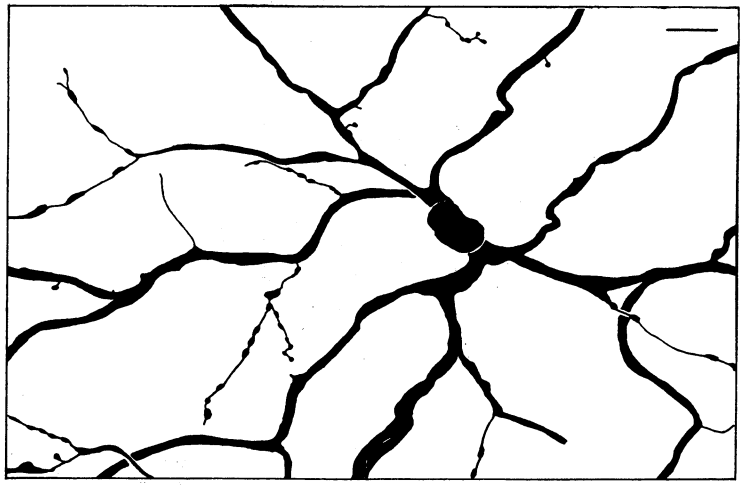

r_{max} = 330 µm
d_{soma} = 13 µm
n_{rami} = 24
r_{rami} = 180 µm (55 %)

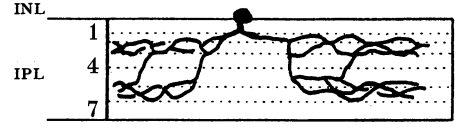

subtype: 39.2–3/5–6
level of stratification: 15–29/52–74 %
number of cells recorded: 1

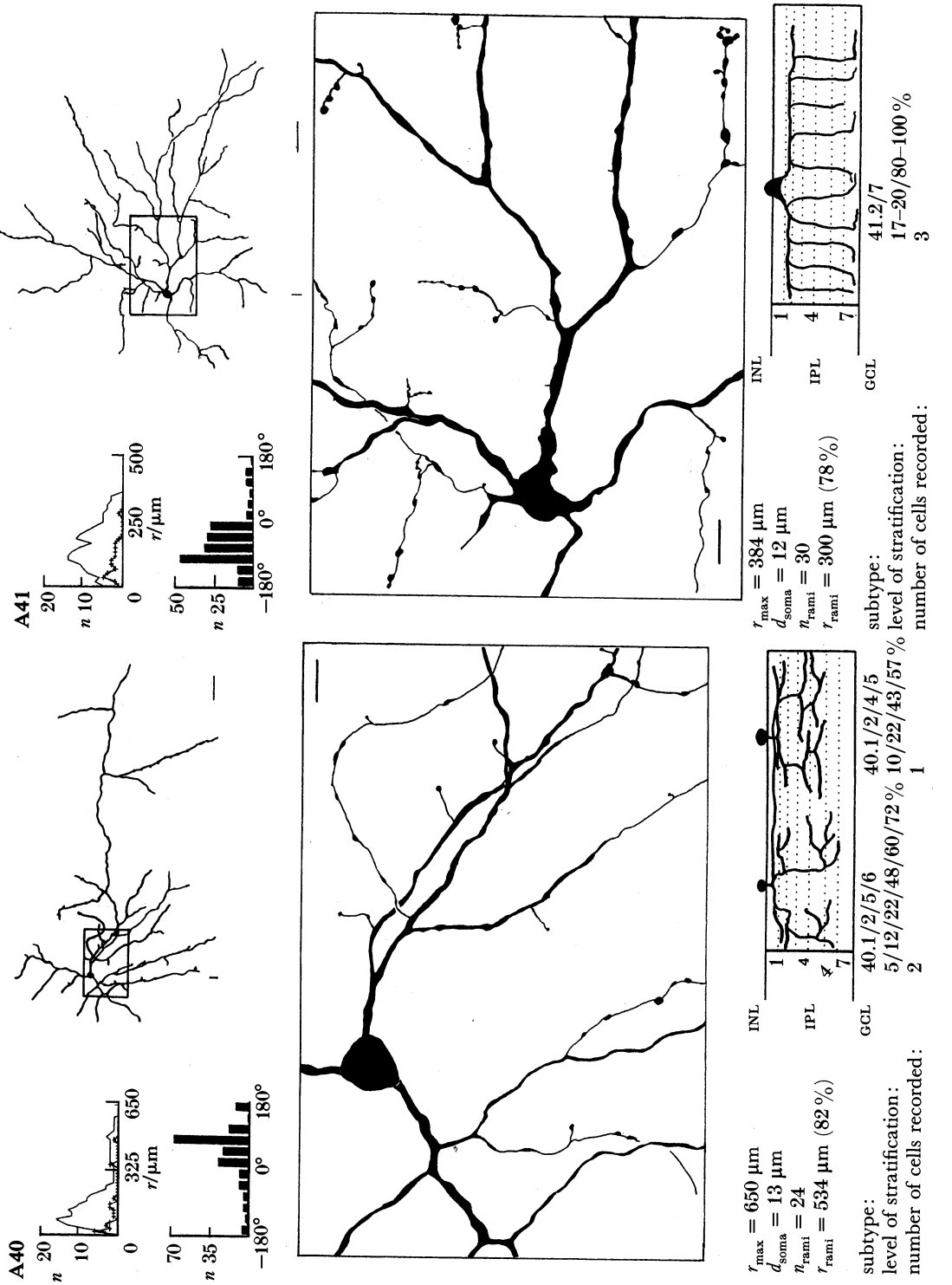
A40
A41
n
r/µm
INL
IPL
GCL
r_{max} = 650 µm
d_{soma} = 13 µm
n_{rami} = 24
r_{rami} = 534 µm (82 %)
r_{max} = 384 µm
d_{soma} = 12 µm
n_{rami} = 30
r_{rami} = 300 µm (78 %)
subtype: 40.1/2/5/6 40.1/2/4/5 41.2/7
level of stratification: 5/12/22/48/60/72 % 10/22/43/57 % 17–20/80–100 %
number of cells recorded: 2 1 3

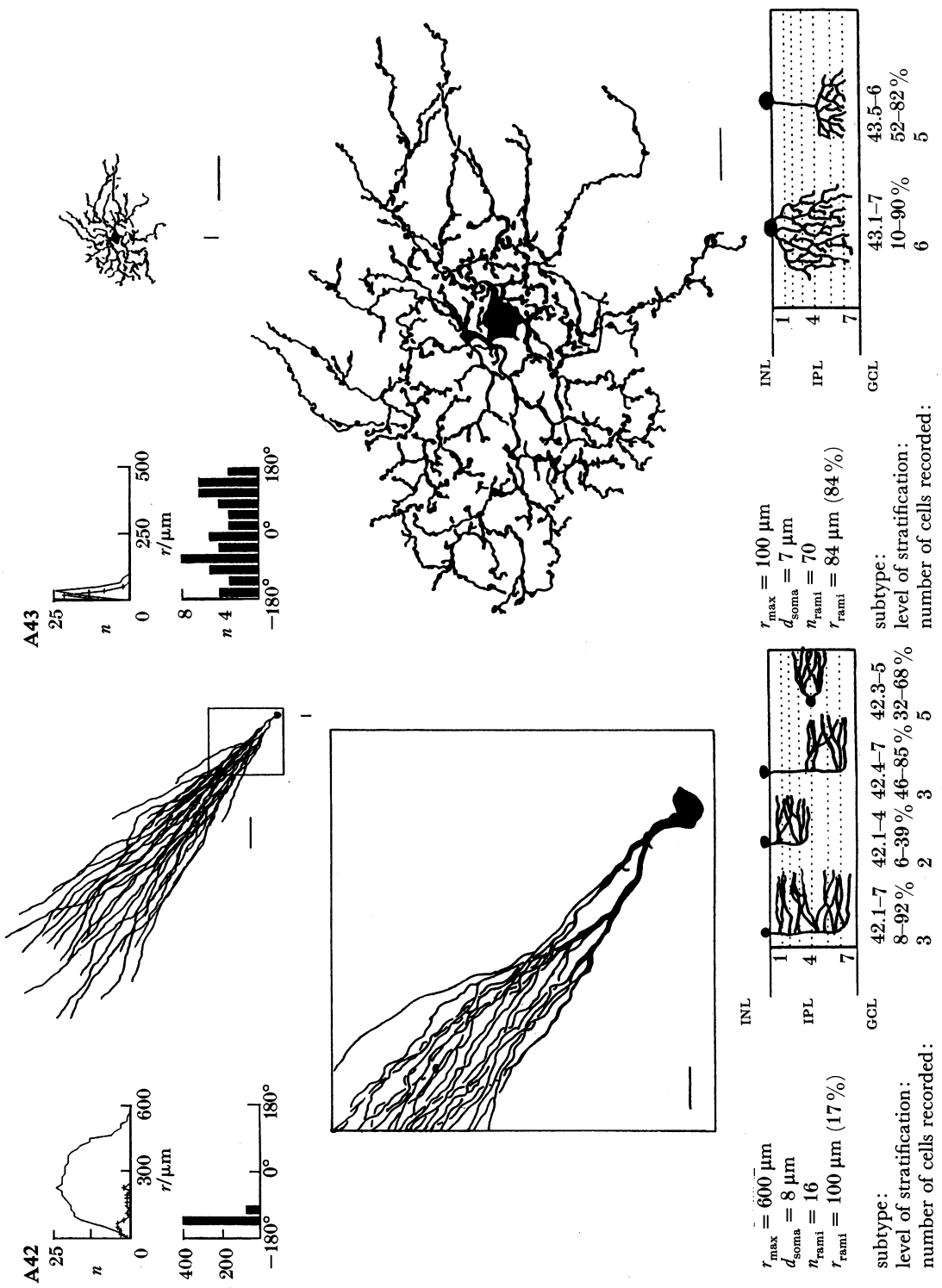
A42
A43
n
r/µm
INL
IPL
GCL
r_{max} = 600 µm
d_{soma} = 8 µm
n_{rami} = 16
r_{rami} = 100 µm (17 %)
r_{max} = 100 µm
d_{soma} = 7 µm
n_{rami} = 70
r_{rami} = 84 µm (84 %)
subtype:
level of stratification:
number of cells recorded:
8–92 % 6–39 % 46–85 % 32–68 %
42.1–7 42.1–4 42.4–7 42.3–5
43.1–7 43.5–6
10–90 % 52–82 %

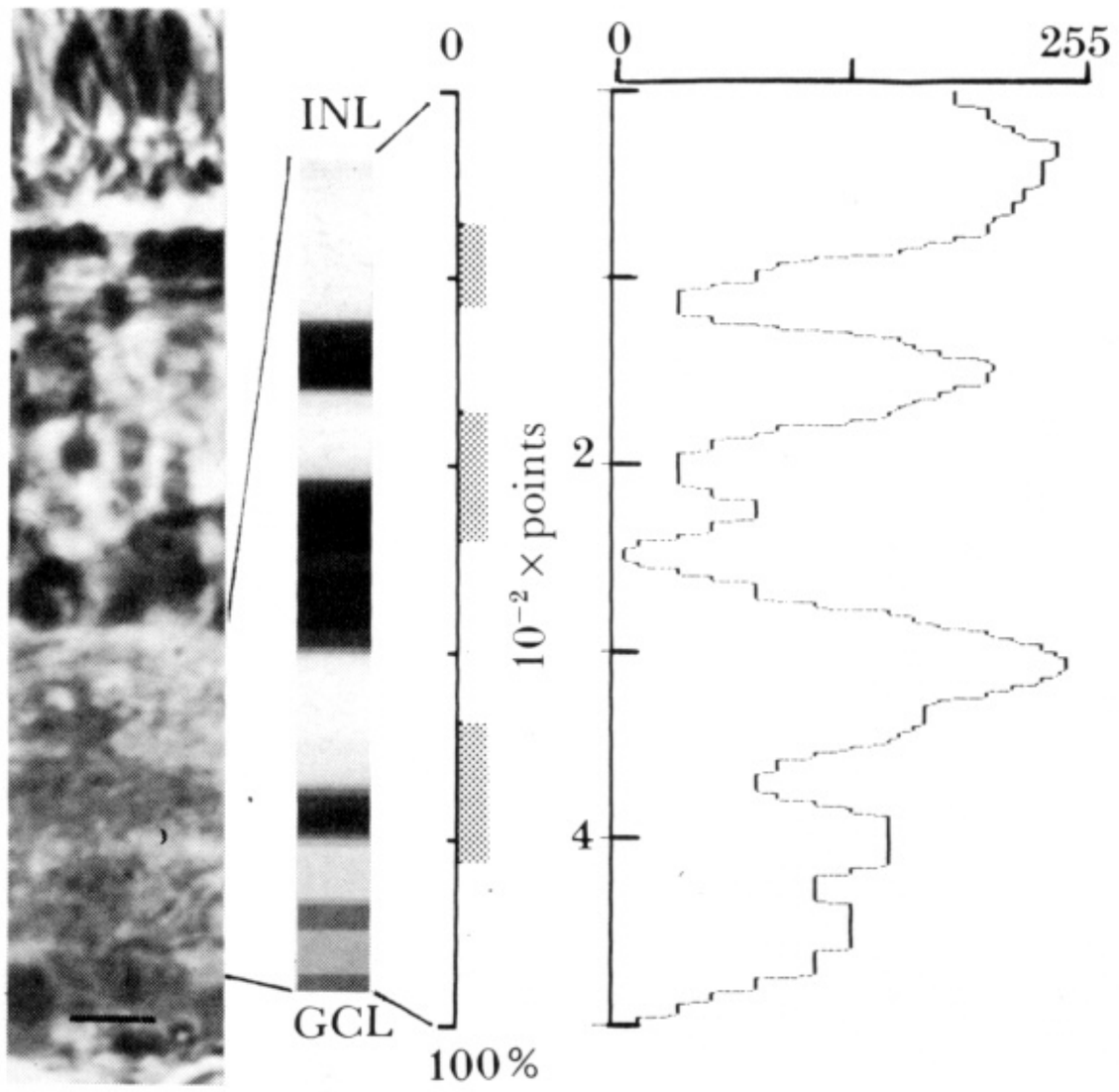

4

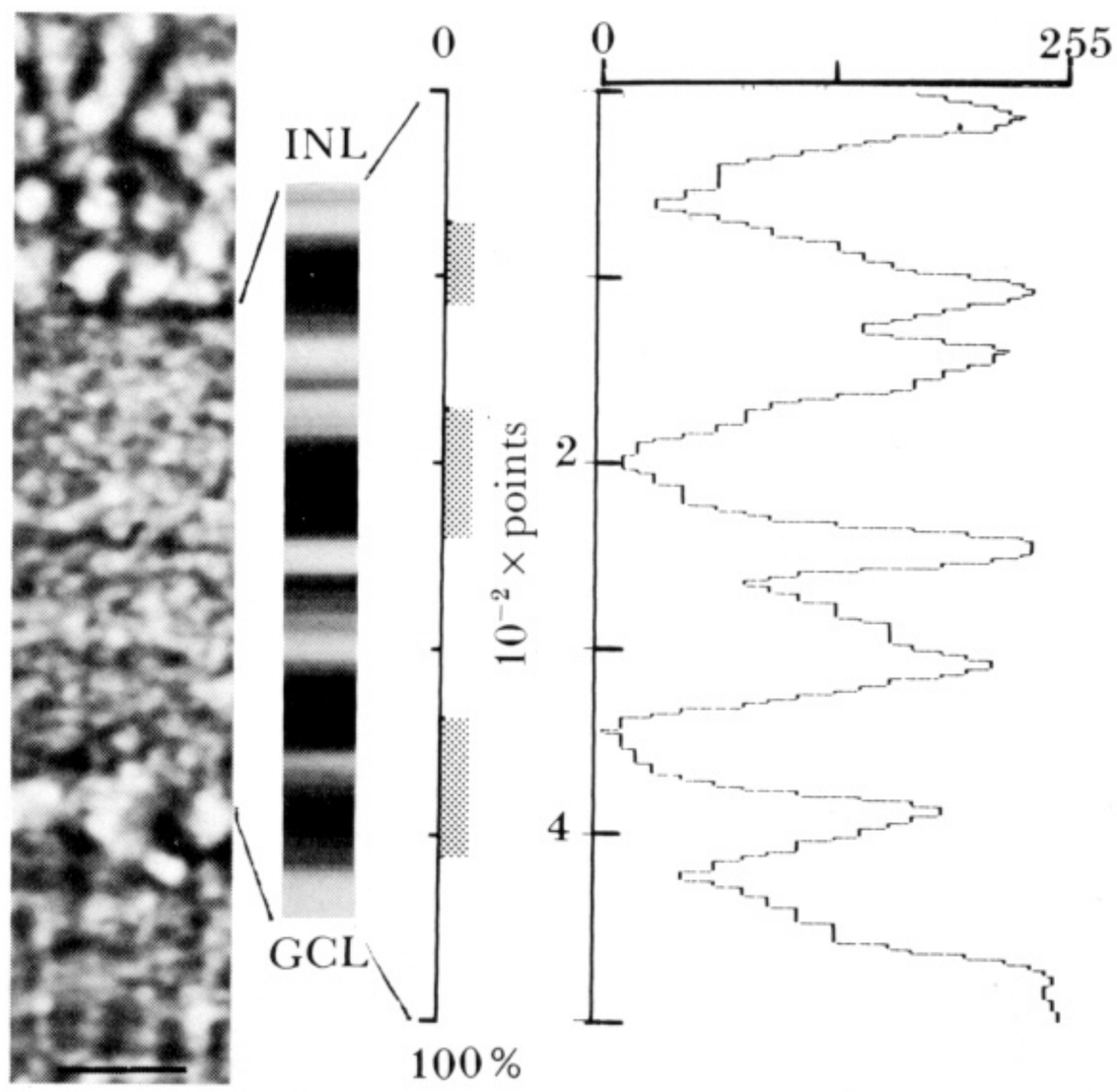

5

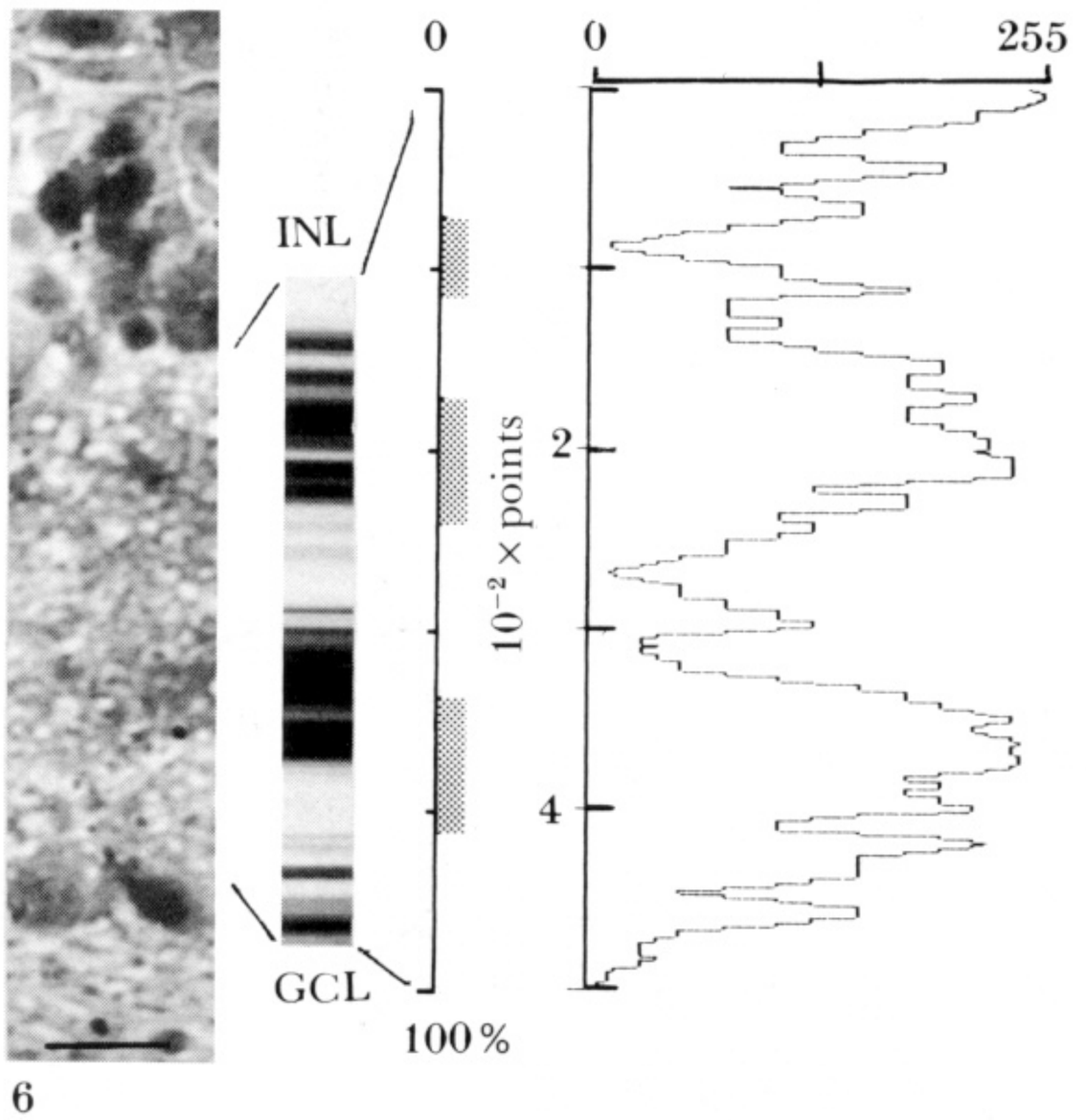

6

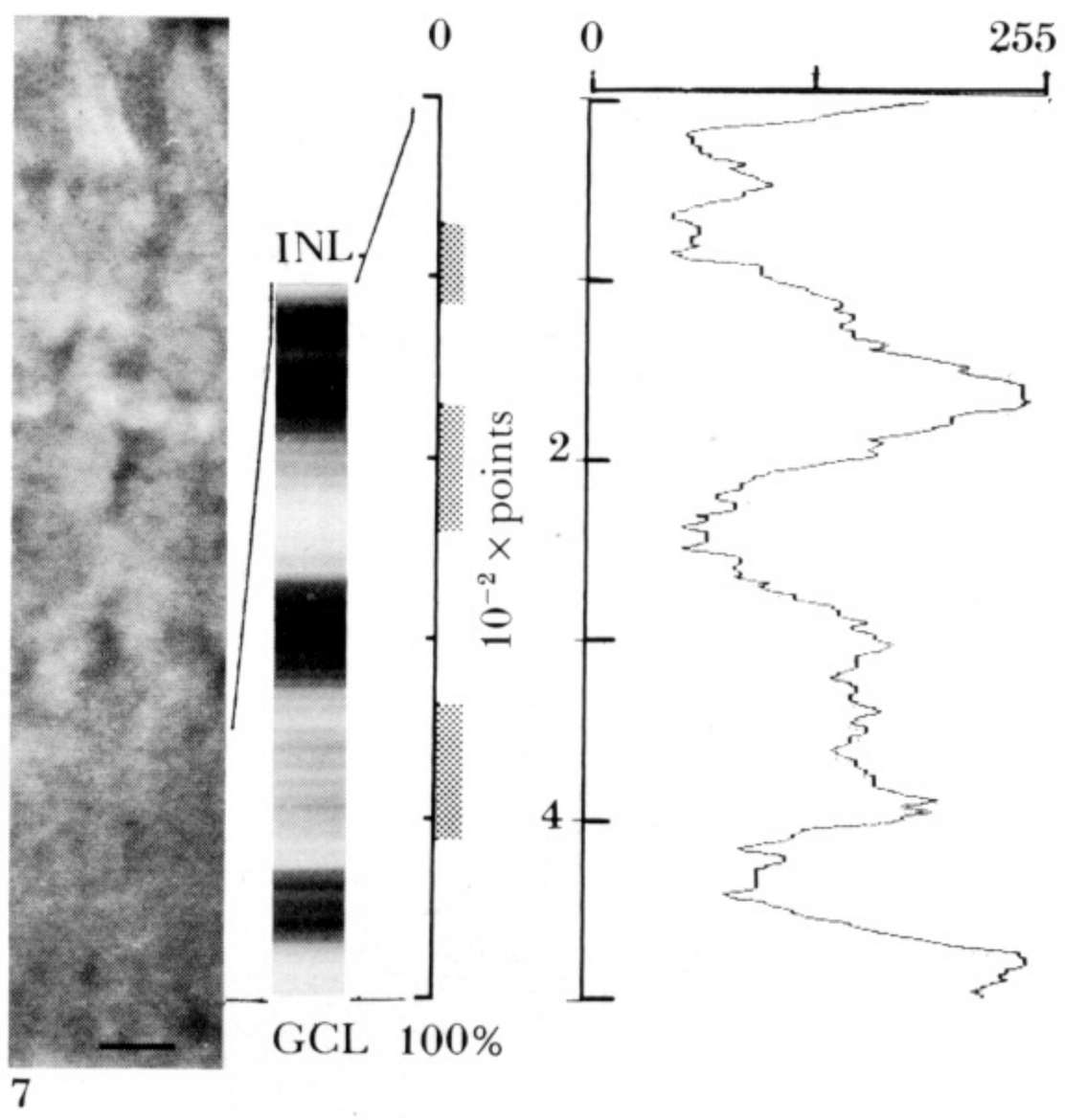

7

FIGURES 4–7. Densitometry of the inner plexiform layer in radial sections after various staining protocols. Each panel consists of a light micrograph of the inner plexiform layer (calibration bar 10 μm) which served as a basis for image analysis on the left; in the centre, the inner plexiform layer is shown after lowpass filtering and scaling of grey values; the densitometric scans through the processed images are shown on the right. Grey values are mapped from 0 (black) to 255 (white); the total width of the IPL is given as a percentage (0 indicates the outer border and 100 the border to the ganglion-cell bodies) and in a resolution of 500 points. (See text for details of the image analysis procedure.)

FIGURE 4. A 50 μm plastic section of Golgi-impregnated material in a region with no impregnated cells.

FIGURE 5. A 50 μm plastic section of control material after immunocytochemistry with the avidin–biotin–HRP visualizing system.

FIGURE 6. A 1 μm plastic section after staining with methylene blue.

FIGURE 7. A 5 μm cryostat section after incubation with rhodaminyl phalloidin for demonstration of F-actin.

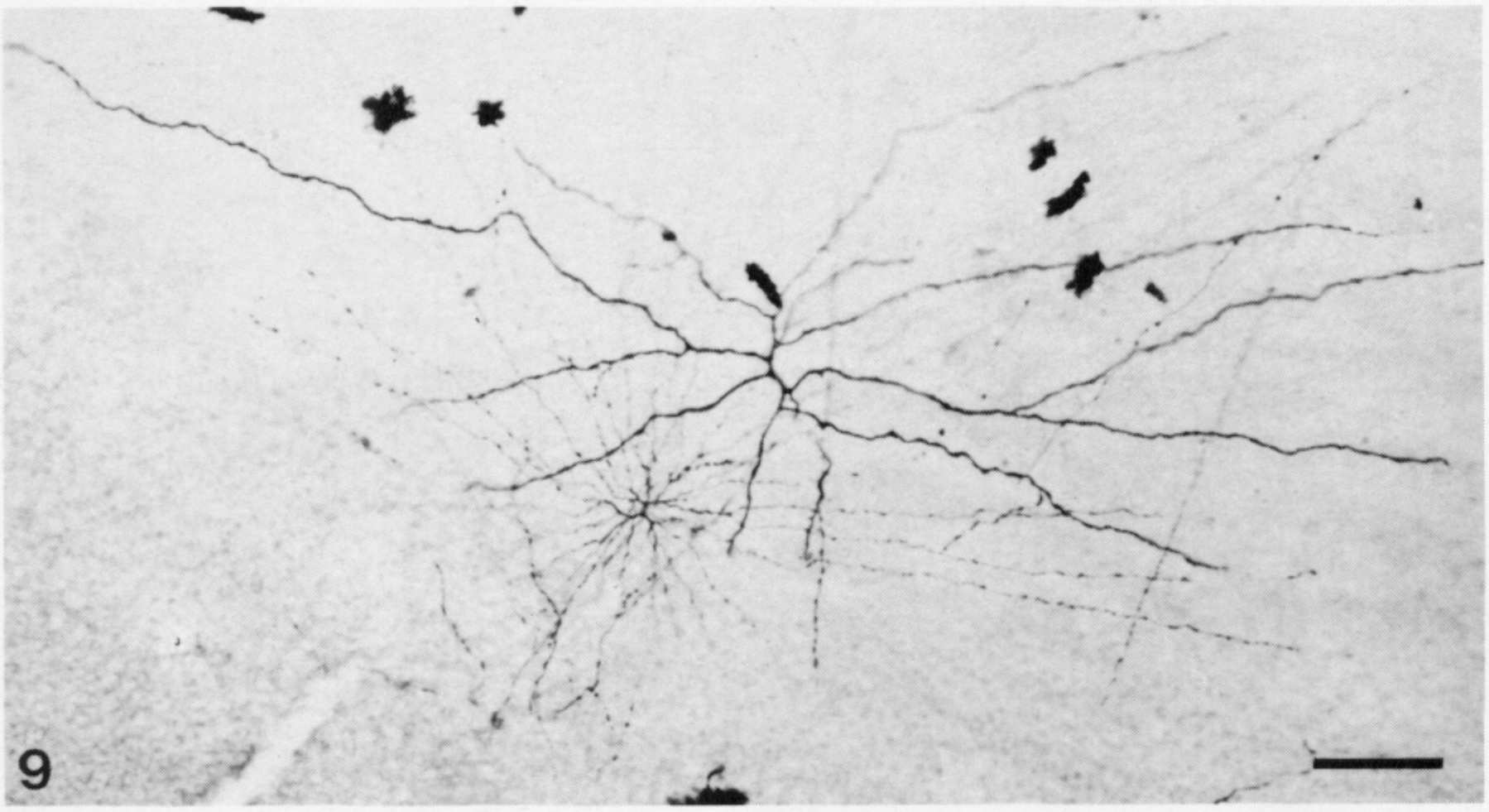

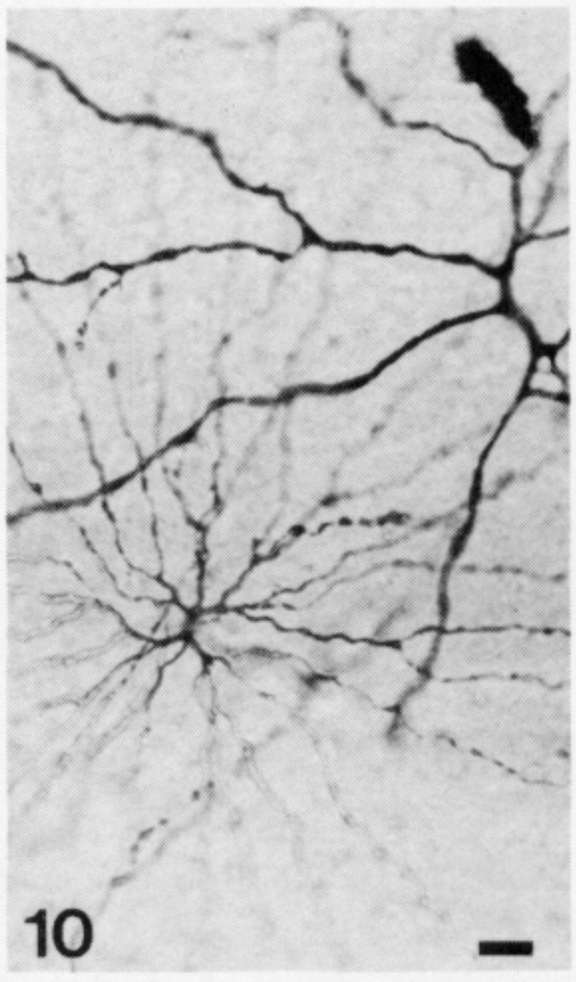

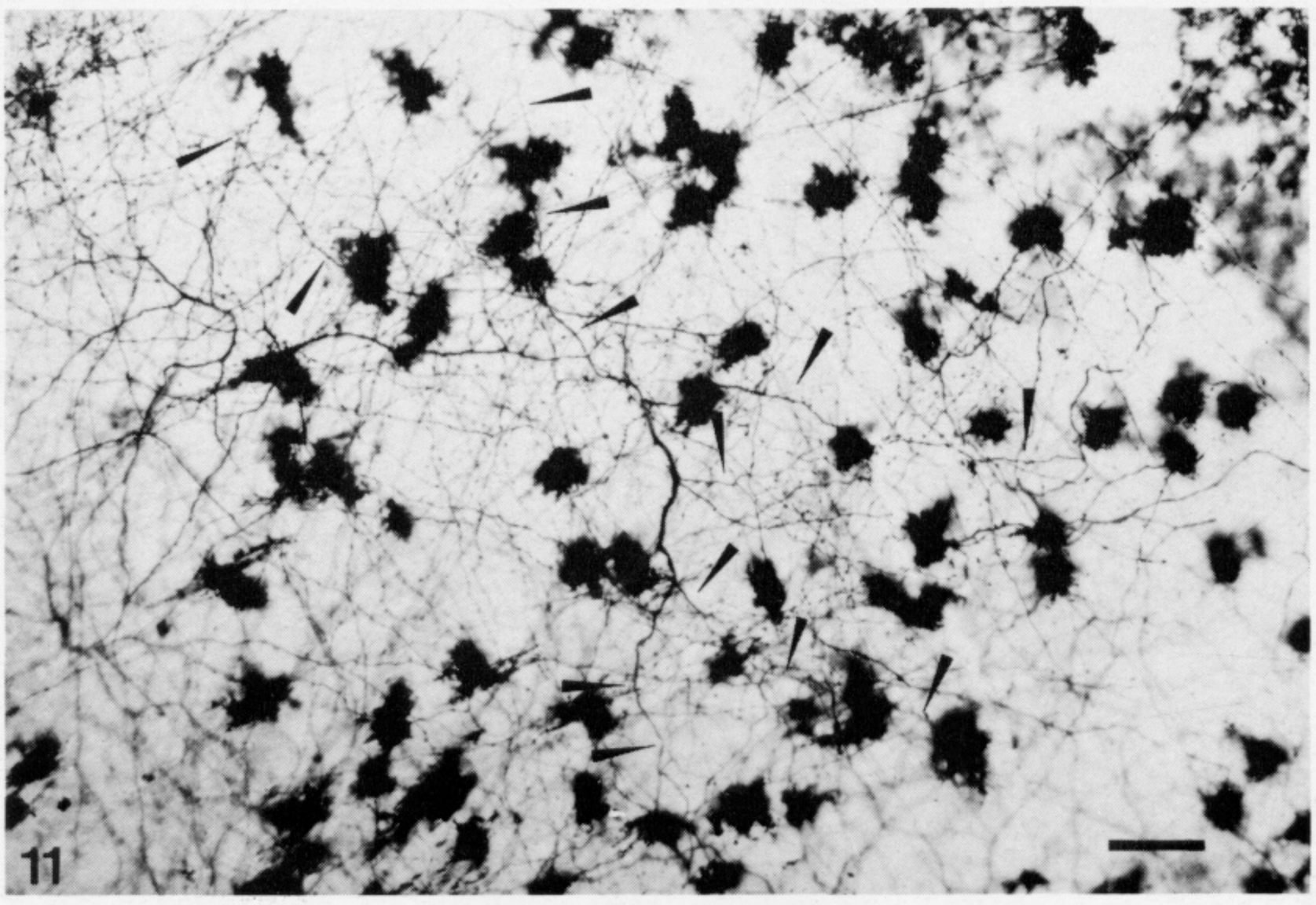

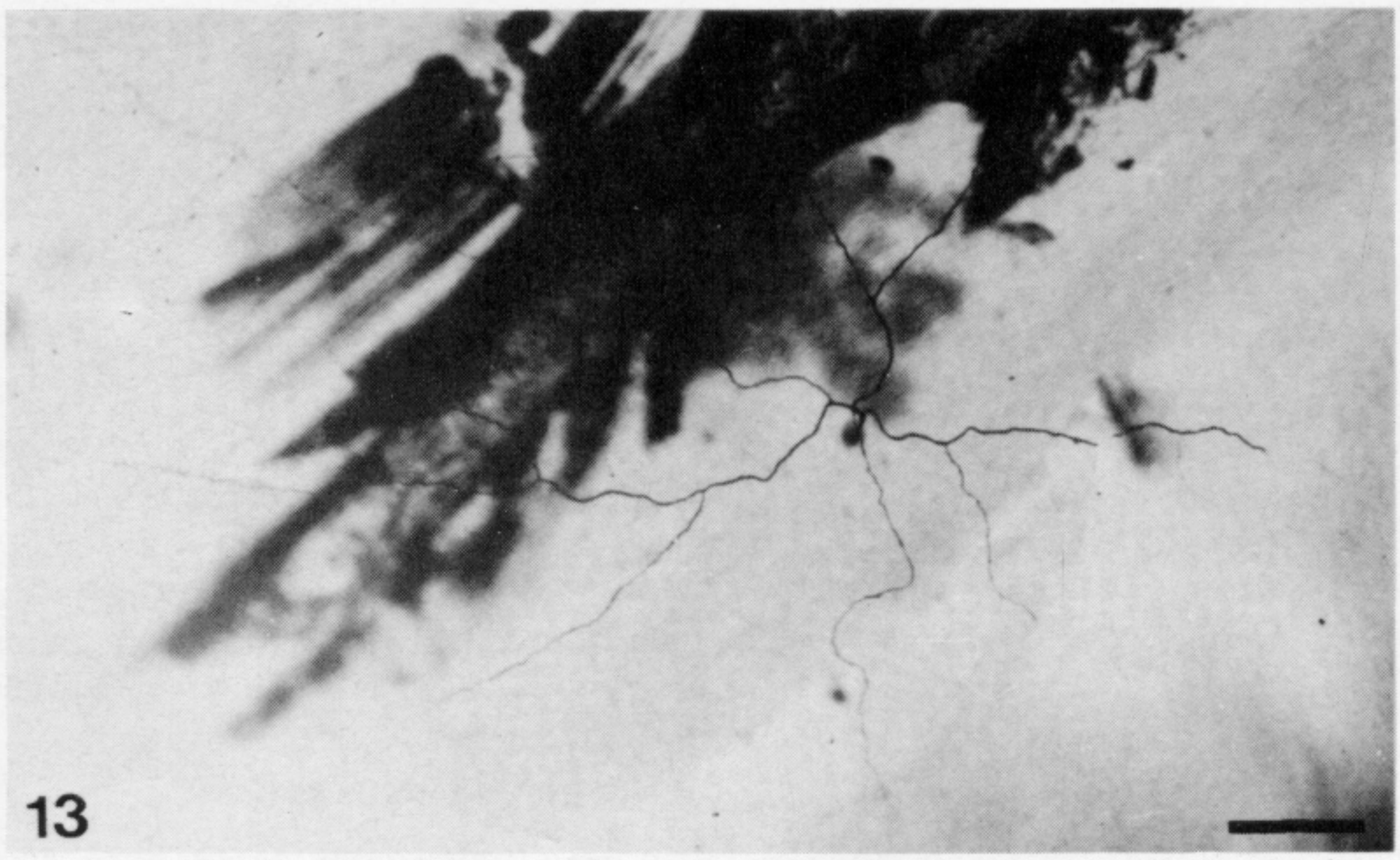

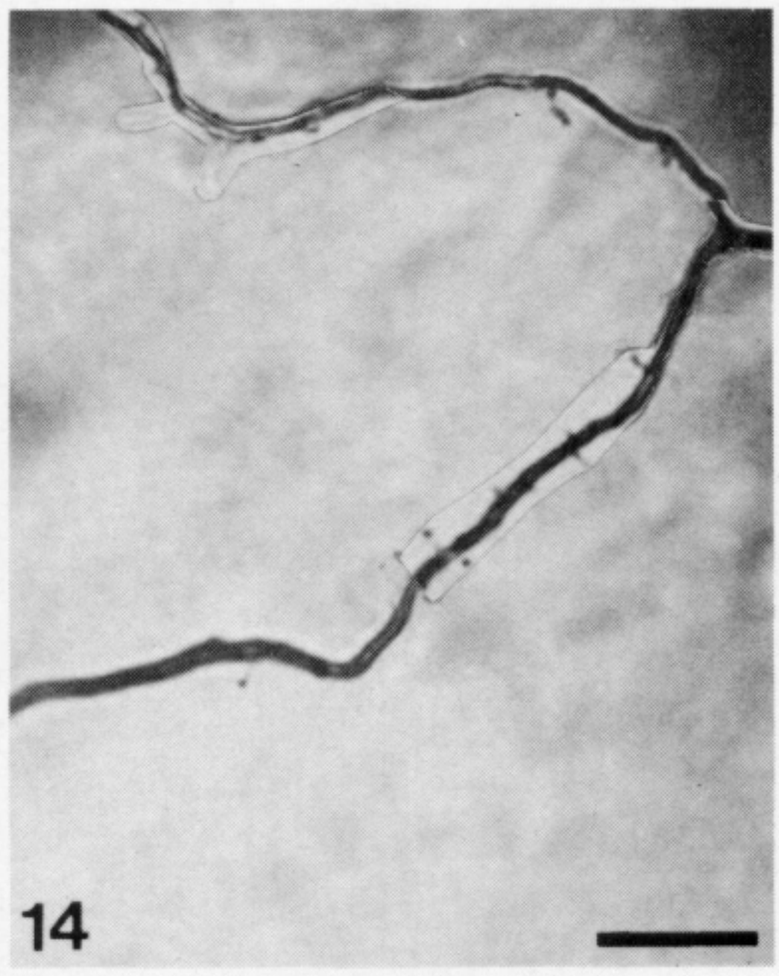

FIGURES 9–14. For description see facing plate 4.

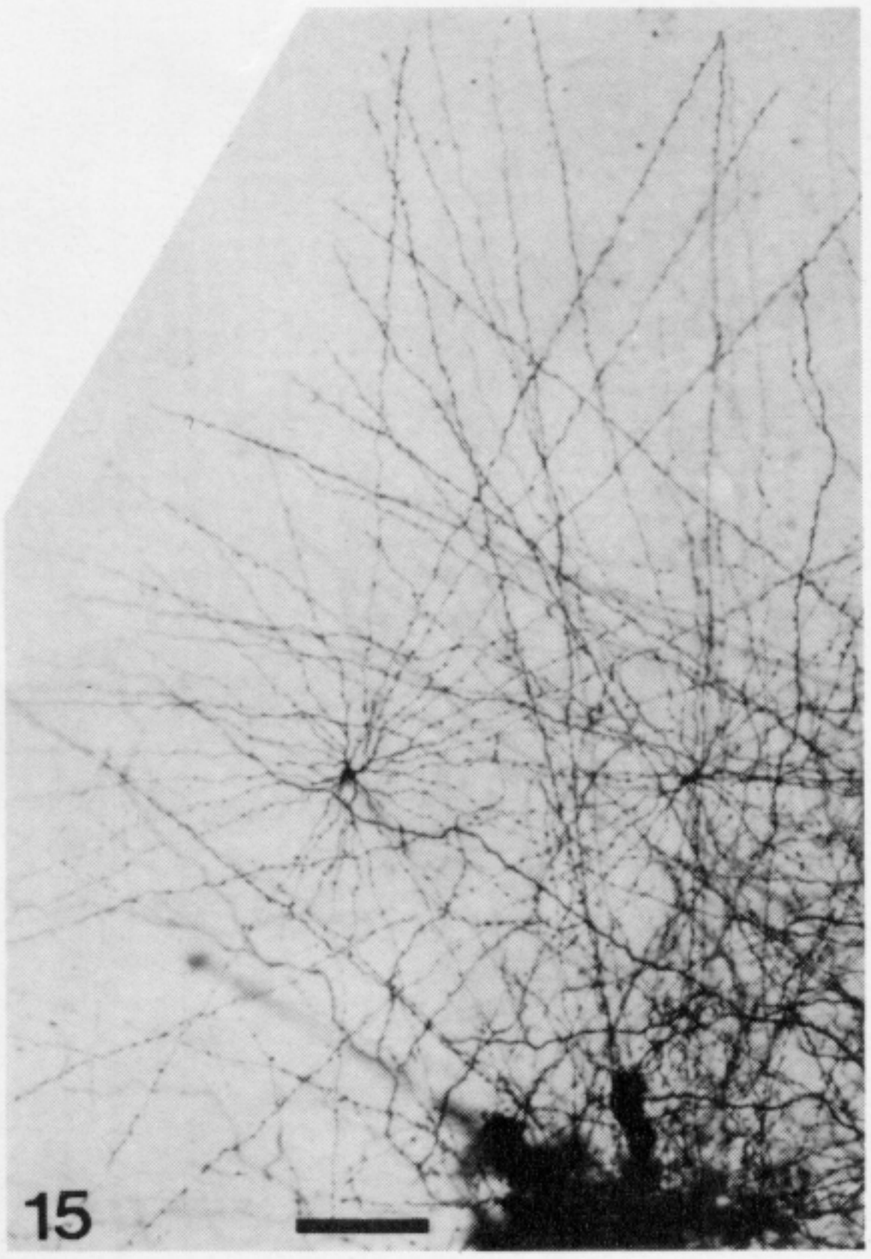

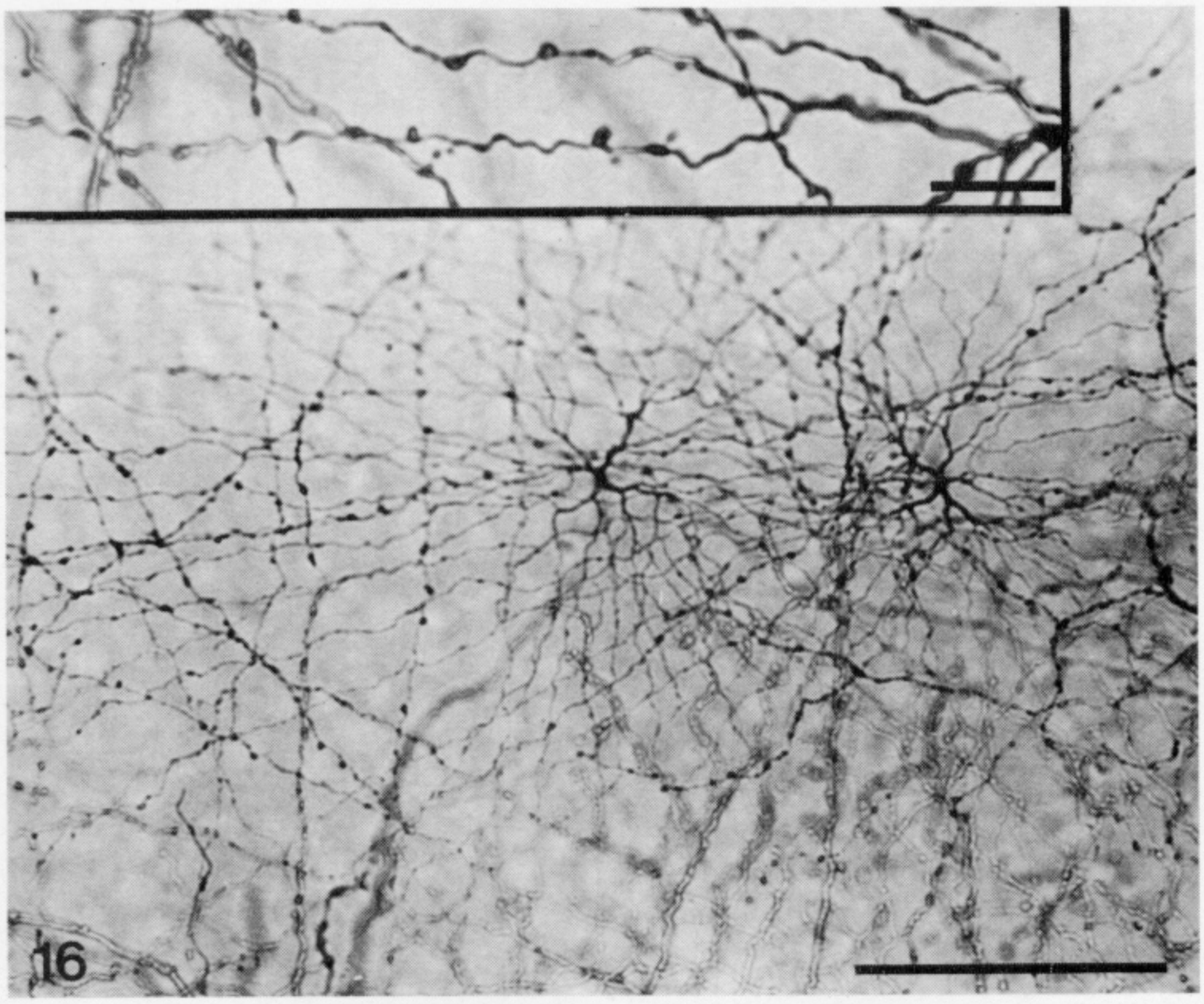

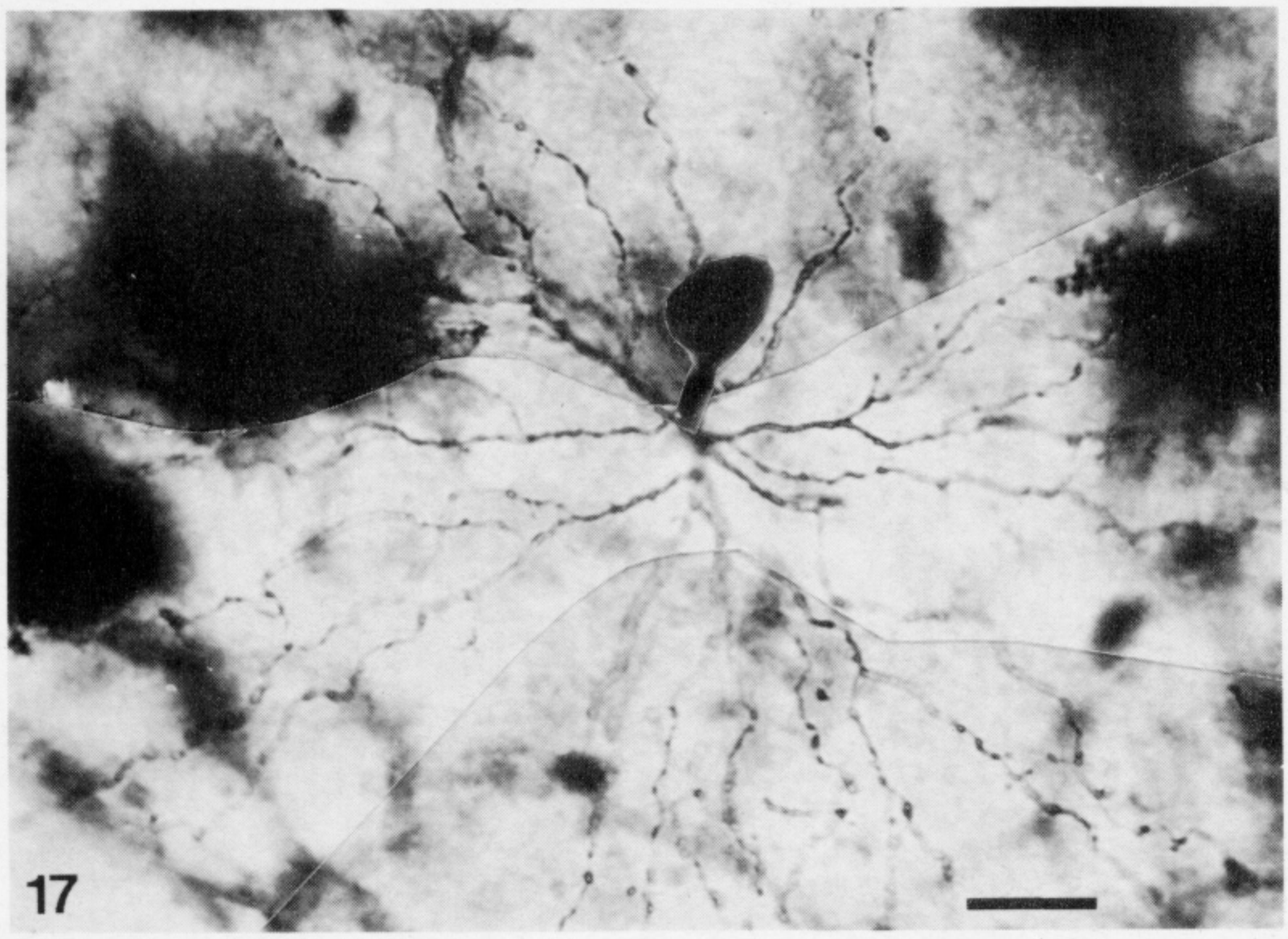

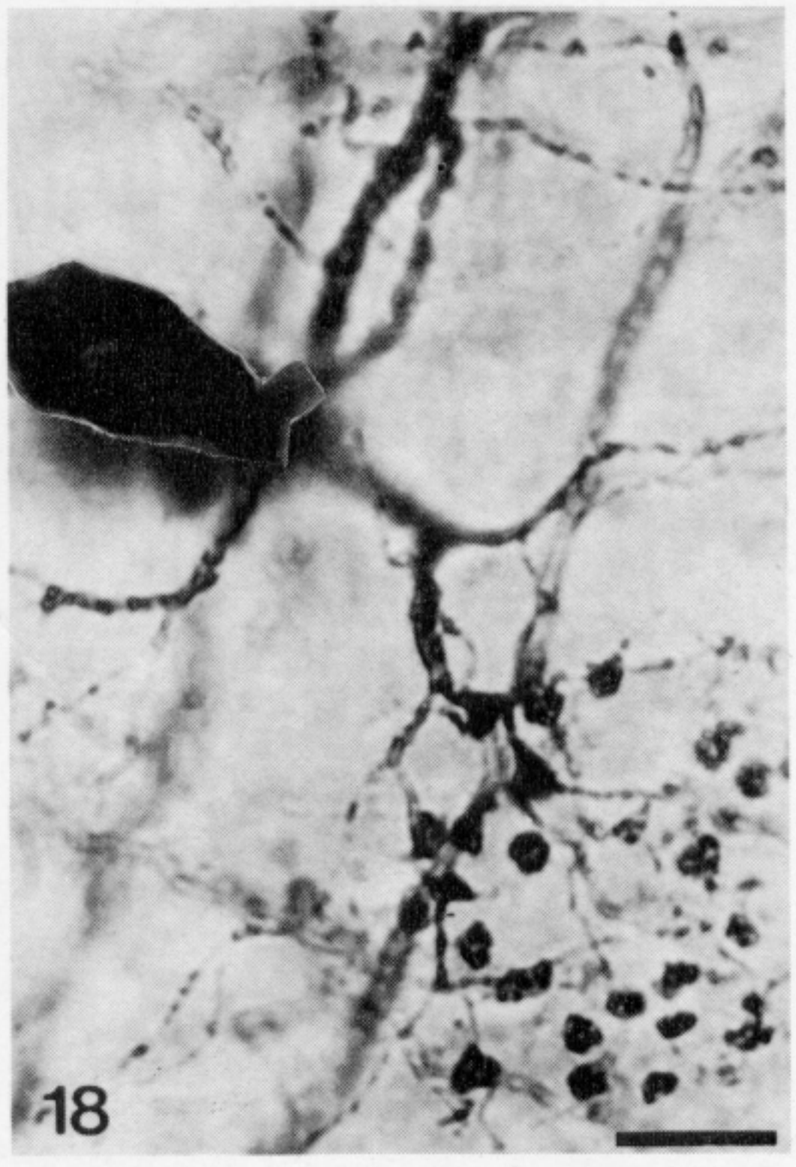

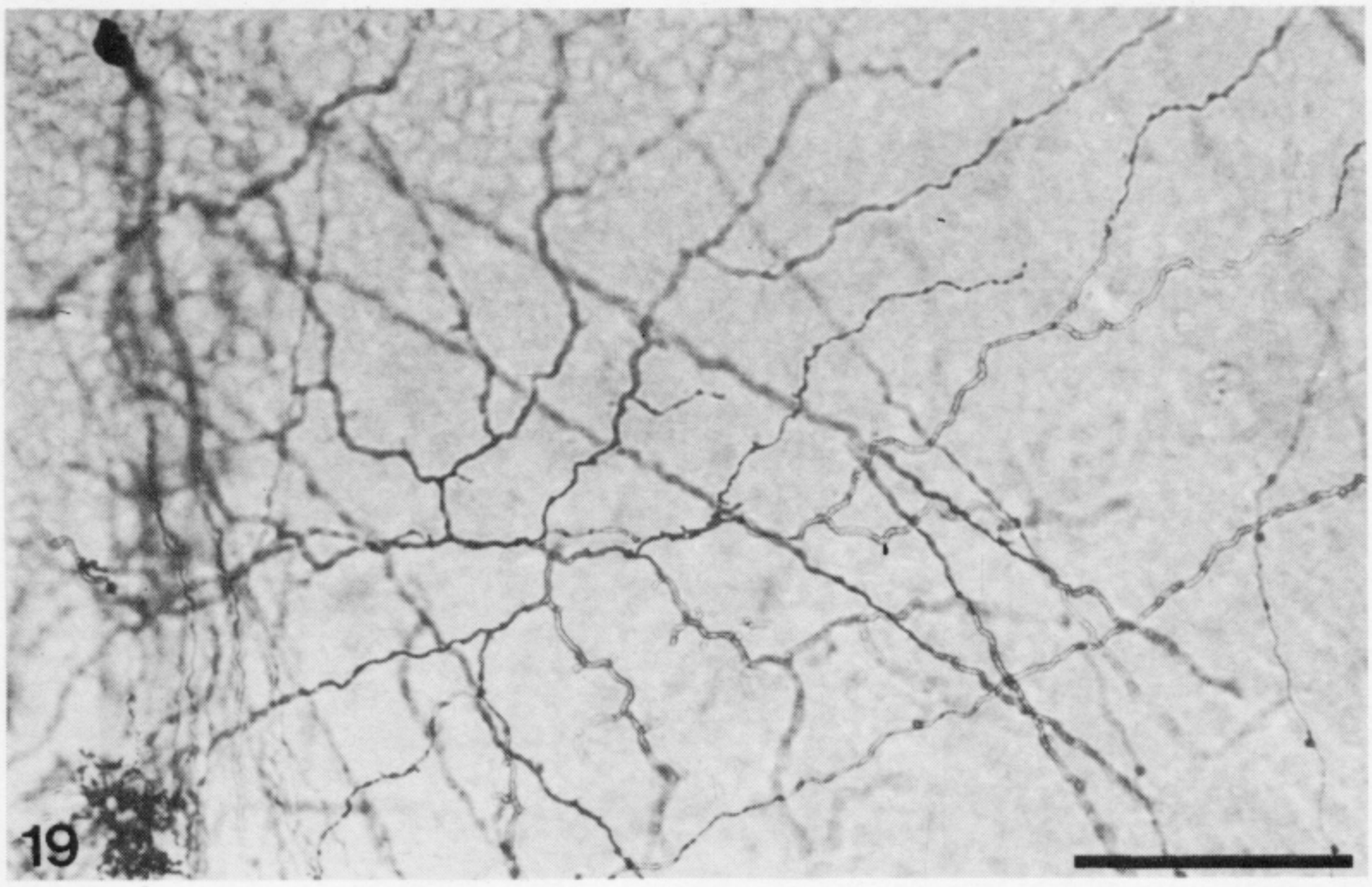

FIGURES 15–20. For description see facing plate 4.

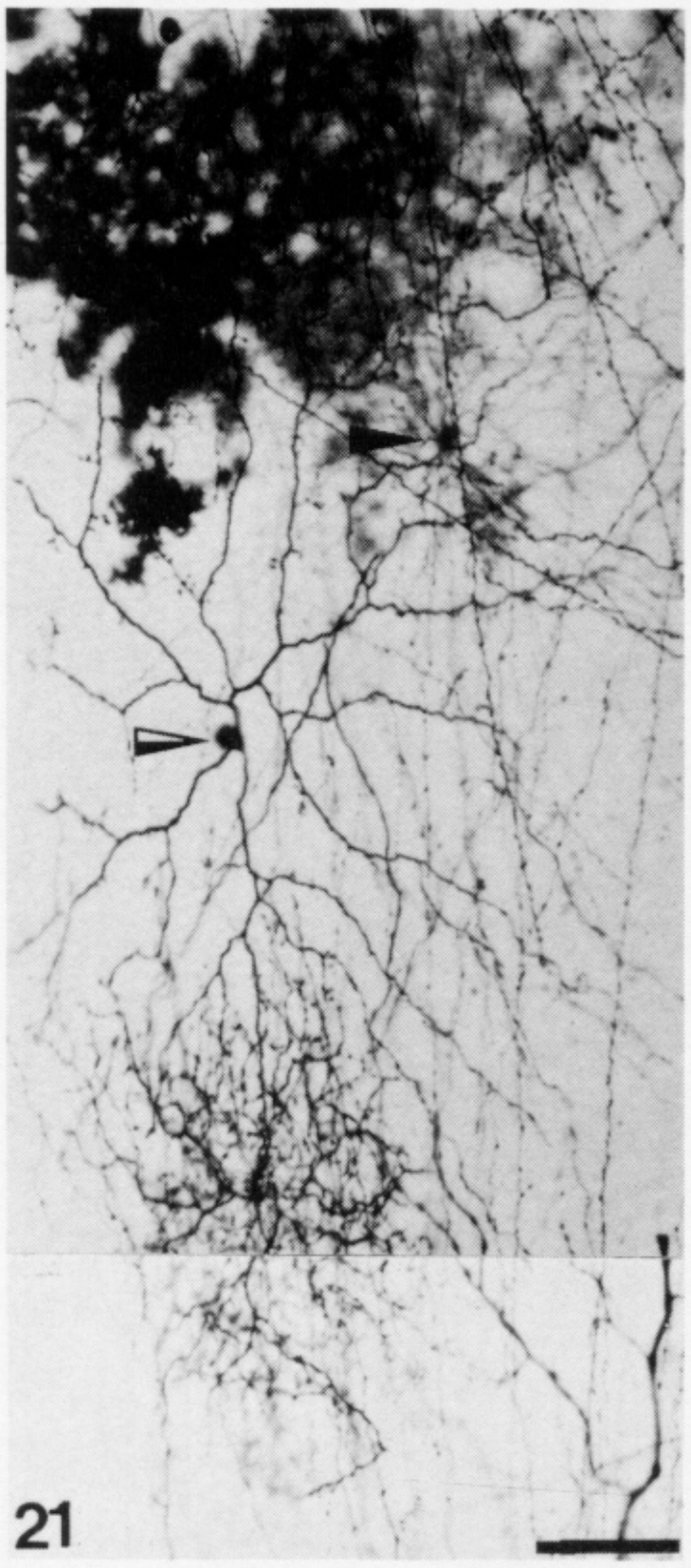

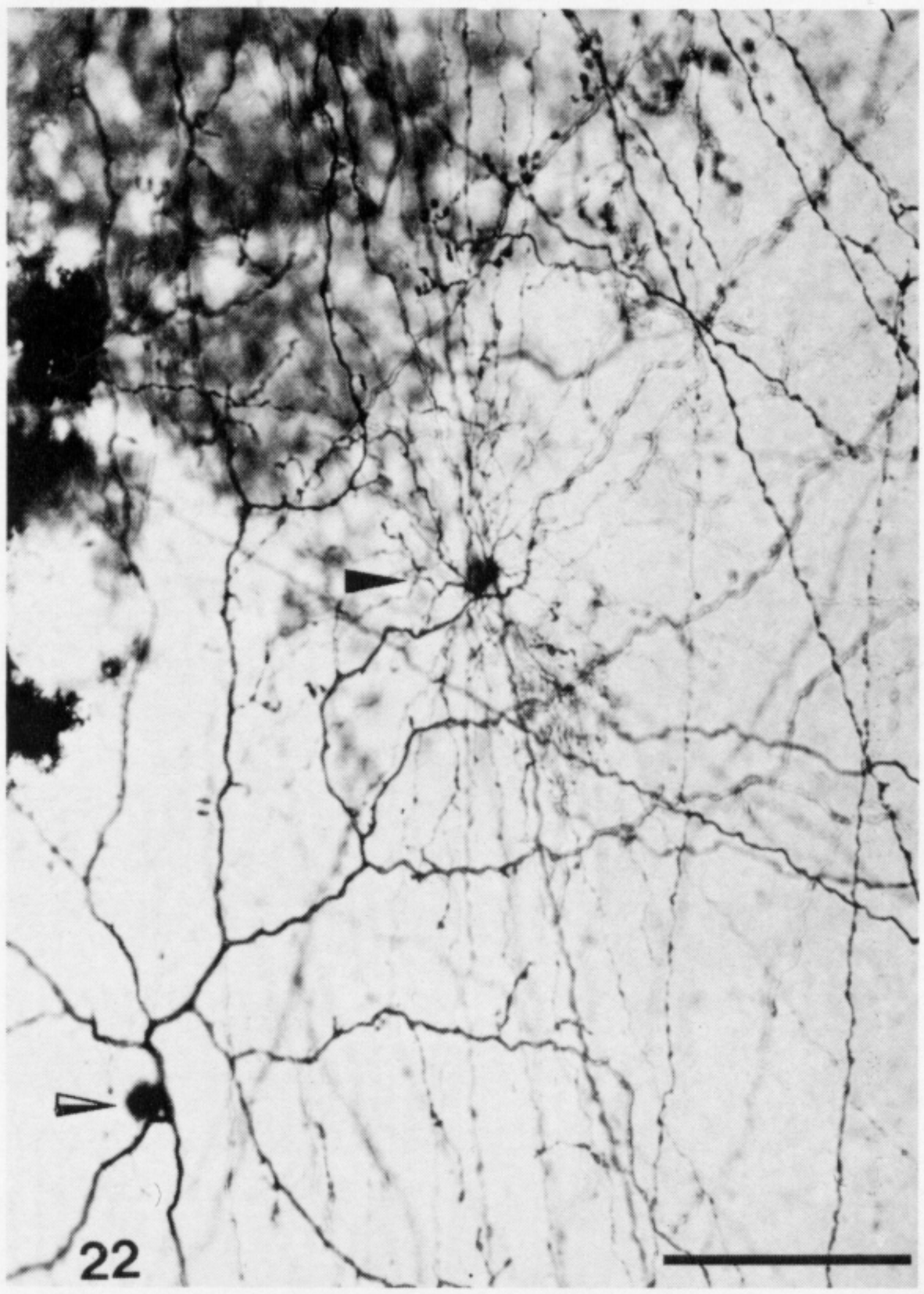

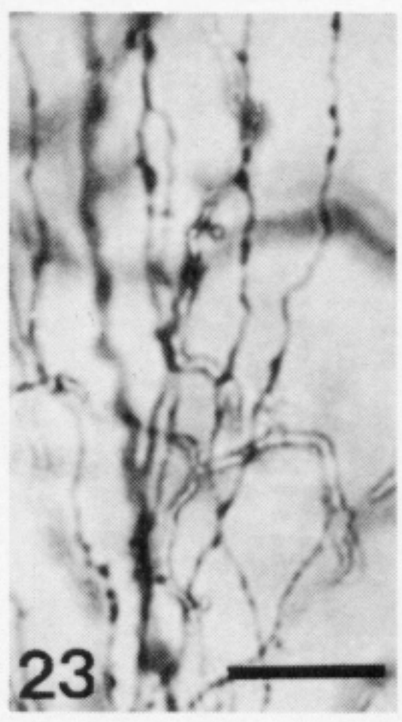

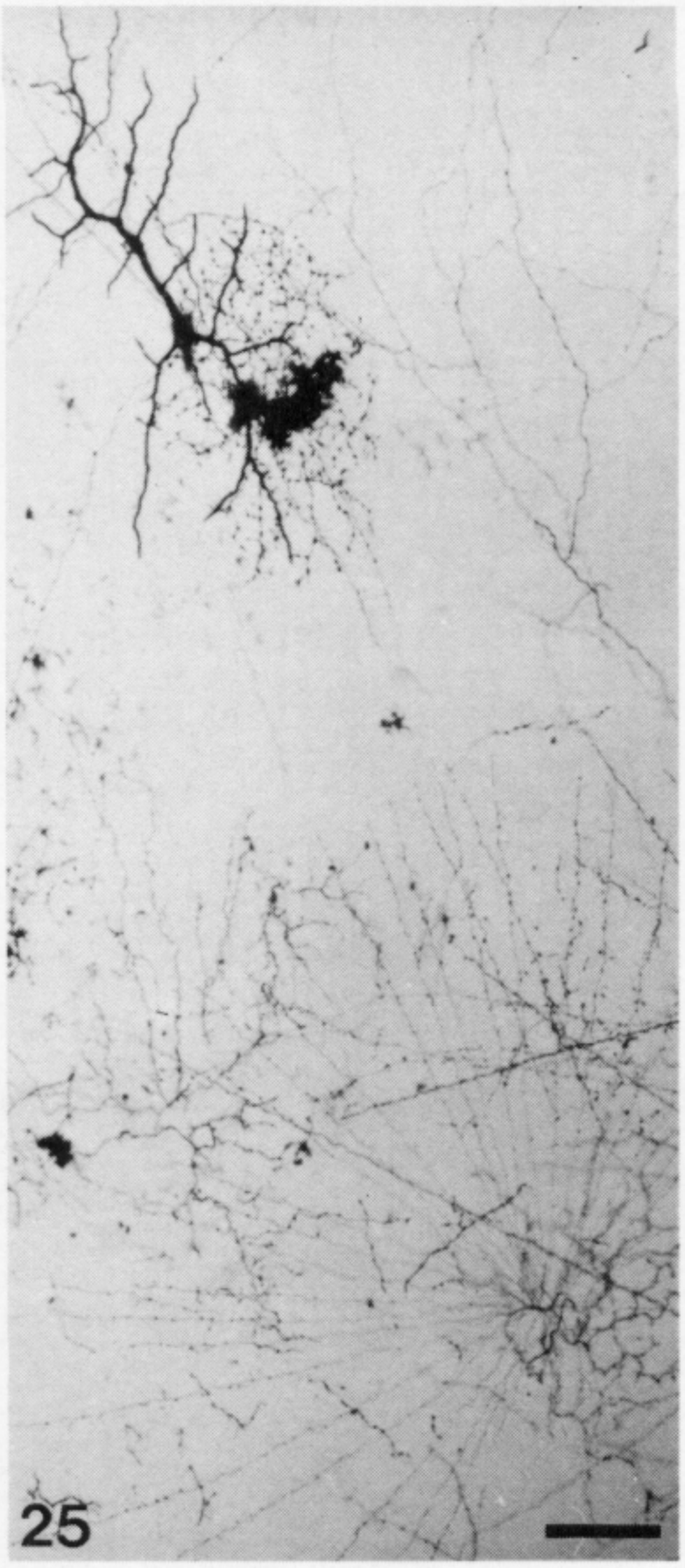

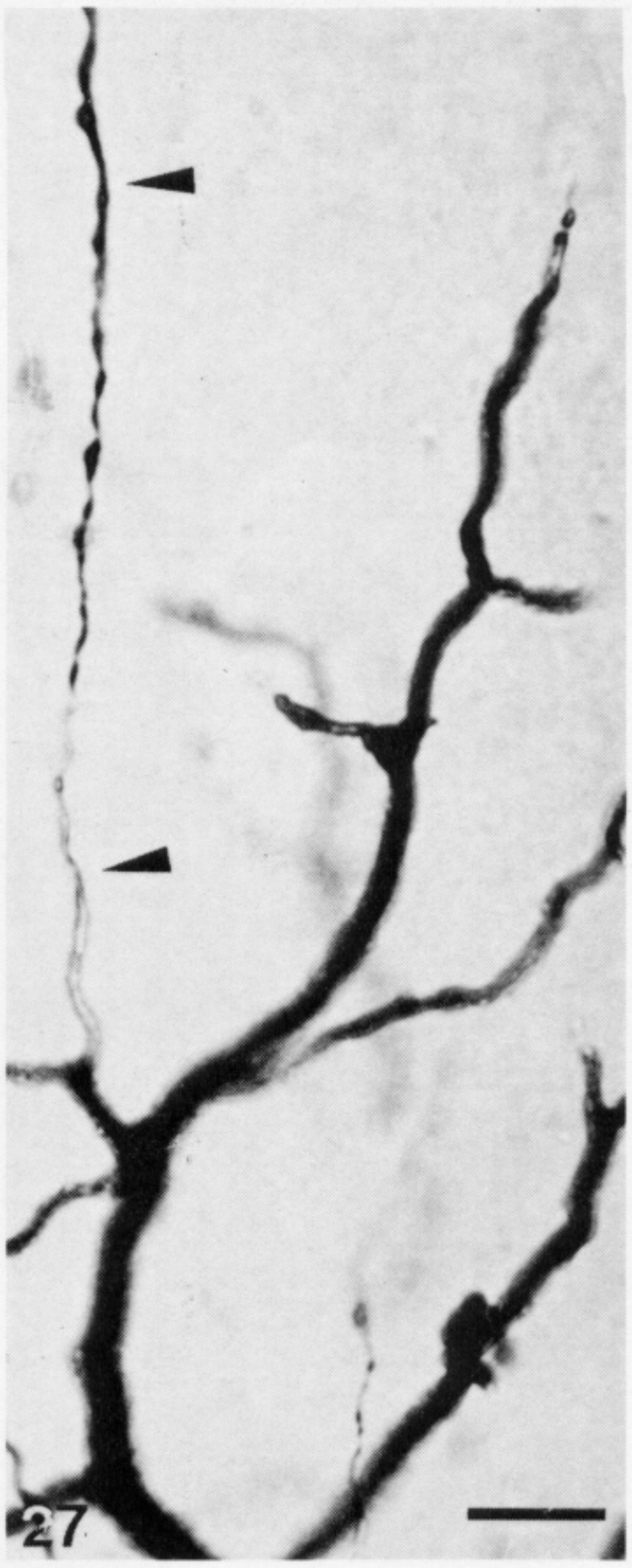

FIGURES 21–27. For description see opposite.

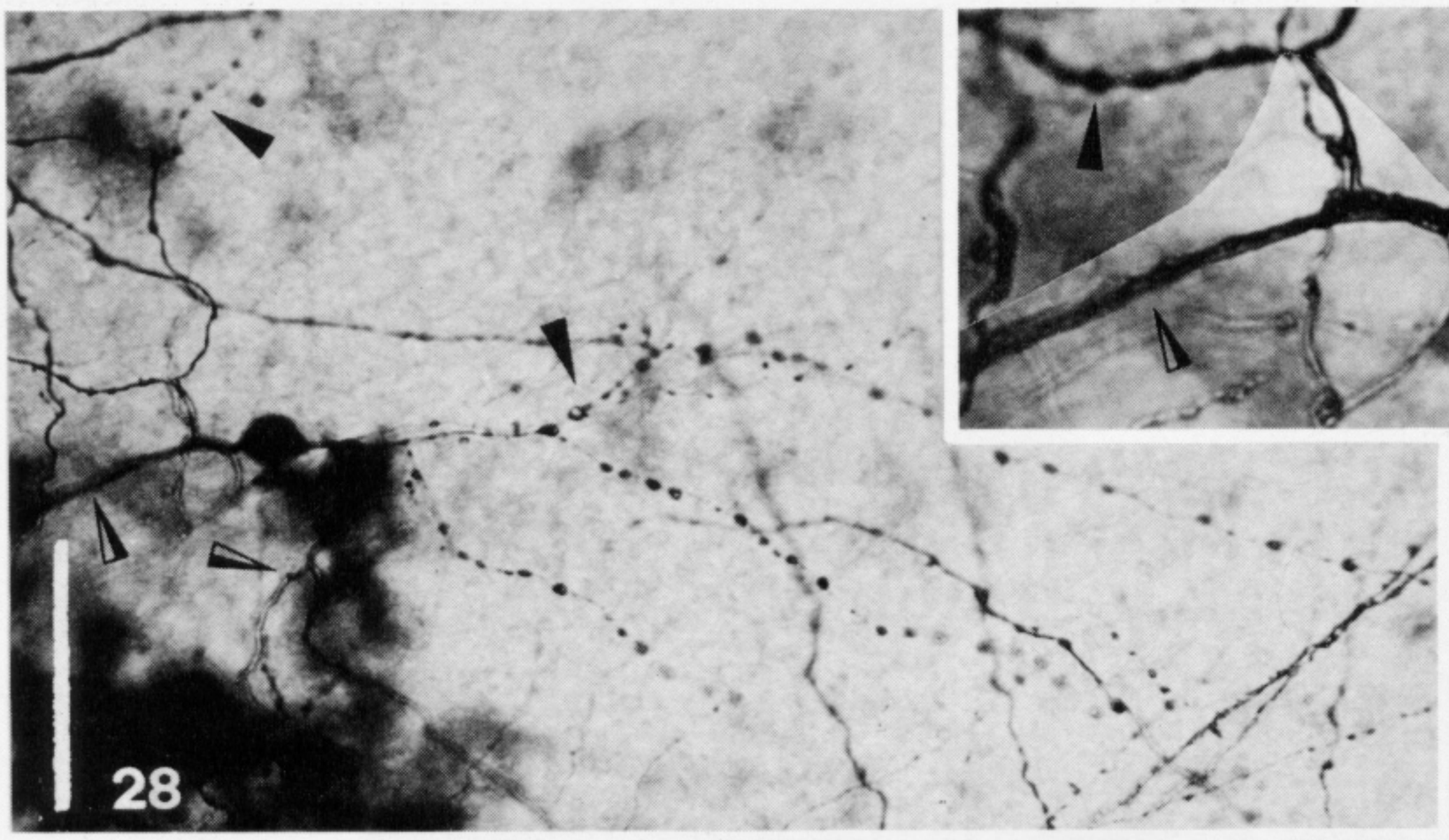

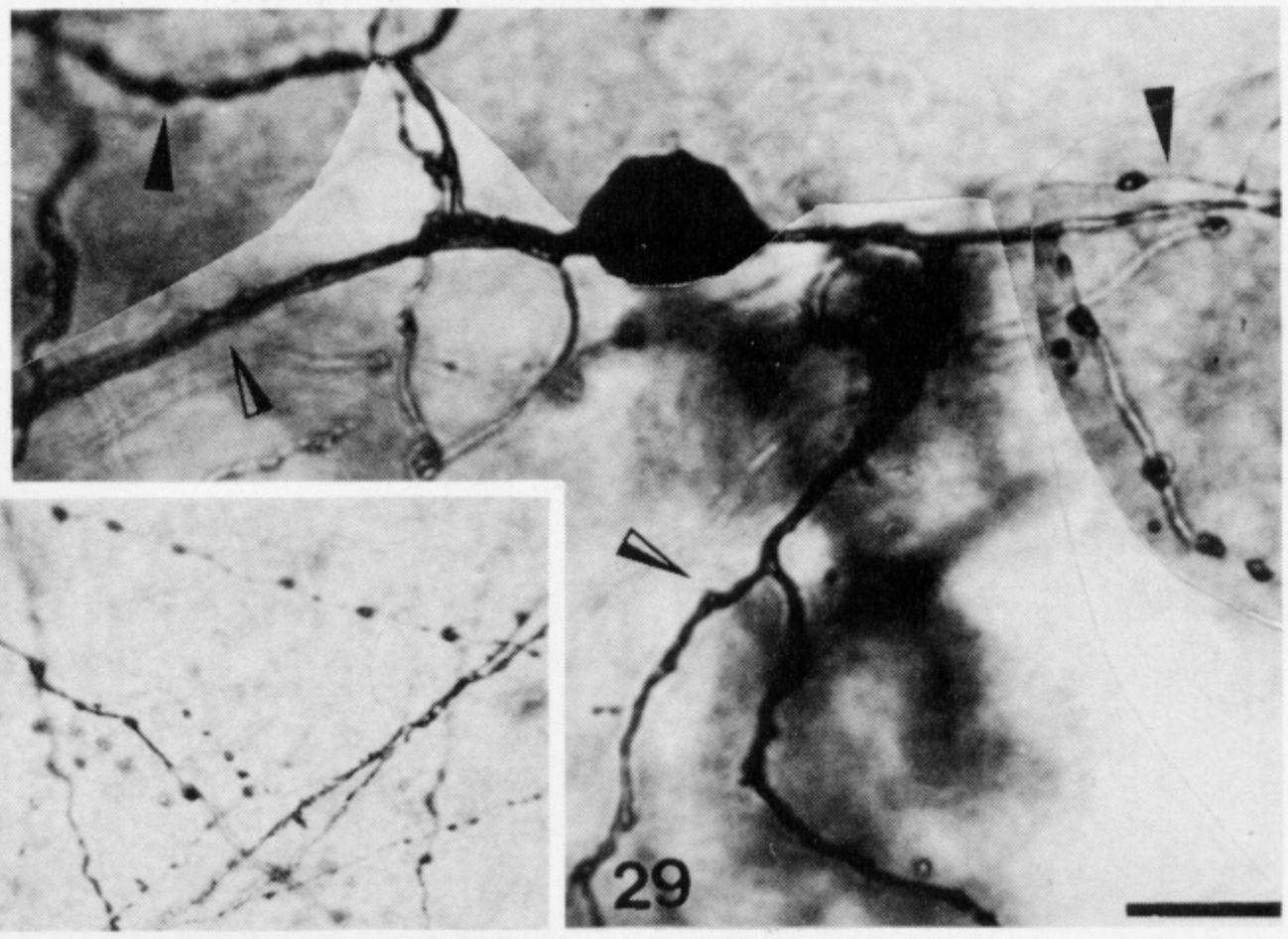

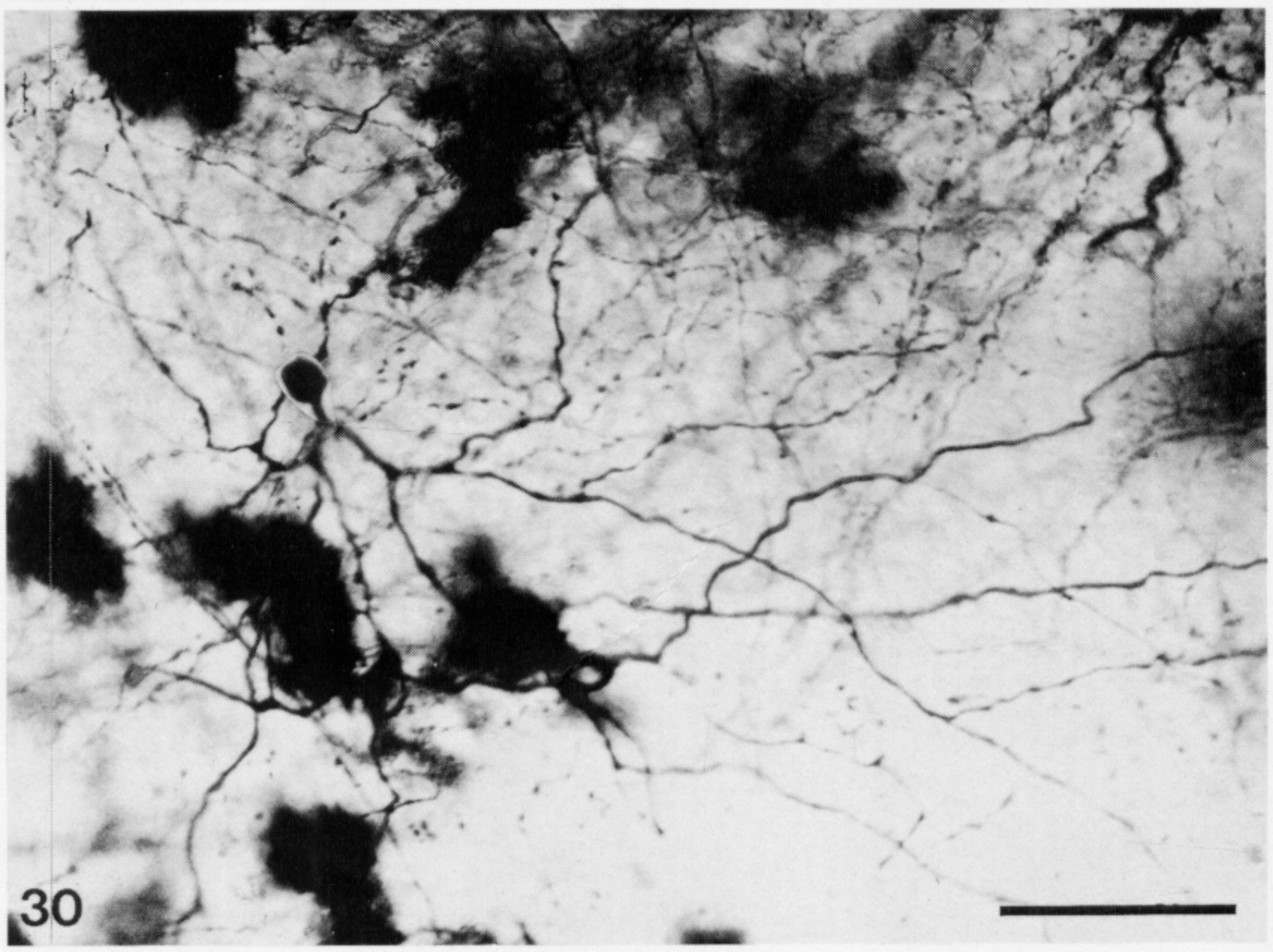

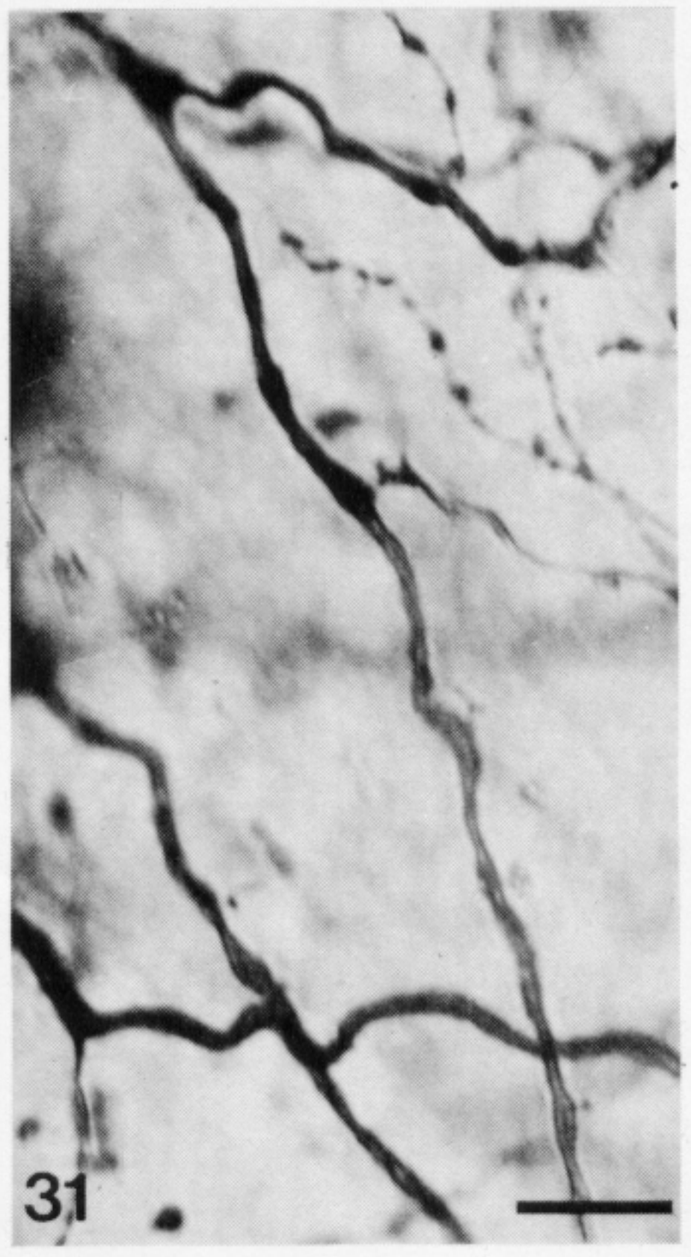

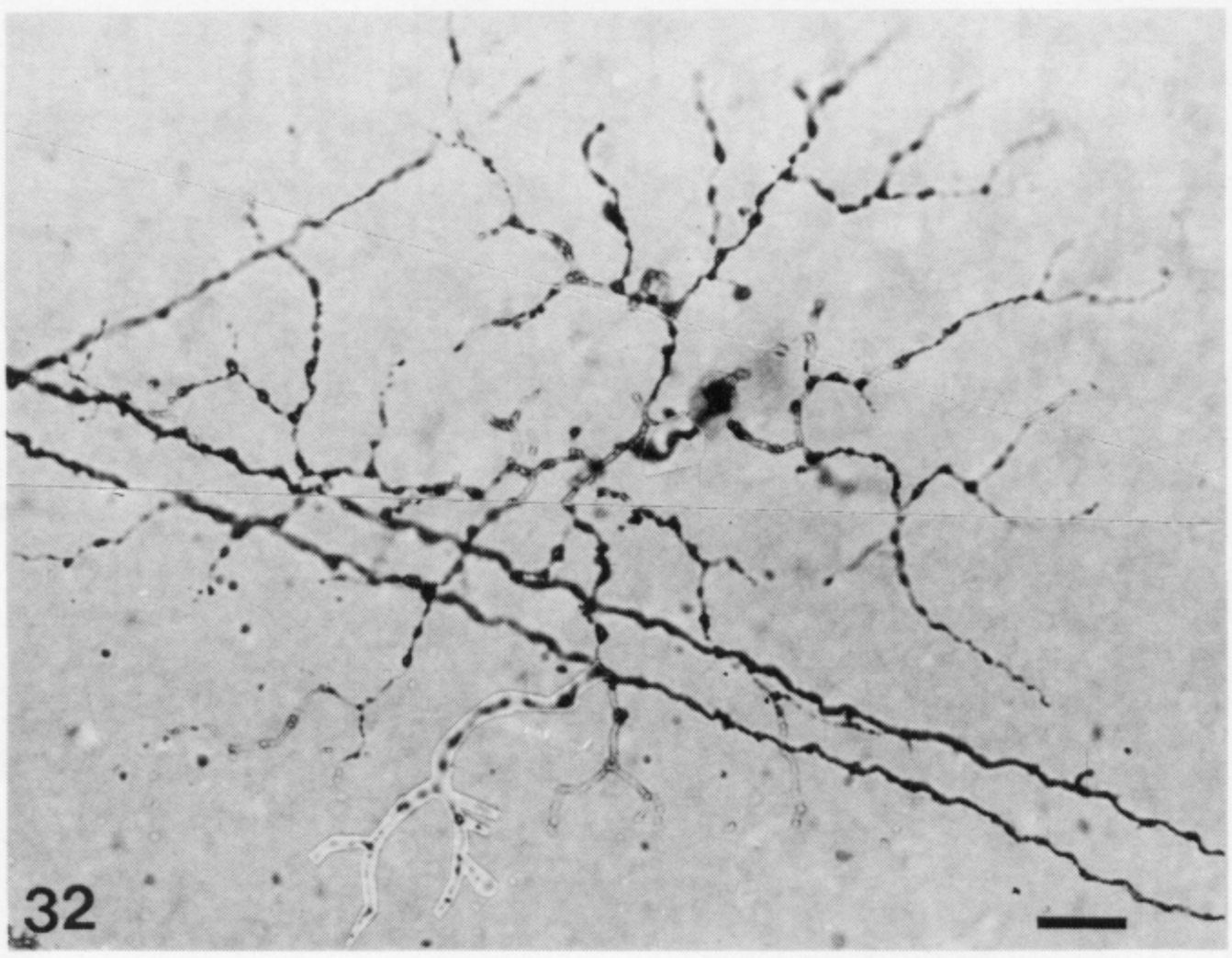

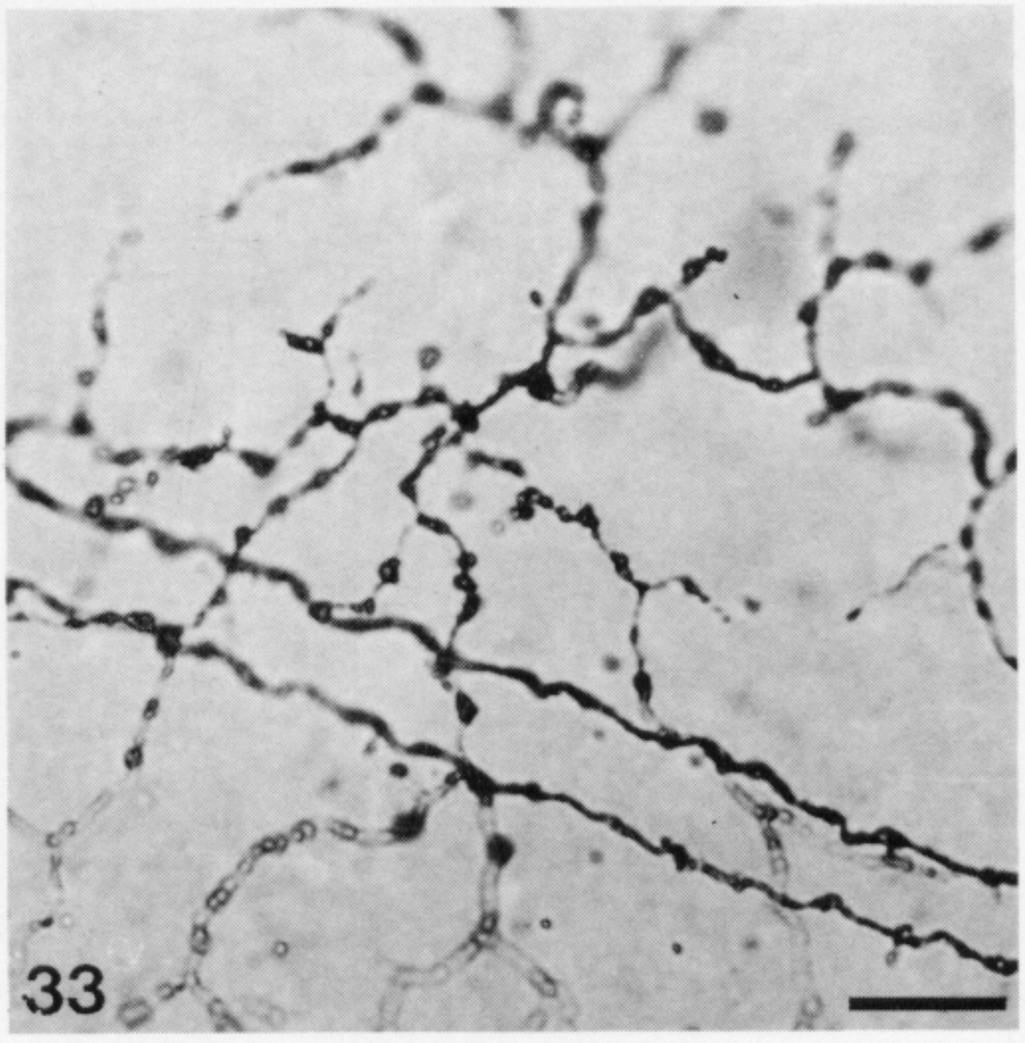

FIGURES 28–33. For description see opposite.

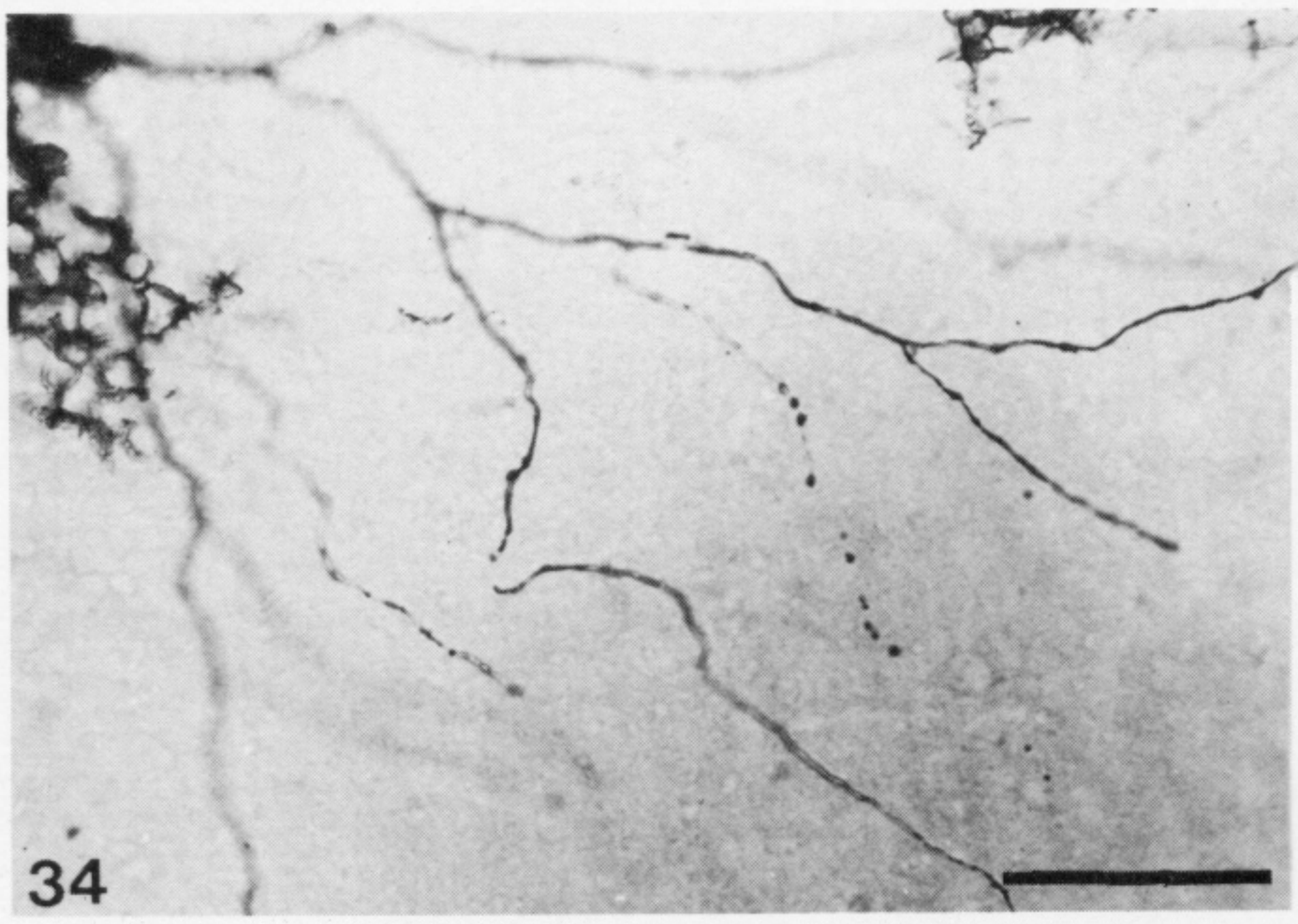

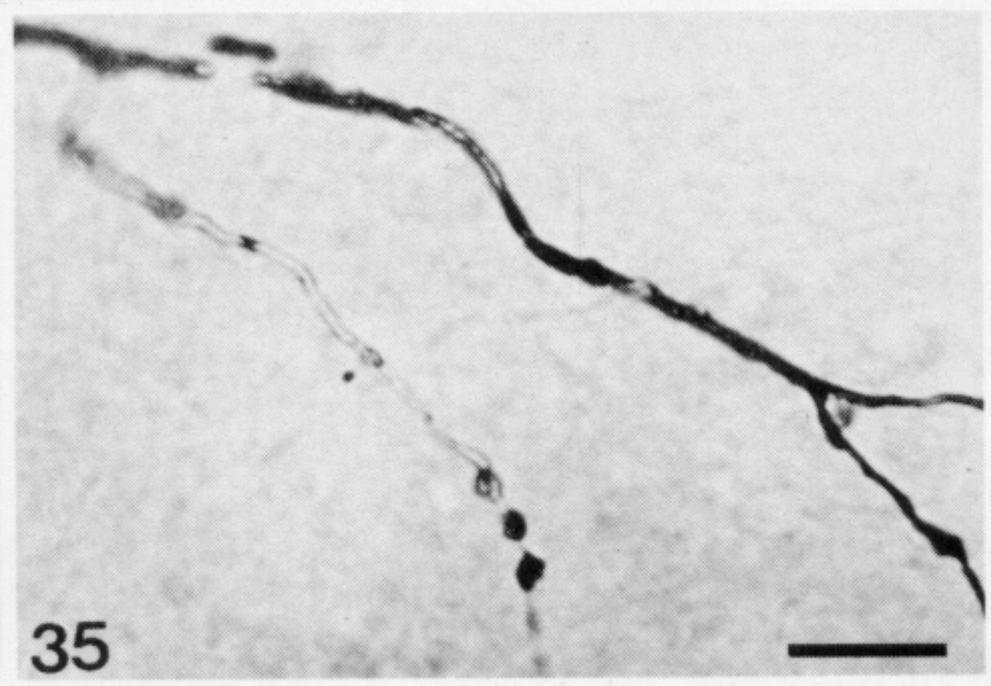

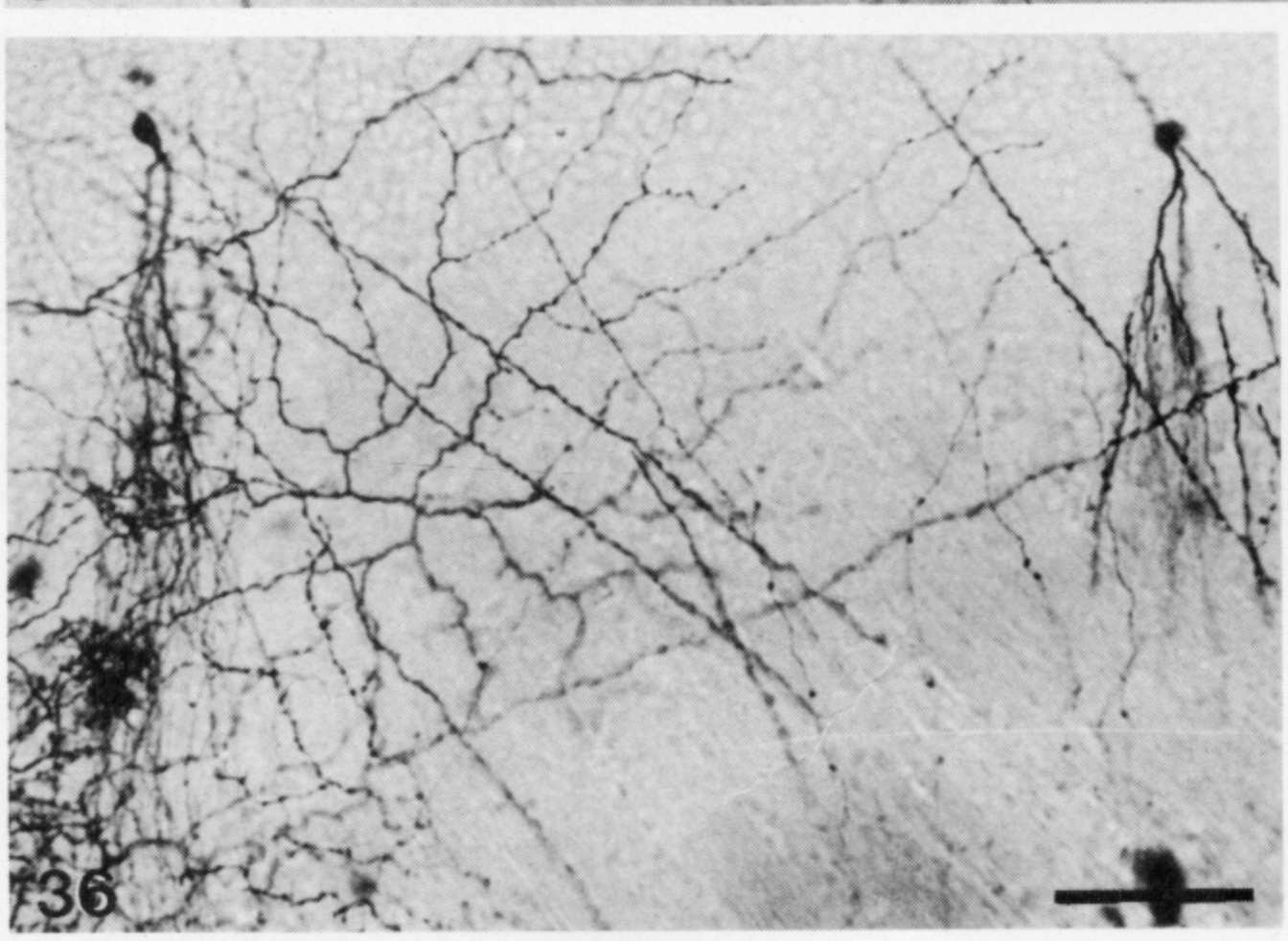

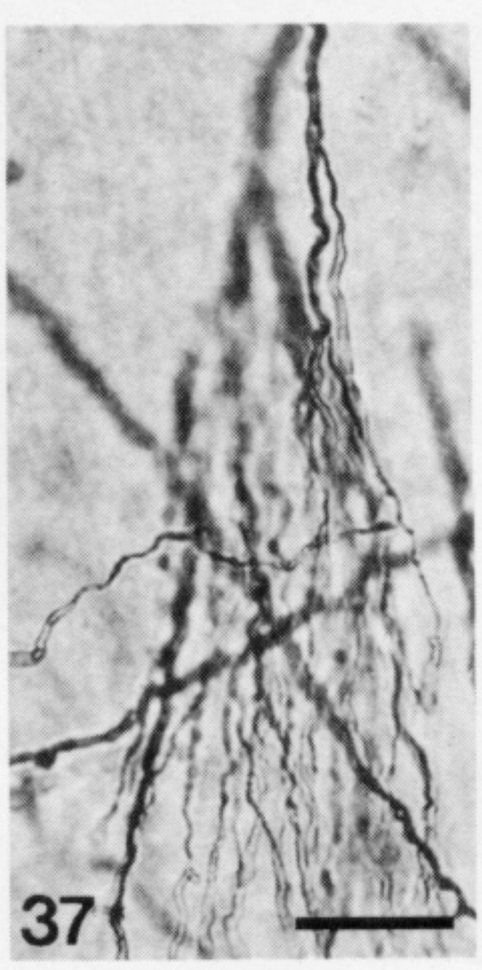

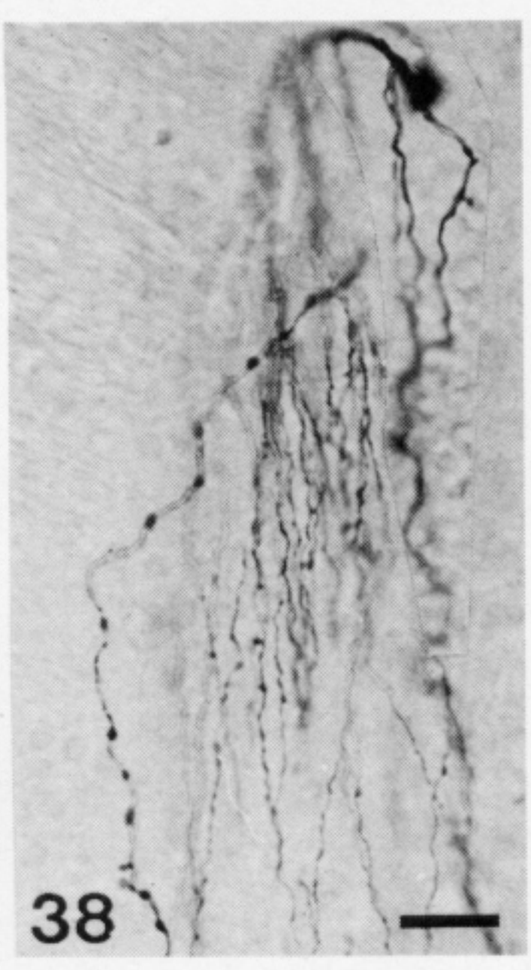

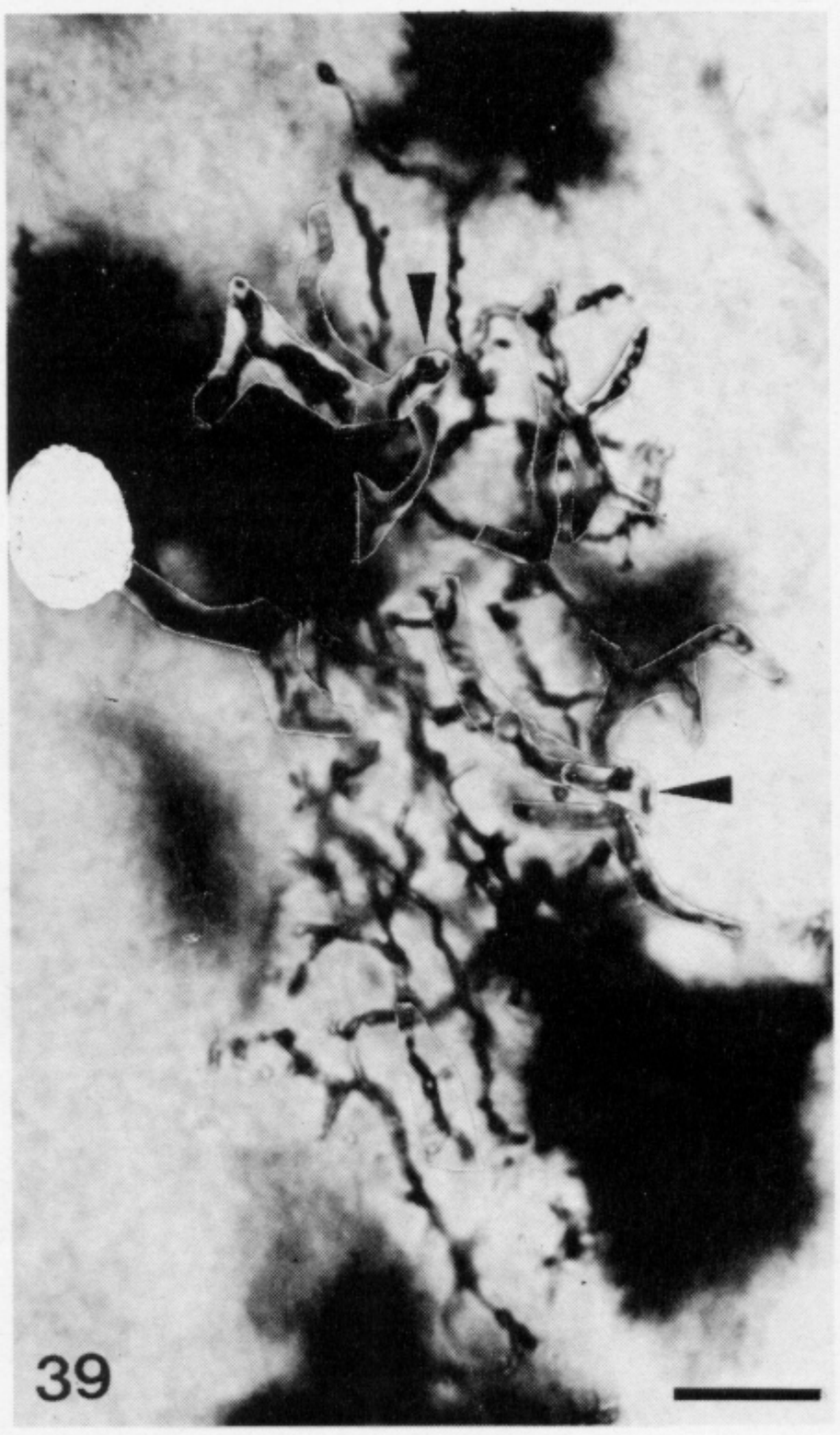

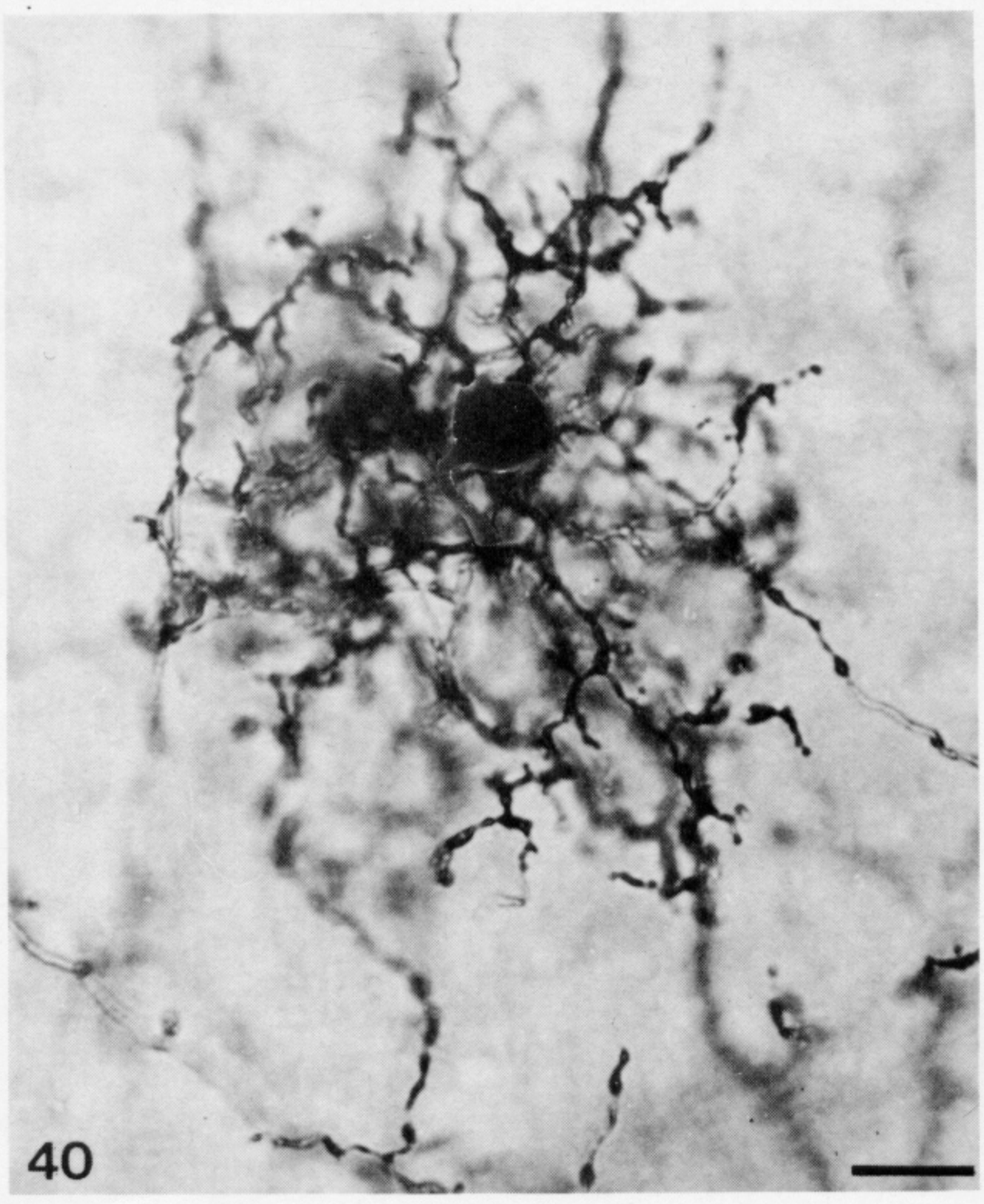

FIGURES 34–40. For description see opposite.

41

FIGURE 41. For description see opposite.